

การสังเคราะห์อนุภาคระดับนาโนเมตรของสไตรีนบิวทาไดอีนโคพอลิเมอร์/ซิลิกา  
และพอลิบิวทาไดอีน/ซิลิกาผ่านดิฟเฟอเรนเชียลไมโครอิมัลชันพอลิเมอไรเซชัน



นางสาวธัญพร ตันเจริญรัตน์

จุฬาลงกรณ์มหาวิทยาลัย

CHULALONGKORN UNIVERSITY

บทคัดย่อและแฟ้มข้อมูลฉบับเต็มของวิทยานิพนธ์ตั้งแต่ปีการศึกษา 2554 ที่ให้บริการในคลังปัญญาจุฬาฯ (CUIR)  
เป็นแฟ้มข้อมูลของนิสิตเจ้าของวิทยานิพนธ์ ที่ส่งผ่านทางบัณฑิตวิทยาลัย

The abstract and full text of theses from the academic year 2011 in Chulalongkorn University Intellectual Repository (CUIR)  
are the thesis authors' files submitted through the University Graduate School.

วิทยานิพนธ์นี้เป็นส่วนหนึ่งของการศึกษาตามหลักสูตรปริญญาวิทยาศาสตรดุษฎีบัณฑิต

สาขาวิชาเคมีเทคนิค ภาควิชาเคมีเทคนิค

คณะวิทยาศาสตร์ จุฬาลงกรณ์มหาวิทยาลัย

ปีการศึกษา 2557

ลิขสิทธิ์ของจุฬาลงกรณ์มหาวิทยาลัย

SYNTHESIS OF STYRENE BUTADIENE COPOLYMER/SiO<sub>2</sub> AND POLYBUTADIENE/SiO<sub>2</sub>  
NANOPARTICLES VIA DIFFERENTIAL MICROEMULSION POLYMERIZATION

Miss Thanyaporn Tancharernrat



A Dissertation Submitted in Partial Fulfillment of the Requirements  
for the Degree of Doctor of Philosophy Program in Chemical Technology

Department of Chemical Technology

Faculty of Science

Chulalongkorn University

Academic Year 2014

Copyright of Chulalongkorn University

Thesis Title	SYNTHESIS OF STYRENE BUTADIENE COPOLYMER/SiO <sub>2</sub> AND POLYBUTADIENE/SiO <sub>2</sub> NANOPARTICLES VIA DIFFERENTIAL MICROEMULSION POLYMERIZATION
By	Miss Thanyaporn Tancharernrat
Field of Study	Chemical Technology
Thesis Advisor	Professor Pattarapan Prasassarakich, Ph.D.
Thesis Co-Advisor	Professor Garry L. Rempel, Ph.D.

---

Accepted by the Faculty of Science, Chulalongkorn University in Partial  
Fulfillment of the Requirements for the Doctoral Degree

..... Dean of the Faculty of Science  
(Professor Supot Hannongbua, Ph.D.)

THESIS COMMITTEE

..... Chairman  
(Associate Professor Kejvalee Pruksathorn, Ph.D.)

..... Thesis Advisor  
(Professor Pattarapan Prasassarakich, Ph.D.)

..... Thesis Co-Advisor  
(Professor Garry L. Rempel, Ph.D.)

..... Examiner  
(Assistant Professor Napida Hinchiranan, Ph.D.)

..... Examiner  
(Associate Professor Sirilux Poompradub, Ph.D.)

..... External Examiner  
(Associate Professor Kitikorn Charmondusit, Ph.D.)

ัญพร ตันเจริญรัตน์ : การสังเคราะห์อนุภาคระดับนาโนเมตรของสไตรีนบิวทาไดอินโคพอลิเมอร์/ซิลิกา และพอลิบิวทาไดอิน/ซิลิกาผ่านดิฟเฟอเรนเชียลไมโครอิมัลชันพอลิเมอไรเซชัน (SYNTHESIS OF STYRENE BUTADIENE COPOLYMER/SiO<sub>2</sub> AND POLYBUTADIENE/SiO<sub>2</sub> NANOPARTICLES VIA DIFFERENTIAL MICROEMULSION POLYMERIZATION) อ.ที่ปรึกษาวิทยานิพนธ์หลัก: ศ. ดร. ภัทรพรรณ ประศาสน์สารกิจ, อ.ที่ปรึกษาวิทยานิพนธ์ร่วม: Prof. Garry L. Rempel Ph.D., 150 หน้า.

ดิฟเฟอเรนเชียลไมโครอิมัลชันพอลิเมอไรเซชัน (DMP) ถูกเลือกเพื่อใช้สังเคราะห์อนุภาคระดับนาโนเมตรของสไตรีนบิวทาไดอินโคพอลิเมอร์-ซิลิกา พอลิบิวทาไดอิน-ซิลิกา และพอลิสไตรีน-ซิลิกา โครงสร้างคอร์เชลล์ถูกออกแบบเพื่อให้เกิดการกระจายตัวของอนุภาคที่ดีเป็นเนื้อเดียวกันโดยลดการเกาะกลุ่มกันของอนุภาคซิลิกา งานวิจัยนี้ศึกษาผลของปริมาณซิลิกา อัตราส่วนของมอนอเมอร์ต่อน้ำ ความเข้มข้นของสารลดแรงตึงผิว และความเข้มข้นของตัวริเริ่มปฏิกิริยา ต่อร้อยละการเปลี่ยนของมอนอเมอร์ ขนาดอนุภาค และประสิทธิภาพการกราฟต์ พบว่าอนุภาคนาโนสไตรีนบิวทาไดอินโคพอลิเมอร์-ซิลิกามีขนาดอยู่ในช่วง 20-50 นาโนเมตร ร้อยละการเปลี่ยนของมอนอเมอร์สูงถึง ร้อยละ 86.6 และประสิทธิภาพการกราฟต์สูงถึงร้อยละ 75.5 โดยใช้ปริมาณสารลดแรงตึงผิวต่ำมาก เพียงแค่ 3 % โดยน้ำหนักของปริมาณมอนอเมอร์ สำหรับการสังเคราะห์พอลิบิวทาไดอิน-ซิลิกาด้วย DMP ร้อยละการเปลี่ยนของมอนอเมอร์สูงถึง ร้อยละ 81.5 ประสิทธิภาพการกราฟต์สูงถึงร้อยละ 78.5 และขนาดอนุภาคเล็กถึง 27 นาโนเมตร ถูกสังเคราะห์เป็นผลสำเร็จ ณ ภาวะที่เหมาะสม สุกทำอนุภาคนาโนพอลิสไตรีน-ซิลิกาที่สังเคราะห์ได้มีขนาดอนุภาคเฉลี่ย 33.5 นาโนเมตร และประสิทธิภาพการกราฟต์สูงถึงร้อยละ 76.3 นอกจากนี้ไดอิมิดรีดักชันถูกนำมาประยุกต์ใช้ในการสังเคราะห์ไฮโดรจีเนตพอลิบิวทาไดอิน-ซิลิกาโดยมีระดับไฮโดรจีเนชันสูงถึงร้อยละ 98.6 ที่อัตราส่วนไฮดราซินต่อไฮโดรเจนเปอร์ออกไซด์เท่ากับ 0.75:1 ไฮโดรจีเนตพอลิบิวทาไดอิน-ซิลิกาที่สังเคราะห์ได้แสดงค่าการสลายตัวทางความร้อนสูงสุดที่ 469.6 องศาเซลเซียส บ่งบอกถึงเสถียรภาพทางความร้อนที่ดี นาโนคอมพอสิตชนิดใหม่ ของสไตรีนบิวทาไดอินโคพอลิเมอร์-ซิลิกา พอลิบิวทาไดอิน-ซิลิกา ไฮโดรจีเนตพอลิบิวทาไดอิน-ซิลิกา และพอลิสไตรีน-ซิลิกาสามารถใช้เป็นสารตัวเติมชนิดใหม่ในน้ำยางธรรมชาติ และยางสไตรีนบิวทาไดอินลาเท็กซ์ โดยเฉพาะยางธรรมชาติเติมไฮโดรจีเนตพอลิบิวทาไดอิน-ซิลิกามีการปรับปรุงสมบัติเชิงกลและสมบัติทางความร้อน รวมถึงมีความต้านทานต่อโอโซนที่ดี

ภาควิชา เคมีเทคนิค

ลายมือชื่อนิสิต .....

สาขาวิชา เคมีเทคนิค

ลายมือชื่อ อ.ที่ปรึกษาหลัก .....

ปีการศึกษา 2557

ลายมือชื่อ อ.ที่ปรึกษาร่วม .....

# # 5472827323 : MAJOR CHEMICAL TECHNOLOGY

KEYWORDS: DIFFERENTIAL MICROEMULSION POLYMERIZATION / DIIMIDE REDUCTION / NANOCOMPOSITE / SILICA / MECHANICAL PROPERTIES / THERMAL PROPERTIES

THANYAPORN TANCHARERNRAT: SYNTHESIS OF STYRENE BUTADIENE COPOLYMER/SiO<sub>2</sub> AND POLYBUTADIENE/SiO<sub>2</sub> NANOPARTICLES VIA DIFFERENTIAL MICROEMULSION POLYMERIZATION. ADVISOR: PROF. PATTARAPAN PRASASSARAKICH, Ph.D., CO-ADVISOR: PROF. GARRY L. REMPEL, Ph.D., 150 pp.

Differential microemulsion polymerization (DMP) was selected for synthesis of styrene butadiene copolymer (SBR)-SiO<sub>2</sub>, polybutadiene (PB)-SiO<sub>2</sub> and polystyrene (PS)-SiO<sub>2</sub> nanoparticles. The core-shell structure was designed to achieve a monodispersion with reduced nanosilica aggregation. The effects of silica loading, monomer to water ratio, surfactant concentration and initiator concentration on monomer conversion, particle size, particle size distribution and grafting efficiency were investigated. SBR-SiO<sub>2</sub> nanoparticles with a size range of 20-50 nm, high monomer conversion of 86.6% and high grafting efficiency of 75.5% were obtained at a low surfactant concentration of 3 wt% based on monomer. For PB-SiO<sub>2</sub> synthesis via DMP, a high monomer conversion (81.5%), grafting efficiency (78.5%) and small particle size (27 nm) was obtained under optimum reaction conditions. In addition, PS-SiO<sub>2</sub> nanoparticles with a small particle size of 33.5 nm and high polymer grafting efficiency of 76.3 was also obtained by DMP. Diimide reduction was applied to synthesize hydrogenated polybutadiene (HPB)-SiO<sub>2</sub>. A high hydrogenation degree of 98.6% was achieved at a ratio of hydrazine to hydrogen peroxide of 0.75:1. HPB-SiO<sub>2</sub> showed a maximum degradation temperature of 469.6 °C resulting in excellent thermal stability. A new nanocomposite of SBR-SiO<sub>2</sub>, PB-SiO<sub>2</sub>, HPB-SiO<sub>2</sub> and PS-SiO<sub>2</sub> could be used as a novel nanofiller in natural rubber and styrene butadiene rubber latex. Especially, NR/HPB-SiO<sub>2</sub> composites had improved mechanical and thermal properties, and exhibited good resistance toward ozone exposure.

Department: Chemical Technology

Field of Study: Chemical Technology

Academic Year: 2014

Student's Signature .....

Advisor's Signature .....

Co-Advisor's Signature .....

## ACKNOWLEDGEMENTS

The author would like to express heartfelt gratitude and sincere appreciation to her advisor, Prof. Dr. Pattarapan Prasassarakich and co-advisor, Prof. Garry L. Rempel for the encouraging guidance, supervision, helpful discussion and support throughout this research. The author also would like to acknowledge Assoc. Prof. Dr. Kejvalee Pruksathorn, Asst. Prof. Dr. Napida Hinchiranan, Assoc. Prof. Dr. Sirilux Poompradub and Assoc. Prof. Dr. Kitikorn Charmondusit for serving as the dissertation chairman and members of the thesis committee, respectively, and for their worthy comments and suggestions.

The author gratefully acknowledges the funding support from the Thailand Research Fund (through the Royal Golden Jubilee Project), Graduate School, Chulalongkorn University as well as the Natural Sciences and Engineering Research Council of Canada (NSERC).

Many thanks also go to the Department of Chemical Technology, Faculty of Science, Chulalongkorn University and Department of Chemical Engineering, University of Waterloo, Canada for providing research facilities throughout this research work.

Finally, the author also expresses her deep gratitude to her family for their love, support and encouragement throughout her Ph.D. program. Special thanks are also extended to her friends in Department of Chemical Technology and the members of the Advanced Rubber Technology and Applied Catalysis Laboratory in Department of Chemical Engineering, University of Waterloo for friendship, support and encouragement.

## CONTENTS

	Page
THAI ABSTRACT .....	iv
ENGLISH ABSTRACT .....	v
ACKNOWLEDGEMENTS .....	vi
CONTENTS .....	vii
LIST OF TABLES .....	xiii
LIST OF FIGURES .....	xv
LIST OF ABBREVIATIONS .....	xxi
CHAPTER I INTRODUCTION.....	1
1.1 Motivation.....	1
1.2 Microemulsion Polymerization.....	2
1.3 Silica Surface Modification .....	7
1.4 Polymer-Silica Nanocomposites .....	10
1.5 Hydrogenation of Diene Rubber .....	16
1.6 Mechanical Properties of Polymer Nanocomposites .....	20
1.7 Thermal Stability of Polymer Nanocomposites.....	23
1.8 Membrane Separation .....	25
1.9 Objective and Scope of Dissertation .....	28
CHAPTER II EXPERIMENTAL AND CHARACTERIZATION.....	31
2.1 Materials .....	31
2.1.1 Preliminary Experiments on Synthesis of Styrene Butadiene Copolymer Nanoparticles .....	31
2.1.2 Synthesis of Styrene Butadiene Copolymer-SiO <sub>2</sub> Nanocomposites.....	31
2.1.3 Synthesis of Polybutadiene-SiO <sub>2</sub> Nanocomposites .....	32

	Page
2.1.4 Hydrogenation of Polybutadiene-SiO <sub>2</sub> Nanocomposites.....	32
2.1.5 Synthesis of Polystyrene- SiO <sub>2</sub> nanocomposites .....	32
2.1.6 Pre-Vulcanization of Natural Rubber Composites .....	33
2.2 Surface Modification of Nanosilica .....	33
2.3 Preliminary Experiments on Synthesis of Styrene Butadiene Copolymer Nanoparticles.....	34
2.4 Synthesis of Styrene Butadiene Copolymer-SiO <sub>2</sub> Nanocomposites .....	37
2.5 Synthesis of Polybutadiene-SiO <sub>2</sub> Nanocomposites.....	39
2.6 Hydrogenation of Polybutadiene-SiO <sub>2</sub> Nanocomposites.....	41
2.7 Synthesis of Polystyrene- SiO <sub>2</sub> Nanocomposites .....	42
2.8 Preparation of NR/SBR-SiO <sub>2</sub> and NR/HPB-SiO <sub>2</sub> Composites.....	44
i) Preparation of NR/SBR-SiO <sub>2</sub> Composites.....	44
ii) Preparation of NR/PB-SiO <sub>2</sub> and NR/HPB-SiO <sub>2</sub> Composites.....	44
2.9 Preparation of SBR/PS-SiO <sub>2</sub> Composites.....	45
2.10 Characterization.....	45
2.10.1 Fourier Transform Infrared Spectroscopy.....	45
2.10.2 <sup>1</sup> H NMR Spectroscopy.....	46
2.10.3 Particle Diameter Measurement.....	46
2.10.4 Morphological Study.....	46
2.10.5 Thermogravimatic Analysis (TGA) .....	47
2.10.6 Differential Scanning Calorimetry (DSC).....	47
2.10.7 Contact Angle Measurement .....	47
2.10.8 Gas Permeability.....	48



	Page
2.11 Mechanical Properties of NR and SBR Composites.....	48
2.12 Thermal Resistance of Vulcanized Rubber.....	49
2.13 Ozone Resistance of Vulcanized Rubber.....	49
2.14 Pervaporation of Water-Ethanol Mixture.....	49
CHAPTER III PRELIMINARY STUDY ON SYNTHESIS OF STYRENE BUTADIENE COPOLYMER NANOPARTICLES VIA DIFFERENTIAL MICROEMULSION POLYMERIZATION.....	
	51
3.1 Introduction .....	51
3.2 Characterization of SBR Nanoparticles .....	52
3.3 Effect of Process Parameters.....	54
3.3.1 Effect of Monomer to Water Ratio.....	54
3.3.2 Effect of Surfactant Concentration .....	55
3.3.3 Effect of Initiator Concentration.....	57
3.4 Morphology of SBR Nanoparticles.....	58
CHAPTER IV PREPARATION OF STYRENE BUTADIENE COPOLYMER-SILICA NANOCOMPOSITES VIA DIFFERENTIAL MICROEMULSION POLYMERIZATION AND NR/SBR-SiO <sub>2</sub> MEMBRANE FOR PERVAPORATION OF A WATER-ETHANOL MIXTURE .....	
	60
4.1 Introduction .....	60
4.2 Characterization of SBR-SiO <sub>2</sub> Nanocomposites .....	61
4.3 Effect of Process Parameters.....	63
4.3.1 Effect of Silica Loading .....	63
4.3.2 Effect of Surfactant Concentration .....	65
4.3.3 Effects of Monomer to Water Ratio.....	66
4.3.4 Effect of Initiator Concentration.....	68

	Page
4.4 Morphology of SBR-SiO <sub>2</sub> Nanocomposites.....	69
4.5 Thermal Properties of NR/SBR-SiO <sub>2</sub> Nanocomposite Membranes.....	72
4.6 Mechanical Properties of NR/SBR-SiO <sub>2</sub> Nanocomposite Membranes.....	73
4.7. Pervaporation .....	74
4.7.1. Effect of SBR-SiO <sub>2</sub> Loading.....	74
4.7.2 Effect of Feed Composition .....	78
CHAPTER V SYNTHESIS OF POLYBUTADIENE-SILICA NANOPARTICLES VIA	
DIFFERENTIAL MICROEMULSION POLYMERIZATION AND THEIR HYDROGENATED	
NANOPARTICLES BY DIIMIDE REDUCTION.....	
5.1 Introduction .....	79
5.2 Characteristics of PB-SiO <sub>2</sub> and HPB-SiO <sub>2</sub> .....	80
5.3 Differential Microemulsion Polymerization (DMP).....	82
5.3.1 Effect of Silica Loading .....	82
5.3.2 Effect of Surfactant Concentration .....	83
5.3.3 Effects of Monomer to Water Ratio.....	85
5.3.4 Effect of Initiator Concentration.....	86
5.4 Diimide Hydrogenation: Effect of N <sub>2</sub> H <sub>4</sub> and H <sub>2</sub> O <sub>2</sub> Concentration .....	87
5.5 Morphology of PB-SiO <sub>2</sub> and HPB-SiO <sub>2</sub> .....	91
5.6 Thermal Properties of PB-SiO <sub>2</sub> and HPB-SiO <sub>2</sub> .....	93
5.7 NR Nanocomposites .....	95
5.7.1 Thermal Properties of NR/PB-SiO <sub>2</sub> and NR/HPB-SiO <sub>2</sub> Composites.....	95
5.7.2. Mechanical Properties of NR/PB-SiO <sub>2</sub> and NR/HPB-SiO <sub>2</sub> Composites .....	98
5.7.3. Thermal Resistance of NR/PB-SiO <sub>2</sub> and NR/HPB-SiO <sub>2</sub> Composites .....	99
5.7.4. Ozone Resistance of NR/PB-SiO <sub>2</sub> and NR/HPB-SiO <sub>2</sub> Nanocomposites .....	102

	Page
CHAPTER VI SBR/PS-SiO <sub>2</sub> NANOCOMPOSITES: PHYSICAL PROPERTIES.....	106
6.1 Introduction .....	106
6.2 Characterization of PS-SiO <sub>2</sub> Nanocomposites .....	107
6.3 Effect of Process Parameters.....	108
6.3.1 Effect of Silica Loading .....	108
6.3.2 Effect of Surfactant Concentration .....	110
6.4 Morphology of PS-SiO <sub>2</sub> Nanocomposites.....	111
6.5 Thermal Properties of PS-SiO <sub>2</sub> Nanoparticles .....	112
6.6 Thermal Properties of SBR/PS-SiO <sub>2</sub> Composites.....	114
6.7 Surface Properties of SBR/PS-SiO <sub>2</sub> Composites .....	116
6.8 Mechanical Properties of SBR/PS-SiO <sub>2</sub> Composites .....	117
6.9 Morphology of SBR/PS-SiO <sub>2</sub> Composites.....	118
CHAPTER VII CONCLUSIONS AND RECOMMENDATIONS .....	119
7.1 Conclusions.....	119
i) Preliminary Study on Synthesis of Styrene Butadiene Copolymer Nanoparticles via Differential Microemulsion Polymerization.....	119
ii) Preparation of Styrene Butadiene Copolymer-Silica Nanocomposites via Differential Microemulsion Polymerization and NR/SBR-SiO <sub>2</sub> Membrane for Pervaporation of Water-Ethanol Mixture.....	119
iii) Synthesis of Polybutadiene-Silica Nanoparticles via Differential Microemulsion Polymerization and their Hydrogenated Nanoparticles by Diimide Reduction .....	120
iv) SBR/PS-SiO <sub>2</sub> Nanocomposites: Physical Properties.....	121
7.2 Recommendations.....	122

	Page
REFERENCES .....	123
APPENDICES.....	136
APPENDIX A Data of Mechanical Properties of NR/SBR-SiO <sub>2</sub> .....	137
APPENDIX B Data of Mechanical Properties of NR/PB-SiO <sub>2</sub> and NR/HPB-SiO <sub>2</sub> .....	138
APPENDIX C Data of Mechanical Properties of SBR/PS-SiO <sub>2</sub> .....	140
APPENDIX D Data of SBR-SiO <sub>2</sub> Synthesis.....	141
APPENDIX E Data of PB-SiO <sub>2</sub> Synthesis .....	143
APPENDIX F Data of PS-SiO <sub>2</sub> Synthesis .....	145
APPENDIX G Calculation of %Hydrogenation.....	146
APPENDIX H Data of Diimide Hydrogenation of Nanosized PB-SiO <sub>2</sub> .....	148
APPENDIX I Classification of Cracking on the Surface of NR Composites for Ozone Resistance Testing .....	149
VITA.....	150

## LIST OF TABLES

Table	Page
1.1 Typical silane coupling agents used for surface modification of silica nanoparticles. ....	9
1.2 Mechanical properties of PP based nanocomposites (Content of SiO <sub>2</sub> = 3.31 vol%) filled with different polymer-grafted SiO <sub>2</sub> . ....	21
4.1 The sizes of SBR-SiO <sub>2</sub> nanoparticle, SiO <sub>2</sub> core and SBR shell. ....	71
4.2 Thermal properties of NR/SBR-SiO <sub>2</sub> nanocomposites membranes. ....	73
4.3 Mechanical properties of NR/SBR-SiO <sub>2</sub> nanocomposites membranes. ....	74
4.4 Contact angle of NR/SBR-SiO <sub>2</sub> nanocomposite membranes. ....	76
5.1 Decomposition temperature of PB-SiO <sub>2</sub> and HPB-SiO <sub>2</sub> nanocomposites. ....	95
5.2 Thermal properties of NR/PB-SiO <sub>2</sub> and NR/HPB-SiO <sub>2</sub> composites. ....	96
5.3 Mechanical properties of NR/PB-SiO <sub>2</sub> and NR/HPB-SiO <sub>2</sub> composites. ....	99
5.4 Cracking of NR, NR/PB-SiO <sub>2</sub> and NR/HPB-SiO <sub>2</sub> nanocomposites. ....	104
6.1 Thermal properties of PS-SiO <sub>2</sub> <sup>a</sup> nanocomposites. ....	114
6.2 Thermal properties of SBR/PS-SiO <sub>2</sub> composite films. ....	115
6.3 Contact angle of SBR/PS-SiO <sub>2</sub> composite films. ....	116
6.4 Mechanical properties of SBR/PS-SiO <sub>2</sub> composites films. ....	117
A-1 Tensile strength, 300% modulus and elongation at break of NR/SBR-SiO <sub>2</sub> composites membranes. ....	137
B-1 Mechanical properties of NR/PB-SiO <sub>2</sub> and NR/HPB-SiO <sub>2</sub> composites before and after ageing. ....	138
B-2 Tensile strength, 300% modulus and elongation at break of NR/PB-SiO <sub>2</sub> and NR/HPB-SiO <sub>2</sub> composites before and after ageing. ....	139

Table	Page
C-1 Tensile strength, 300% modulus and elongation at break of SBR/PS-SiO <sub>2</sub> composites membranes. ....	140
D-1 Data of effect of silica loading on SBR-SiO <sub>2</sub> .....	141
D-2 Data of effect of surfactant concentration on SBR-SiO <sub>2</sub> . ....	141
D-3 Data of effect of monomer to water ratio on SBR-SiO <sub>2</sub> .....	142
D-4 Data of effect of initiator concentration on SBR-SiO <sub>2</sub> .....	142
E-1 Data of effect of silica loading on PB-SiO <sub>2</sub> .....	143
E-2 Data of effect of surfactant concentration on PB-SiO <sub>2</sub> . ....	143
E-3 Data of effect of monomer to water ratio on PB-SiO <sub>2</sub> .....	144
E-4 Data of effect of initiator concentration on PB-SiO <sub>2</sub> .....	144
F-1 Data of effect of silica loading on PS-SiO <sub>2</sub> .....	145
F-2 Data of effect of surfactant concentration on PS-SiO <sub>2</sub> .....	145
H-1 Data of effect of N <sub>2</sub> H <sub>4</sub> concentration on HPB-SiO <sub>2</sub> . ....	148
H-2 Data of effect of H <sub>2</sub> O <sub>2</sub> concentration on HPB-SiO <sub>2</sub> . ....	148

## LIST OF FIGURES

Figure	Page
1. 1 Isotropic microemulsion domains in the phase diagram of multicompartment systems.....	3
1. 2 Schematic polymerization mechanism in oil-in-water microemulsions. (I) Microdroplets are initiated by free radicals (a) with water-soluble initiator or (b) oil-soluble initiator. (II) Particle growth (c) by monomer diffusion through the continuous phase and (d) by collision between droplets (nonionic surfactant). (III) End of polymerization: polymer particles and empty micelles.....	4
1. 3 Proposed mechanism: differential microemulsion polymerization of MMA. ....	7
1. 4 Grafting and polycondensation mechanism of silane on silica particles, with Y is the organic functional group.....	10
1. 5 Agglomerated nanoparticles dispersed in a polymer matrix.....	12
1. 6 The possible structure of grafted nanoparticles dispersed in a polymer matrix.....	13
1. 7 The proposed formation mechanism of nanosize-SiO <sub>2</sub> encapsulated by nanosized PIP with core/shell morphology.....	16
1. 8 Proposed diimide latex reduction mechanism.....	18
1. 9 Schematic diagram of the pervaporation process. (a) Vacuum pervaporation, (b) purge gas pervaporation. ....	26
1. 10 Schematic representation of the pervaporation transport mechanism. (a) Solution-diffusion model, (b) pore flow model. ....	27
2. 1 The schematic diagram of silica surface modification. ....	34
2. 2 Schematic drawing of nanosized SBR polymerization apparatus. ....	36
2. 3 The schematic diagram of SBR synthesis.....	36

Figure	Page
2. 4	The schematic diagram of SBR-SiO <sub>2</sub> synthesis. .... 38
2. 5	The schematic diagram of PB-SiO <sub>2</sub> synthesis. .... 40
2. 6	The schematic diagram of HPB-SiO <sub>2</sub> synthesis..... 41
2. 7	The schematic diagram of PS-SiO <sub>2</sub> synthesis..... 43
2. 8	Appearance of SBR/PS-SiO <sub>2</sub> composite film..... 45
2. 9	Schematics of pervaporation equipment. .... 50
3. 1	FTIR spectrum of SBR nanoparticles..... 53
3. 2	<sup>1</sup> H-NMR spectrum of SBR nanoparticle in CDCl <sub>3</sub> ..... 53
3. 3	Effect of monomer to water ratio (M/H <sub>2</sub> O) on; (◆) %Conversion, (■) %Polymer content, (▲) Particle size. Condition: SDS = 5 wt%, KPS = 2 wt% based on monomer. .... 55
3. 4	Effect of surfactant concentration on; (a) (◆) %Conversion, (■) %Polymer content, (▲) Particle size and (b) characteristic of the latex. Condition: M/H <sub>2</sub> O = 0.2, KPS = 2 wt% based on monomer. .... 56
3. 5	Effect of initiator concentration on; (a) (◆) %Conversion, (■) %Polymer content, (▲) Particle size and (b) characteristic of the latex. Condition: M/H <sub>2</sub> O = 0.2, SDS = 3 wt% based on monomer..... 58
3. 6	TEM micrograph and particle size distribution of SBR nanoparticles. Condition: M/H <sub>2</sub> O = 0.3, SDS = 5 wt%, KPS = 2 wt% based on monomer. .... 59
4. 1	FTIR spectrum of (a) Modified SiO <sub>2</sub> and (b) SBR-SiO <sub>2</sub> . .... 62
4. 2	<sup>1</sup> H-NMR spectrum of SBR-SiO <sub>2</sub> in CDCl <sub>3</sub> . .... 62
4. 3	Effect of silica loading on; (◆) %Conversion, (■) %Si encapsulation eff, (▲) Particle size. Condition: M/H <sub>2</sub> O = 0.2, SDS = 5 wt%, KPS = 2 wt% based on monomer..... 64



Figure	Page
4. 4 Effect of (a) Silica encapsulated (b) Silica mixed with SBR on characteristic of the latex.....	64
4. 5 Effect of surfactant concentration on; (a) (◆) %Conversion, (■) %GE, (▲) Particle size. Condition and (b) characteristic of latex: SiO <sub>2</sub> = 10 wt%, M/H <sub>2</sub> O = 0.2, KPS = 2 wt% based on monomer. ....	66
4. 6 Effect of monomer to water ratio (M/H <sub>2</sub> O) on; (◆) %Conversion, (■) %GE, (▲) Particle size. Condition: SiO <sub>2</sub> = 10 wt%, SDS = 5 wt%, KPS = 2 wt% based on monomer. ....	67
4. 7 Effect of initiator concentration on; (◆) %Conversion, (■) %GE, (▲) Particle size. Condition: SiO <sub>2</sub> = 10 wt%, M/H <sub>2</sub> O = 0.2, SDS = 3 wt% based on monomer.....	68
4. 8 TEM imaging of composite samples (a) SBR-SiO <sub>2</sub> (1 wt% SDS), (b) SBR-SiO <sub>2</sub> (3 wt% SDS), (c) SBR-SiO <sub>2</sub> (10 wt% SDS) and (d) SBR/untreated SiO <sub>2</sub> (3 wt% SDS) at 10 wt% silica loading. Condition: SiO <sub>2</sub> = 10 wt%, M/H <sub>2</sub> O = 0.2, KPS = 2 wt% based on monomer.....	70
4. 9 A schematic of formation mechanism of SBR-SiO <sub>2</sub> core-shell nanoparticles... 71	
4. 10 Effect of SBR-SiO <sub>2</sub> loading (wt%) in membrane on; (a) total permeate fluxes (◆), partial water flux (■) and partial ethanol flux (▲) and (b) pervaporation selectivity at 5 vol% water concentration in feed.....	77
4. 11 Effect of water concentration (vol%) in feed on partial water and partial ethanol fluxes for NR/SBR-SiO <sub>2</sub> nanocomposite membranes with SBR-SiO <sub>2</sub> loading of 10 wt% (◆, ◇), 20 wt% (■, □), 30 wt% (▲, △) and 40 wt% (●, ○).....	78
5. 1 FTIR spectrum of (a) SiO <sub>2</sub> , Modified SiO <sub>2</sub> and (b) PB-SiO <sub>2</sub> , HPB-SiO <sub>2</sub> .....	81

Figure	Page
5. 2 Effect of silica loading on; (a) (◆) %Conversion, (■) %Si encapsulation eff, (▲) Particle size and (b) characteristics of the latex. Condition: M/H <sub>2</sub> O = 0.2, SDS = 5 wt%, KPS = 3 wt% based on monomer.....	83
5. 3 Effect of surfactant concentration on; (a) (◆) %Conversion, (■) %GE, (▲) Particle size and (b) characteristics of the latex. Condition: SiO <sub>2</sub> = 10 wt%, M/H <sub>2</sub> O = 0.2, KPS = 2 wt% based on monomer.....	84
5. 4 Effect of monomer to water ratio (M/H <sub>2</sub> O) on; (◆) %Conversion, (■) %GE, (▲) Particle size. Condition: SiO <sub>2</sub> = 10 wt%, SDS = 7 wt%, KPS = 2 wt% based on monomer. ....	86
5. 5 Effect of initiator concentration on; (◆) %Conversion, (■) %GE, (▲) Particle size. Condition: SiO <sub>2</sub> = 10 wt%, M/H <sub>2</sub> O = 0.2, SDS = 5 wt% based on monomer.....	87
5. 6 <sup>1</sup> H-NMR spectra of (a) PB-SiO <sub>2</sub> and (b) HPB-SiO <sub>2</sub> at 98.6 %HD. ....	89
5. 7 Hydrogenation of PB-SiO <sub>2</sub> ; (a) effect of [N <sub>2</sub> H <sub>4</sub> ] at [H <sub>2</sub> O <sub>2</sub> ] = 4 mol/L and (b) effect of [H <sub>2</sub> O <sub>2</sub> ] at [N <sub>2</sub> H <sub>4</sub> ] = 3 mol/L on hydrogenation degree (●) and particle size (▲). Condition: [H <sub>3</sub> BO <sub>3</sub> ] = 0.15 mol/L, [C=C] = 1 mol/L, T = 70 °C, time = 5 h.....	90
5. 8 TEM micrographs and particle size distribution of samples (a) PB-SiO <sub>2</sub> and (b) HPB-SiO <sub>2</sub> at 98.6 %HD. ....	92
5. 9 A schematic of formation mechanism of modified SiO <sub>2</sub> , PB-SiO <sub>2</sub> and HPB-SiO <sub>2</sub> nanoparticles.....	93
5. 10 TGA thermograms of (a) PB-SiO <sub>2</sub> (5 %SiO <sub>2</sub> ), (b) PB-SiO <sub>2</sub> (10 %SiO <sub>2</sub> ), (c) PB-SiO <sub>2</sub> (15 %SiO <sub>2</sub> ), (d) PB-SiO <sub>2</sub> (20 %SiO <sub>2</sub> ) and (e) HPB-SiO <sub>2</sub> (10 %SiO <sub>2</sub> , 98.6 %HD).....	94

Figure	Page
5. 11 Temperature dependence of (a) weight loss and (b) DTG for NR/HPB-SiO <sub>2</sub> composites.....	97
5. 12 Mechanical properties of NR, NR/PB-SiO <sub>2</sub> and NR/HPB-SiO <sub>2</sub> before and after aging: (a) tensile strength (MPa), (b) modulus at 300% strain (MPa) and (c) elongation at break (%)......	101
5. 13 Surface of NR/PB-SiO <sub>2</sub> and NR/HPB-SiO <sub>2</sub> composites after ozone exposure for 72 h; (a) NR, (b) NR/PB-SiO <sub>2</sub> (90:10), (c) NR/PB-SiO <sub>2</sub> (80:20), (d) NR/PB-SiO <sub>2</sub> (70:30), (e) NR/HPB-SiO <sub>2</sub> (90:10), (f) NR/HPB-SiO <sub>2</sub> (80:20), (g) NR/HPB-SiO <sub>2</sub> (70:30). .....	105
6. 1 FTIR spectrum of (a) Modified SiO <sub>2</sub> and (b) PS-SiO <sub>2</sub> .....	108
6. 2 Effect of silica loading on; (a) (◆) %Conversion, (■) %Si encapsulation eff, (▲) Particle size and (b) characteristics of the latex. Condition: M/H <sub>2</sub> O = 0.3, SDS = 3 wt%, KPS = 2 wt% based on monomer.....	109
6. 3 Effect of surfactant concentration on; (a) (◆) %Conversion, (■) %GE, (▲) Particle size and (b) characteristics of the latex. Condition: SiO <sub>2</sub> = 10 wt%, M/H <sub>2</sub> O = 0.3, KPS = 2 wt% based on monomer.....	111
6. 4 TEM imaging of PS-SiO <sub>2</sub> nanocomposite samples (a) 1 wt% SDS, (b) 3 wt% SDS and (c) 10 wt% SDS at 10 wt% silica loading. Condition: SiO <sub>2</sub> = 10 wt%, M/H <sub>2</sub> O = 0.3, KPS = 2 wt% based on monomer.....	112
6. 5 TGA thermograms of (a) Pure PS, (b) PS-SiO <sub>2</sub> (5 %SiO <sub>2</sub> ), (c) PS-SiO <sub>2</sub> (7.5 %SiO <sub>2</sub> ), (d) PS-SiO <sub>2</sub> (10 %SiO <sub>2</sub> ), (e) PS-SiO <sub>2</sub> (15 %SiO <sub>2</sub> ) and (f) PS-SiO <sub>2</sub> (20 %SiO <sub>2</sub> )......	113
6. 6 DSC thermograms of (a) SBR, (b) SBR/PS-SiO <sub>2</sub> (90:10) and (c) SBR/PS-SiO <sub>2</sub> (80:20)......	115

Figure	Page
6. 7 SEM micrographs (15000x) of (a) SBR, (b) SBR/PS-SiO <sub>2</sub> (90:10) and (c) SBR/PS-SiO <sub>2</sub> (80:20).....	118
G-1 <sup>1</sup> H-NMR spectra of HPB-SiO <sub>2</sub> at 98.6 %HD.....	146



## LIST OF ABBREVIATIONS

ASTM	: American Society for Testing and Materials
BD	: 1,3 Butadiene
DLS	: Dynamic Light Scattering Technique
DMP	: Differential Microemulsion Polymerization
$D_n$	: Number Average Diameter
DRC	: Dry Rubber Content
EPM	: Ethylene-Propylene Rubber
EPDM	: Ethylene-Propylene Diene Monomer
DRC	: Dry Rubber Content
DSC	: Differential Scanning Calorimetry
FTIR	: Fourier Transform Infrared Spectroscopy
GE	: Grafting Efficiency
HD	: Hydrogenation Degree
HPB	: Hydrogenated Polybutadiene
ISO	: International Standardization for Organization
KPS	: Potassium Persulfate
NBR	: Acrylonitrile-Butadiene Rubber
NMR	: Nuclear Magnetic Resonance Spectroscopy
NR	: Natural Rubber
$OsO_4$	: Osmium Tetroxide
PB	: Polybutadiene
SBR	: Styrene Butadiene Rubber
SDS	: Sodium Dodecyl Sulfate
ST	: Styrene
TEM	: Transmission Electron Microscope
$T_g$	: Glass Transition Temperature
TGA	: Thermogravimetric Analysis

$T_{id}$	: Initial Decomposition Temperature
$T_{max}$	: Maximum Decomposition Temperature
VTS	: Vinyl Trimethoxy Silane
ZDEC	: Zincediethyl Dithiocarbamate
ZnO	: Zinc Oxide



## CHAPTER I

### INTRODUCTION

#### 1.1 Motivation

Polymer nanocomposite materials (polymer/filler) have increasing potential for future applications due to the advantageous properties of the organic polymer species such as elasticity, processibility with inorganic fillers providing high thermal stability and reinforcement. One of the most common inorganic systems is nanosilica that has many functional properties and effective reinforcement. Therefore, polymer/silica nanocomposites have attracted substantial academic and industrial interest and have been employed in a variety of applications. However, the difficulties as an access to well dispersed silica in polymer matrix are due to the large quantity of hydroxyl groups on the surface of the nanosilica and the high surface energy and polarity, resulting in inferior compatibility and less stability between the polymer matrix and nanosilica; thus severe agglomeration and weak polymer-filler interaction occurs. Therefore, the severe agglomeration of nanosilica in a polymer matrix cannot be broken down with high speed shearing or milling via mechanical mixing methods because the electrostatic forces holding the particles together are stronger than the shear force created by the velocity gradient. The great advantage provided by nanosilica can only be achieved if the particles are finely dispersed in the polymer matrix.

Thus, differential microemulsion polymerization (DMP) was developed to provide a “new green process technology” for synthesis of polymer/silica hybrid particles and to achieve the effective compatibility and uniform dispersion of nanosilica particles in the polymer matrix and good colloidal stability. Using DMP becomes more attractive because water as the media is non-toxic, non-flammable, inexpensive, and is an environmentally friendly solvent. Moreover, it is desirable to reduce the surfactant concentration under mild reaction conditions. So, DMP could be an alternative route in this area for realization of a green commercial process for synthesis of polymer nanocomposite materials.

## 1.2 Microemulsion Polymerization

Polymerization in a microemulsion is a new polymerization technique which allows the preparation of ultrafine latex particles with narrow particle size distribution, high molecular weight polymer products and special dispersion with high solid-content and provides alternative opportunities for producing polymer nanoparticles and polymer nanocomposites [1-3]. Microemulsion polymerization was first proposed and developed by Stoffer et al. in the early 1980s [4]. Many investigations have been carried out in recent years, and both microemulsion (O/W, oil in water) and inverse microemulsion (W/O, water in oil) polymerization could be used to synthesize nanosized polymer particles. The particles produced in this system were very small ranging from 10 to 100 nm. Microemulsions are thermodynamically stable, isotropic, and optically transparent dispersions of two immiscible liquids, oil and water, obtained in the presence of a surfactant system. A spherical oil-in-water or water-in-oil, microemulsion consists of small microdroplets surrounded by a surfactant monolayer as shown in Figure 1.1. The small size of the droplets is commonly used as a criterion for the preparation of the microemulsion [5]. The thermodynamic stability of microemulsions results from the very low interfacial tension of the small droplets. Thus, the formation of the microemulsion is a spontaneous process. However, a large amount of surfactant (about 10–15% based on monomer weight) is needed for achieving thermodynamic stability of the microemulsion. Microemulsions have been successfully used in a variety of chemical reactions because they provide effective qualities of thermodynamic stability, optical transparency, very large interfacial area and very low interfacial tension, and solubilization of substrates [6]. A variety of polymeric materials have been obtained by microemulsion polymerization.

The mechanism of microemulsion polymerization is similar to emulsion polymerization with a large amount of surfactant. Candau, F. [7, 8] reported that the mechanism of o/w microemulsion polymerization is now well accepted. The polymerization mechanism in oil-in-water microemulsions is shown in Figure 1.2. It can be explained in that in the first step, the polymerization is initiated by the entry of radicals into the droplets (water soluble initiator) or by radicals generated within the



oil droplets (oil-soluble initiator). In the second step (Figure 1.2c and d), nucleated particles grow by diffusion of monomer from inactive droplets through the continuous phase or by collision-coalescence with neighboring droplets. Since the particles are usually larger than the starting droplets, new micelles are formed. At the end of the polymerization, particles are accompanied by empty small surfactant micelles.

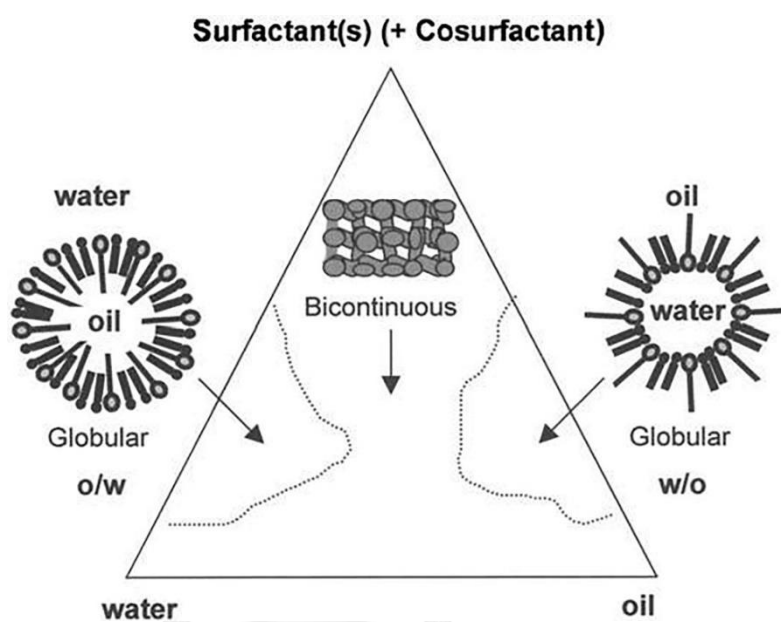
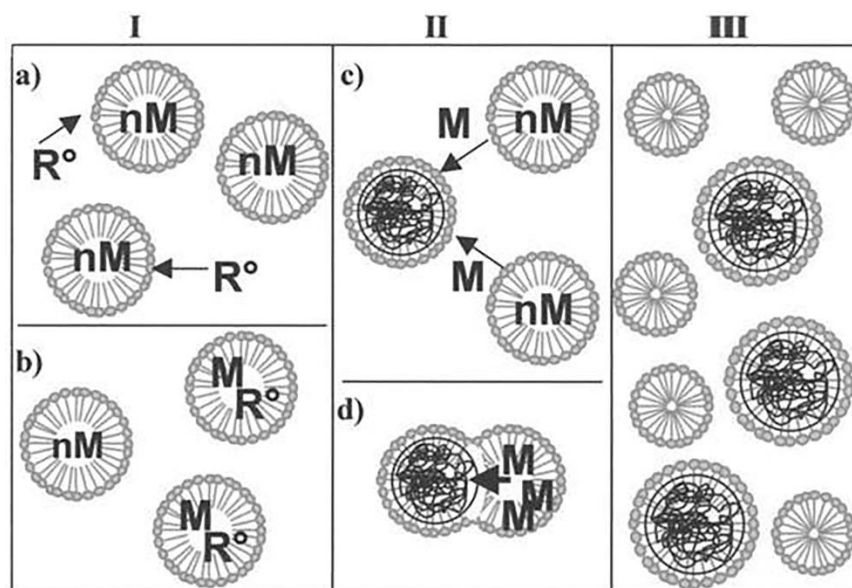


Figure 1. 1 Isotropic microemulsion domains in the phase diagram of multicompartments systems [5].



**Figure 1. 2** Schematic polymerization mechanism in oil-in-water microemulsions. (I) Microdroplets are initiated by free radicals (a) with water-soluble initiator or (b) oil-soluble initiator. (II) Particle growth (c) by monomer diffusion through the continuous phase and (d) by collision between droplets (nonionic surfactant). (III) End of polymerization: polymer particles and empty micelles [7, 8].

Gan et al. [9] investigated the synthesis of polystyrene via microemulsion polymerization. Water-soluble KPS as initiator, cetyltrimethyl ammonium bromide (CTAB) as surfactant and a glycol type cosurfactant were used in this system. This system could produce a small particle of diameter ( $D_n$  20-40 nm) and a high molecular weight ( $\bar{M}_w = 5-10 \times 10^6$ ).

Roy and Devi [10] studied the preparation of poly(methyl methacrylate) (PMMA) via o/w microemulsion polymerization using sodium dodecyl sulphate (SDS) as surfactant and potassium persulphate (KPS) as water-soluble initiator. The average particle size of PMMA latex formed was found to be 45 nm. Moreover, the high molecular weight ( $\bar{M}_w = 8.03 \times 10^5$ ) and low polydispersity were achieved due to

predominance of nucleation in monomer droplets in the microemulsion polymerization.

Larpernt et al. [11] reported the synthesis of polystyrene (PS) by o/w microemulsion polymerization using SDS as surfactant and hydroxyalkyl acrylates or methacrylates as cosurfactants. The stable suspensions of well-defined highly functionalized nanoparticles (15 – 25 nm) were achieved whereas the monomer conversion increased to 100% at room temperature. However, the monomer content was extremely low and usually lower than the surfactant concentration used.

However, in a microemulsion polymerization system, the surfactant used was high, sometimes even higher than the amount of monomer. Low surfactant concentration and high polymer content are desirable for industrial applications. This is a drawback that considerably limits the potential uses of microemulsion polymerization and has hampered the process from being scaled up to an industrial level due to the high cost of surfactant and post-treatment for removing the surfactant after polymerization. The surfactants are not only expensive but also have significantly negative impact on the physical properties of polymers. It can be seen that microemulsion polymerization presents lots of challenges, such as how to decrease surfactant concentration, how to increase monomer content and how to improve the purity of the final products. Therefore, possible and effective techniques for microemulsion polymerization are in great demand, and many methods have been tried out, for example, taking advantages of high efficiency surfactants and conducting seed microemulsion polymerization. Meanwhile, differential microemulsion polymerization may be another new and potential one.

Differential microemulsion polymerization (DMP) was proposed in a reaction system similar to emulsion polymerization. It is composed of water, surfactant, a water insoluble monomer (e.g., styrene, ST), and a water-soluble initiator (e.g., ammonium persulfate, APS) and requires a certain temperature to initiate the polymerization and suitable agitation to form an emulsion. The monomer feed is provided continuously as very small droplets and slowly added to the polymerization system under mild agitation. This method could be used to make similar particles as in traditional

microemulsion polymerization. However, DMP requires a much smaller amount of surfactant.

He et al. [12] reported the synthesis of PMMA nanosized particles by differential microemulsion polymerization using APS as initiator and SDS as surfactant. The amount of surfactant has a great influence on the particle size and polymer content. Moreover, PMMA particles of less than 20 nm can be obtained at an extremely low surfactant concentration of 5.5% based on monomer weight, which is difficult to be realized by conventional methods. The physical model proposed for differential microemulsion polymerization of PMMA is illustrated in Figure. 1.3 [13]. In the reaction system for the differential microemulsion polymerization, once the reaction is initiated, there are initiators, radicals (primary radicals, monomer radicals, and polymer radicals), as well as a very small amount of monomer and micelles in the water phase. The initiator decomposes in the water phase to generate primary radicals. Some of the primary radicals could attack monomers to produce polymer radicals. These polymer radicals propagate in the water phase leading to a critical chain length and precipitate to form polymer particles (homogeneous nucleation) or enter into monomer-swollen micelles to generate polymer particles (heterogeneous nucleation). The radicals in the water phase could also be terminated by combination or disproportion or be captured by either active (polymer particles having free radicals in them) or dead polymer particles.

Yuan et al. [14] studied the synthesis of PMMA nanoparticles via differential microemulsion polymerization using APS as initiator and SDS as surfactant. This method is suitable for obtaining PMMA with a particle size of less than 20 nm by using a very low amount of surfactant of 3 wt% based on monomer weight. Moreover, high monomer conversion of 95% and high molecular weight of  $1.3 \times 10^5$  were obtained.

Differential microemulsion polymerization has many advantages for the synthesis of nanosized polymer latex particles with high monomer conversion and high polymer content by using an extremely low surfactant concentration. Additionally, DMP is an environmental friendly process which is suitable for a green commercial industry due to the absence of organic solvents under mild reaction conditions.

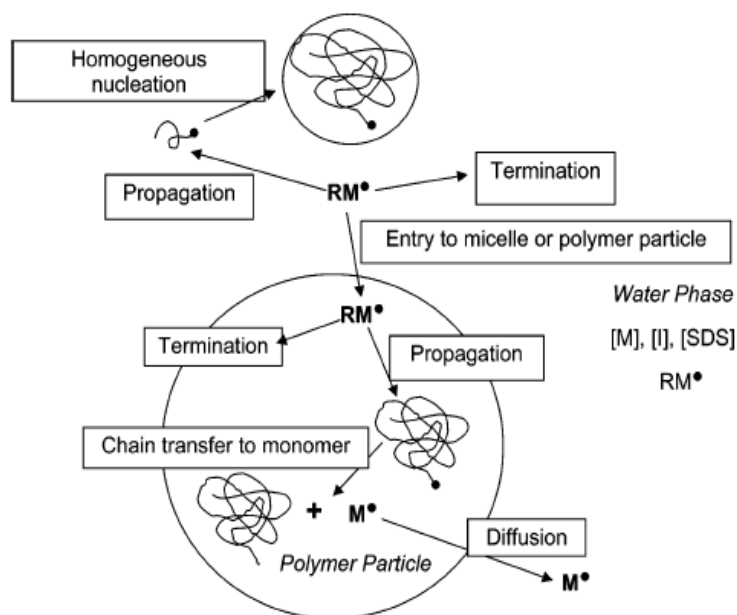


**Figure 1. 3** Proposed mechanism: differential microemulsion polymerization of MMA [13].

### 1.3 Silica Surface Modification

One of the most common fillers is nanosilica which has many functional properties. It has been widely used in colloidal products, paints, catalysis and chromatographic separations since silica is chemically inert and optically transparent [15]. Moreover, nanosilica has a noticeable reinforcing effect due to its high surface area which leads to a dramatic increase in the interfacial area in the polymer matrix. However, the hydroxyl group ( $-OH$ ) on the silica surface absorbs moisture, and has the highest polarity. Thus, the difficulties in obtaining a well dispersed silica in rubber matrix are due to the large quantity of hydroxyl groups on the surface of the nanosilica and the high surface energy and polarity, resulting in inferior compatibility and less stability between the polymer matrix and nanosilica; thus severe agglomeration and weak rubber-filler interactions occurred. The applications of nanosilica are quite limited.

Silica particles with a hydrophilic surface easily adhere to each other through hydrogen bonding and form irregular agglomerates. This hydrophilic surface does not

process good compatibility with the polymer. Therefore, mechanical mixing/dispersion methods such as high speed shearing or milling are not effective to break down the agglomeration because the electrostatic forces holding the particles together are stronger than the shear force created by the velocity gradient [16]. The great advantage provided by nanosilica can only be achieved if the particles are finely dispersed in the polymer matrix. This problem could be resolved by a surface modification method of silica nanoparticles.

In general, surface modification of nanosilica can be carried out by either chemical or physical methods. For physical methods, electrostatic interactions and other types of Van der Waals interactions are the main driving forces in preliminary silica surface modification. The procedure usually involves surfactants or macromolecules adsorbed onto its surface. In principle, a polar group of surfactants is adsorbed to the surface of silica by an electrostatic interaction. As a consequence, the physical attraction between the silica particles within the agglomerates is reduced, making it easy for the silica particles to become incorporated into the polymer matrix [17, 18]. For example, silica was treated with the cationic surfactant cetyltrimethylammonium bromide (CTAB) to improve the interaction between  $\text{SiO}_2$  and the polymer [19] or  $\text{SiO}_2$  nanoparticles were modified with stearic acid to improve their dispersion and the adhesion between the filler and polymer matrix [20]. However, both of these types of interaction are physical in nature which tends to be weak compared to chemical reactions.

Therefore, chemical treatment of the nanoparticle surface is necessary to achieve better compatibility and dispersion of the filler in the polymer latex. Chemical methods involve modification either with modifying agents or by grafting polymers. Silane coupling agents are often used to treat the silica surface due to their unique bifunctional structure. They generally have hydrolyzable ends, which are capable of reacting with the silanol groups on the silica surface through hydrolysis and polycondensation to form siloxane linkages (Si-O-Si bonds), and an organofunctional end, which has the ability to initiate the desired chemical reactions [21]. The general structure of the coupling agents can be represented as  $\text{RSiX}_3$  [22], where the X represents the hydrolyzable groups, which are typically chloro, ethoxy, or methoxy

groups. The organofunctional, R, group can have a variety of functionalities depending on the requirements of the polymer. The functional group X reacts with hydroxyl groups on the SiO<sub>2</sub> surface, while the alkyl chain may react with the polymer. Hydrophobic silica can thus be obtained. Some typical silane coupling agents used for surface modification of nanosilica are presented in Table 1.1.

**Table 1. 1** Typical silane coupling agents used for surface modification of silica nanoparticles [22].

name	chemical structure
aminopropyl methyldiethoxysilane	$\text{H}_2\text{N}(\text{CH}_2)_3(\text{CH}_3)\text{Si}(\text{OC}_2\text{H}_5)_2$
(3-acryloxypropyl)methyldimethoxysilane	$\text{CH}_2=\text{CHCOO}(\text{CH}_2)_3(\text{CH}_3)\text{Si}(\text{OCH}_3)_2$
3-aminopropyltriethoxysilane	$\text{H}_2\text{N}(\text{CH}_2)_3\text{Si}(\text{OC}_2\text{H}_5)_3$
3-aminopropyltrimethoxysilane	$\text{H}_2\text{N}(\text{CH}_2)_3\text{Si}(\text{OCH}_3)_3$
(3-acryloxypropyl)trimethoxysilane	$\text{CH}_2=\text{CHCOO}(\text{CH}_2)_3\text{Si}(\text{OCH}_3)_3$
aminophenyltrimethoxysilane	$\text{H}_2\text{NPhSi}(\text{OCH}_3)_3$
bis(triethoxysilylpropyl)tetrasulfane	$(\text{C}_2\text{H}_5\text{O})_3\text{Si}(\text{CH}_2)_3\text{S}_4(\text{CH}_2)_3\text{Si}(\text{OC}_2\text{H}_5)_3$
dimethyldichlorosilane	$(\text{CH}_3)_2\text{SiCl}_2$
3-glycidoxypropyltrimethoxysilane, 3-glycidyloxypropyltrimethoxysilane	$\text{CH}_2(\text{O})\text{CHCH}_2\text{O}(\text{CH}_2)_3\text{Si}(\text{OCH}_3)_3$
3-isocyanatopropyltriethoxysilane	$\text{OCN}(\text{CH}_2)_3\text{Si}(\text{OC}_2\text{H}_5)_3$
methacryloxymethyltriethoxysilane	$\text{CH}_2=\text{C}(\text{CH}_3)\text{COOCH}_2\text{Si}(\text{OC}_2\text{H}_5)_3$
methacrylic acid 3-(trimethoxysilyl) propyl ester, 3-(trimethoxysilyl)propyl methacrylate, 3-methacryloxypropyltrimethoxysilane	$\text{CH}_2=\text{C}(\text{CH}_3)\text{COO}(\text{CH}_2)_3\text{Si}(\text{OCH}_3)_3$
methacryloxypropyltriethoxysilane	$\text{CH}_2=\text{C}(\text{CH}_3)\text{COO}(\text{CH}_2)_3\text{Si}(\text{OC}_2\text{H}_5)_3$
mercaptopropyl triethoxysilane	$\text{SH}(\text{CH}_2)_3\text{Si}(\text{OC}_2\text{H}_5)_3$
methyltriethoxysilane	$\text{CH}_3\text{Si}(\text{OC}_2\text{H}_5)_3$
phenyltrimethoxysilane	$\text{PhSi}(\text{OCH}_3)_3$
vinyltriethoxysilane	$\text{CH}_2=\text{CHSi}(\text{OC}_2\text{H}_5)_3$
vinyltrimethoxysilane	$\text{CH}_2=\text{CHSi}(\text{OCH}_3)_3$

Alkyl silane coupling agent are mainly used in chemical surface modification to obtain a hydrophobic surface [23, 24]. Haldorai et al. [25] reported that silica nanoparticles can be surface modified by methacryloxypropyl trimethoxysilane (MPTMS) which is capable of copolymerizing with styrene and provides a reactive C=C bond. Additionally, Lin et al. [26] revealed that 3-glycidoxypropyl trimethoxysilane was successfully grafted onto the surface of silica particles. The mechanism of silane treatment is described in many papers, and there are three models of grafting (grafting and polycondensation) as shown in Figure 1.4 [27]. For the first model, the first

molecule of silane is grafted onto the surface of inorganic particles, and others are condensed on the one that has been grafted. The second model, which is geometrically impossible, assumes that the silane forms three siloxane bonds. The last and more realistic one involves the grafting reaction of the silane and condensation. The ideal result of silica surface treatment is to break down silica nanoparticle agglomerates, to produce nanostructural composites and to achieve the homogeneity of the nano-size silica in the polymer matrix.

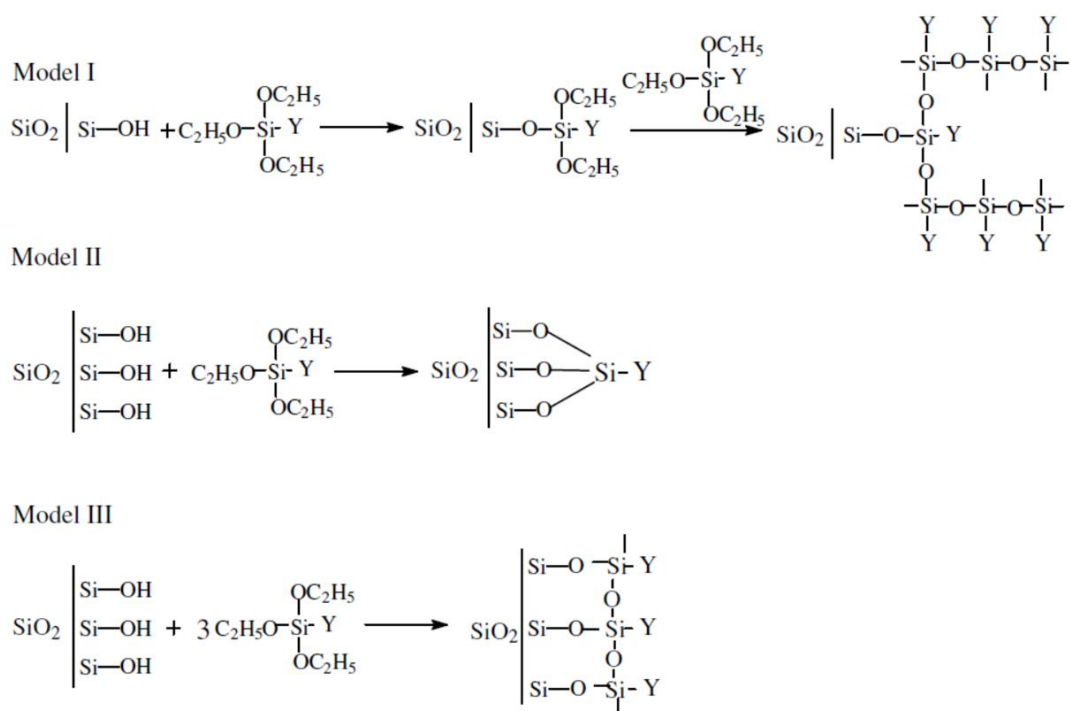


**Figure 1. 4** Grafting and polycondensation mechanism of silane on silica particles, with Y is the organic functional group [27].

#### 1.4 Polymer-Silica Nanocomposites

Organic/inorganic materials are called nanocomposites, when inorganic phases become nanosized. Organic/inorganic nanocomposites are generally organic polymer composites with inorganic nanoscale building blocks. They combine the advantages of the inorganic material (e.g., rigidity, thermal stability) and the organic polymer (e.g., flexibility, dielectric, ductility, and processability). Moreover, they usually contain



special properties of nanofillers leading to materials with improved properties. The small size of the fillers leads to a dramatic increase in interfacial area as compared with traditional composites. This interfacial area creates a significant volume fraction of interfacial polymer with properties different from the bulk polymer even at low loadings [28-30]. Inorganic nanoscale, silica is viewed as being very important. Therefore, polymer/silica nanocomposites have attracted substantial academic and industrial interest. They have received much attention in recent years and have been employed in a variety of applications.

The traditional and simplest method of preparing polymer/silica composites is direct mixing of the silica into the polymer. The mixing can generally be done by melt blending and solution blending. The main difficulty in the mixing process is always the effective dispersion of the silica nanoparticles in the polymer matrix, because they usually tend to agglomerate. Melt blending is most commonly used because of its efficiency, operability, and environmental containment. However, making a homogeneous dispersion of nanoparticles in a polymeric matrix is a very difficult task due to the strong tendency of nanoparticles to agglomerate. Therefore, nanoparticle filled polymers sometimes contain a number of loosened clusters of particles as shown in Figure 1.5 and exhibit properties even worse than conventional particle/polymer systems [31]. Pérez et al. [32] reported that the addition of silica into styrene-butadiene rubber (SBR) by melt blending to prepare SBR/silica nanocomposites resulted in increasing the glass transition temperature ( $T_g$ ) and thermal resistance while the modulus and tensile strength slightly increased due to the adhesion of the filler in the rubber nanocomposites. The polymer and polymer blend like polypropylene (PP) [33, 34], polyethylene (PE) [35, 36] and polystyrene (PS) [37] filled with nanosilica have also been reported. Solution blending, is a liquid-state powder processing method that provides a good molecular level of mixing and is widely used in material preparation and processing. Some of the limitations of melt mixing can be overcome when both the polymer and the nanoparticles are well dissolved or dispersed in solution. However, a high amount of solvent and a high cost depending on the solvent and its recovery are required. Many polymers exhibit good mixing with silica using this method [38, 39].

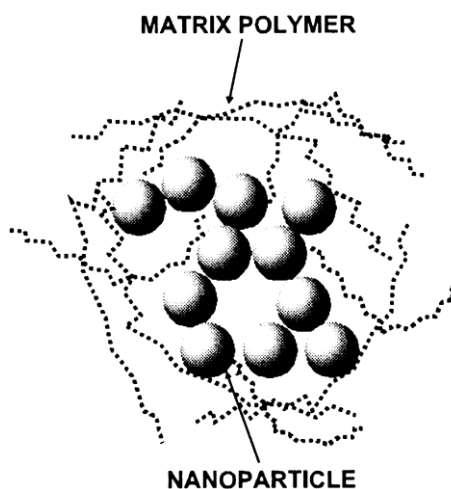


**Figure 1. 5** Agglomerated nanoparticles dispersed in a polymer matrix [31].

The preparation of polymer/silica nanocomposites by direct mixing leads to physisorption, which is a relatively weak interaction and it is sensitive to temperature and chemical reagents resulting in easy desorption. Thus, many chemical methods have been applied to produce polymer/silica nanocomposites providing strong covalent bonds with functional groups. Grafting of polymer chains onto silica nanoparticles is one of the effective methods to increase the hydrophobicity of the particles and to improve interfacial interactions in nanocomposites resulting in better compatibility and dispersion of silica particles in the polymer matrix. It was found that modification of nanoparticles through graft polymerization was very effective to prepare nanocomposites because of an increase in hydrophobicity of the nanoparticles that is beneficial to the filler/matrix miscibility, and an improved interfacial interaction yielded by the molecular entanglement between the grafting polymer on the nanoparticles and the matrix polymer [40, 41]. The dispersion of the modified nanoparticles by polymer grafting and main polymer matrix is shown in Figure 1.6 [31]. Grafting polymer on the silica surface by polymerization is characterized by many advantages, such as simple, low cost, easy to be controlled and broader applicability. According to Lee et al. [42], polystyrene/silica composite particles have been successfully synthesized via soap-free emulsion polymerization initiated with conventional anionic KPS through radical chain polymerization. The incorporation of

silica particles provided an enhancement in the thermal stability due to the strong interaction between silica and the polystyrene molecules.

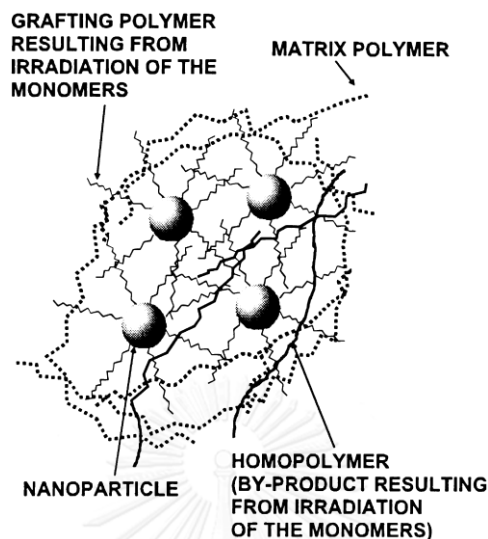


**Figure 1. 6** The possible structure of grafted nanoparticles dispersed in a polymer matrix [31].

Much research has been reported on the preparation of polymer/silica nanocomposites by using dispersion polymerization [43-47], suspension-dispersion polymerization [48-50] and emulsion polymerization [51-58]. Zhu et al. [48] investigated the preparation of core-shell poly(methyl methacrylate) (PMMA)-SiO<sub>2</sub> nanoparticles by suspension dispersion polymerization (SDP) in an aqueous system. The core-shell nanoparticles were subsequently used as filler in a poly(vinyl chloride) (PVC) matrix. It was found that PMMA covering the surface of SiO<sub>2</sub> nanoparticles improved the dispersion of nanosilica dispersion in a PVC matrix and enhanced the interfacial adhesion between SiO<sub>2</sub> and the PVC matrix. Moreover, the PVC composites exhibited increased tensile strength, elongation at break and heat resistance. Haldorai et al. [25] reported the preparation of silica/polystyrene core-shell composite nanospheres using radical dispersion polymerization in a hydrophobic ionic liquid with poly(vinylpyrrolidone) as stabilizer. Silica nanoparticles were first surface modified by the silane coupling agent methacryloxypropyltrimethoxysilane (MPTMS), which is

capable of copolymerizing with styrene and provided a reactive C=C bond. Silica/polystyrene core-shell morphology with an average particle size of around 250 nm was obtained.

Emulsion polymerization is frequently and effectively used to synthesize inorganic/polymer hybrid particles. Espiard et al. [56-58] reported the encapsulation of silica particles through emulsion polymerization using 3-(trimethoxysilyl)propyl methacrylate (MPS) as coupling agent. The silane molecule allowed the grafting of a significant amount of polymer from the early stages of polymerization; thus MPS provided reactive double bonds for covalent attachment of the growing polymer chains on the silica surface. Ding et al. [59] studied the synthesis of monodisperse polystyrene/SiO<sub>2</sub> composite particles (PSCP) with a core-shell structure via in situ emulsion polymerization of styrene (ST) on the surface of silica nanoparticles modified with oleic acid. The C=C bonds of oleic acid were covalently attached to the silanol groups at the surface of nanosized silica to induce coating. The average diameters of the core-shell particles were in the range of 150 –180 nm. Mahdavian et al. [60] reported the preparation of poly(ST-MMA)/SiO<sub>2</sub> via emulsion polymerization. Nano-SiO<sub>2</sub> was modified with oleic acid and composite particles in the range of 90-200 nm with a high silica encapsulation efficiency of 87.2% were obtained. Emulsion polymerization can control the reaction rate, particle size and morphology effectively.

Recently, emulsion polymerization has been developed to obtain smaller size diameter particles by using miniemulsion [61-65] or microemulsion [66, 67] polymerization. Tiarks et al. [68] studied the synthesis of polymer/silica nanocomposites by using miniemulsion polymerization. Polymer emulsions made with a variety of monomers, including St, BA, and MAA were generated by the miniemulsion process in the presence of a coupling comonomer, a hydrophobe, and silica nanoparticles. The overall size of the particles was in the range of 100 nm at a surfactant level of 15 wt% based on monomer weight. The polymer/silica structures as “raspberry” hybrids where whole clusters of silica nanoparticles are completely embedded in the polymer particle could be made. Qi et al. [69] investigated acrylate polymer/silica nanocomposite particles that were prepared through miniemulsion polymerization. The encapsulation efficiency of silica was greater than 95%, the degree

of grafting of acrylate polymer onto silica was about 60%, and the particle size was smaller than 100 nm when a surfactant level of 20 wt% based on the monomer weight was used. The miniemulsion is a relatively stable oil-in-water dispersion, which is typically obtained by shearing a system containing monomer, water, surfactant and a costabilizer. Xu et al. [67] reported that the PMMA/SiO<sub>2</sub> nanocomposite particles could be prepared through microemulsion polymerization by using silica particles coated with 3-(trimethoxysilyl) propyl-methacrylate (MSMA). This technique could produce particles with a diameter smaller than 100 nm, however the surfactant amount used was about 40 wt% based on the monomer weight.

However, both microemulsion and miniemulsion polymerization required a high amount of surfactant. The surfactants are not only expensive but also have a significant negative impact on the physical properties of the polymers. Moreover, the concentration of such surfactant molecules in solution needs to be tuned carefully because latex formation in the free micelles in the emulsion can be observed at higher concentrations of surfactant (above critical micelle concentration, CMC). These molecules are usually only weakly bonded to the surface and can therefore desorb easily [70]. Differential microemulsion polymerization was developed because it is desirable to reduce the surfactant concentration under mild reaction conditions and also to yield nanosized particles with high conversion. Chuayjuljit et al. [71] reported the preparation of nanolatex of polystyrene-encapsulated silica via in situ differential microemulsion polymerization. Hybrid nanoparticles with core-shell morphology with an average diameter of 40 nm were subsequently used as filler for the natural rubber nanocomposite. PS-encapsulated nanosilica apparently improved the tensile strength, modulus at 300% strain and flammability of the NR. Kongsinlark et al. [72] studied the synthesis of monodispersed polyisoprene-silica nanoparticles via differential microemulsion polymerization and PIP-SiO<sub>2</sub> nanoparticles of 20–60 nm were produced with a narrow size distribution resulting in a reduced nano-SiO<sub>2</sub> aggregation in the PIP matrix. The surfactant concentration used was around 3% based on monomer weight. The monomer conversion was 87% and the polymer grafting efficiency was as high as 78%. The proposed formation mechanism of nanosize-SiO<sub>2</sub> encapsulated by nanosized PIP with core/shell morphology is illustrated in Figure 1.7.

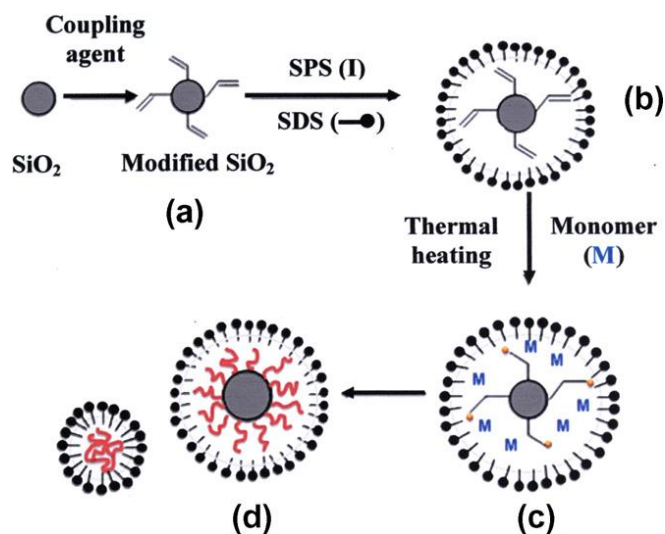


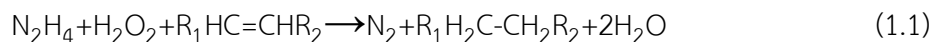
**Figure 1. 7** The proposed formation mechanism of nanosize- $\text{SiO}_2$  encapsulated by nanosized PIP with core/shell morphology [72].

### 1.5 Hydrogenation of Diene Rubber

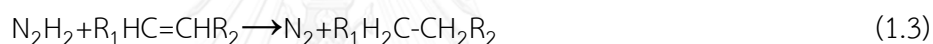
Hydrogenation is one important method of chemical modification, which improves the physical, chemical and thermal properties of diene-based elastomers. Rubbers such as polybutadiene (PB) and polyisoprene (PIP) suffer from a drawback in their thermal and ozone stability due to the  $\text{C}=\text{C}$  in their polymer backbones. The  $\text{C}=\text{C}$  of the rubber are sensitive to oxygen, ozone and heat resulting in rubber degradation and the reduction of mechanical and thermal properties. Hydrogenation of diene-based rubbers is a very useful process to obtain hydrogenated rubber and improve its thermal properties and oxidative stability while maintaining its elastomeric properties [73].

The diimide hydrogenation method as a potential alternative of the conventional hydrogenation technology in which high pressure gaseous hydrogen, organic solvents, and expensive transition-metal catalysts are not necessary, has received increasing attention in the area of the hydrogenation of rubbers in latex form [74-82]. The reaction between hydrogen peroxide and hydrazine is favorable to

hydrogenate rubber in latex form. The overall diimide hydrogenation of unsaturated polymer latex is presented in Eq. 1.1.



The reactants involved in this reaction system include hydrazine, hydrogen peroxide, and an unsaturated polymer. Boric acid is sometimes used as a promoter. The reaction of diimide hydrogenation can be divided into two steps in accordance with Eq. (1.2) the reaction between hydrazine and hydrogen peroxide to produce the diimide molecules and Eq. (1.3) the reaction between diimide and carbon-carbon double bonds to form the hydrogenated polymer.



However, according to the reactivity of diimide, two side reaction possibly occur. One is diimide decomposition as presented in Eq. 1.4 that is the reaction of diimide with hydrogenperoxide to generate nitrogen gas, which most likely occurs at the interface. The other side reaction is diimide disproportionation as shown in Eq. 1.5 being the reaction between two diimide molecules to produce hydrazine and to release nitrogen gas, which most likely occurs in the rubber phase.



The reaction of Eq. 1.2 may occur at the interface of the rubber particles and also in the bulk aqueous phase. Diimide generated in the aqueous phase would not be available for the hydrogenation reaction in the organic phase. Thus, this competition affects the efficiency of the diimide utilization in the aqueous phase. Diimide may get consumed by way of Eq. 1.4 either at the interface or in the aqueous phase before it

can diffuse into the rubber particles. Moreover, the radical source for gel formation and the crosslinking process is observed according to Eq. 1.5 [74, 78, 80].

Parker et al. [75] studied the hydrogenation by diimide reduction to prepare a highly saturated nitrile butadiene rubber (NBR) latex. The diimide hydrogenating agent was generated by the  $\text{N}_2\text{H}_4$  and  $\text{H}_2\text{O}_2$  system at the surface of the polymer particles. Carboxylated surfactants, which were adsorbed at the latex particle surface, played an important role by forming hydrazinium carboxylates with hydrazine and copper ions. The generated  $\text{N}_2\text{H}_2$  intermediates were stabilized by copper ions ( $\text{Cu}^{2+}$ ) to effectively reduce the carbon-carbon double bonds. The mechanism for diimide hydrogenation of nitrile rubber catalyzed by cupric ions is proposed in Figure 1.8.

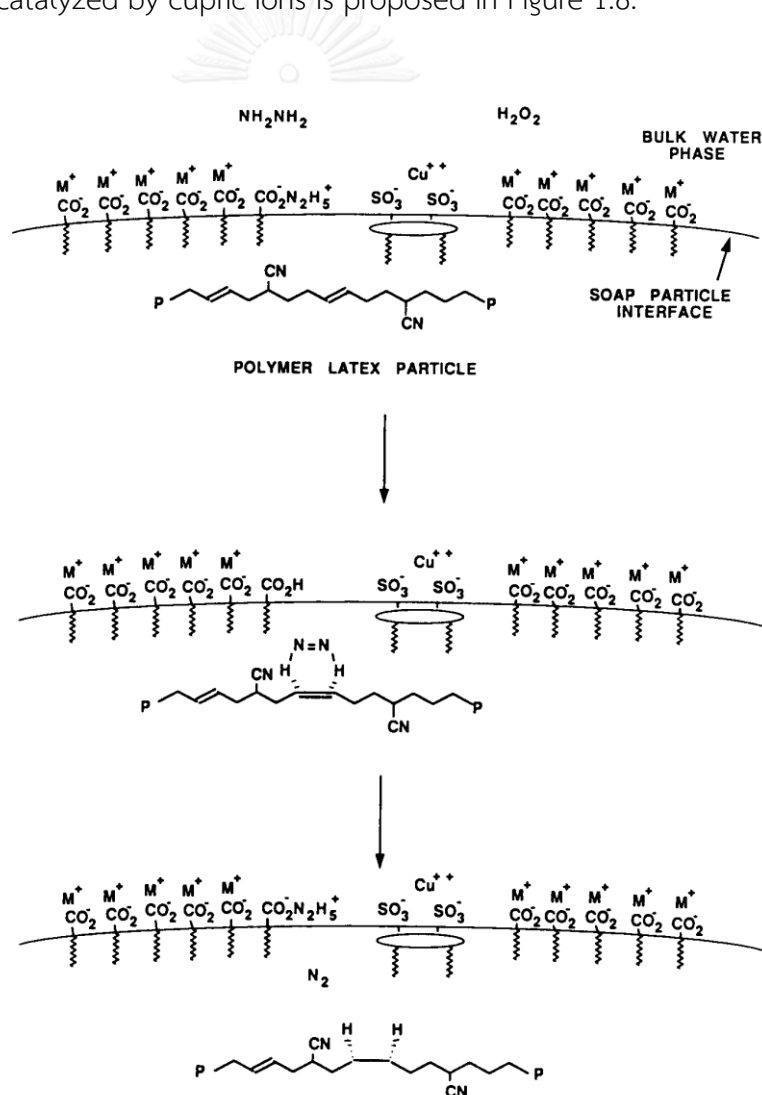


Figure 1. 8 Proposed diimide latex reduction mechanism [75].



He et al. [76] studied the diimide hydrogenation of styrene-butadiene rubber (SBR) latex. It was observed that the hydrogenation of carbon-carbon double bonds depended on the latex particle size and the extent of crosslinking in the particles. The SBR latex with a diameter of 50 nm could be hydrogenated to the extent of 91% using a mole ratio of  $N_2H_4$  to  $H_2O_2$  of 1 per mole of carbon-carbon double bonds. For the SBR latex with a diameter of 230 nm, the hydrogenation degree was only 42%. The effect of particle size on the % hydrogenation could be explained according to a "layer model". The copper ion promoter was postulated as staying at the surface of the latex particles. By modulating the concentration of copper ions at the particle surface, a higher degree of hydrogenation could be attained. However, the gel fraction of SBR latex was increased after the hydrogenation.

Xie et al. [79] reported on the hydrogenation of NBR latex using hydrazine and hydrogen peroxide, with copper sulfate as catalyst and without pressurized hydrogen and organic solvent by reduction of the gel content of the hydrogenation product to 15% while maintaining a high hydrogenation degree of 87%. HNBR behaves as an oil resistant, thermoplastic elastomer with good thermooxidation resistance. The retention after thermal aging was quite good, maintaining 98% of its tensile strength and 96% of its ultimate elongation.

Mahittikul et al. [81] reported on the hydrogenation of natural rubber latex (NRL) via diimide reduction to produce a strictly alternating ethylene-propylene copolymer in  $N_2H_4$  and  $H_2O_2$  system using cupric acetate as catalyst. The cupric acetate is a highly active catalyst for the reaction and the addition of a controlled amount of gelatin demonstrated a beneficial effect on the degree of hydrogenation. A hydrogenation degree of 67.8% was achieved at a ratio of hydrogen peroxide to hydrazine of 1:1. The main factors controlling the hydrogenation of NRL via diimide reduction were the concentration of rubber and hydrazine.

Simma et al. [82] studied the hydrogenation of skim natural rubber (SNR) by the diimide reduction method to improve thermal and ozone stability of SNR in a system of  $N_2H_4$  and  $H_2O_2$  using copper sulfate as catalyst. A high hydrogenation degree of 65% was achieved at a ratio of hydrogen peroxide to hydrazine of 1.6:1 and a low copper sulfate concentration of 49.5  $\mu M$ . The increase in the decomposition

temperature of hydrogenated SNR indicated that diimide hydrogenation increased the thermal stability of SNR. Moreover, the HSNR/NR had high resistance to surface cracking caused by ozone.

Kongsinlark et al. [83] studied the use of the diimide reduction to hydrogenate polyisoprene (PIP)-silica nanocomposites using the  $N_2H_4$  and  $H_2O_2$  system with boric acid as promoter. Their results provided a hydrogenation degree of 98% at a ratio of hydrogen peroxide to hydrazine of 1.5:1. The nanosized HPIP- $SiO_2$  at 98 % hydrogenation showed a maximum degradation temperature of 521 °C resulting in excellent thermal stability, compared with unfilled PIP (387 °C). A new nanocomposite of HPIP- $SiO_2$  could be used as a novel nanofiller in natural rubber. Additionally, HPIP- $SiO_2$ /NR composites had improved mechanical properties and exhibited a good retention of tensile strength after thermal aging and good resistance toward ozone exposure.

## 1.6 Mechanical Properties of Polymer Nanocomposites

One of the important reasons for adding inorganic fillers to polymers is to improve their mechanical performance; the mechanical properties of polymer nanocomposites being a major concern [84]. The mechanical behavior of a polymer can be characterized by its stress–strain properties. A tensile test is the most widely used method to evaluate the mechanical properties of the resultant nanocomposites, and accordingly Young's modulus, tensile strength, and the elongation at break are three main parameters obtained. These vary with the silica content, but the variation trends are different.

**Table 1. 2** Mechanical properties of PP based nanocomposites (Content of SiO<sub>2</sub> = 3.31 vol%) filled with different polymer-grafted SiO<sub>2</sub> [85].

Grafting polymers	Nanocomposites						neat PP
	PS	PBA	PVA	PEA	PMMA	PMA	
Tensile strength (MPa)	34.1	33.3	33.0	26.8	35.2	33.9	32.0
Young's modulus (GPa)	0.92	0.86	0.81	0.88	0.89	0.85	0.75
Elongation at break (%)	9.3	12.6	11.0	4.6	12.0	11.9	11.7

The mechanical properties of polypropylene (PP) nanocomposites filled with SiO<sub>2</sub> particles grafted with various polymers at a fixed SiO<sub>2</sub> fraction were summarized in Table 1.2 [85]. Although the monomers of the grafting polymers should have different compatibilities with PP, all the grafting polymers except PEA exhibited an improvement in the tensile strength of the nanocomposites. It can be concluded that entanglement of the grafting polymer segments with the PP molecules dominated the interfacial interaction in the nanocomposites. Thus, a PP matrix with a higher molecular weight should be entangled more effectively leading to a higher tensile strength increment.

Bikiaris et al. [86] reported the properties of isotactic polypropylene (iPP)/SiO<sub>2</sub> nanocomposites with untreated and surface treated silica nanoparticles prepared by melt compounding. A small improvement in mechanical properties such as tensile strength and elongation at break was observed after nanoparticle addition. A maximum in mechanical properties appeared at a silica content of 2.5 wt% in both surface treated and untreated SiO<sub>2</sub> nanoparticles. A nanoparticle content higher than 2.5 wt% in the polymer matrix resulted in decreased mechanical properties. This was attributed to the increased tendency of SiO<sub>2</sub> nanoparticles to form agglomerates at higher concentrations.

Rubber is a high molecular weight polymeric material, with high elongation and excellent resilience possessing low tensile strength and modulus and poor creep characteristics leading to its limits for rubber applications. Silica is one of the reinforcing substances currently used; so fillers as silica are frequently added to rubbers in order to improve the mechanical properties of the composites.

Suzuki et al. [87] studied the effect of rubber/filler interactions on the stress-strain behavior for silica filled styrene-butadiene rubber (SBR) vulcanizates. The rubber/filler interactions were controlled by the modification of the silica surface using several kinds of silane coupling agents such as decyltrimethoxysilane (DS) and bis-(3-triethoxysilylpropyl)-tetrasulfide (TESPT). A chemical structure of TESPT produced a strong chemical bonding between SBR and silica, which enhanced the tensile stress at a larger strain. Moreover, in the case of mono-functional coupling agents, the tensile stress at a larger strain decreased with an increase in the length of the alkyl chains in the coupling agents. The results suggested that monofunctional coupling agents with long alkyl units worked as a plasticizer for rubber molecules.

According to Peng et al. [88], natural rubber/silica (NR/SiO<sub>2</sub>) was prepared by combining self-assembly and latex-compounding techniques. The SiO<sub>2</sub> nanoparticles were homogeneously distributed in the NR matrix as nano-clusters with an average size ranging from 60 to 150 nm at 6.5 wt% of SiO<sub>2</sub> loading. It was found that the incorporation of silica nanoparticles into the elastomer matrix leads to a significant improvement in the mechanical properties of the host elastomer. The tensile strength, tensile modulus as well as tear strength of the resulting nanocomposite markedly increased at SiO<sub>2</sub> loadings of 2.5–4 wt%. This phenomenon can be explained in that when inorganic nanofillers are homogeneously distributed in polymer matrixes, they will macroscopically form an inorganic network, which mutually penetrates the polymer matrix and restricts sliding of the polymer molecules, and therefore increases the mechanical properties of the polymer hosts including tear resistance.

Lui et al. [89] studied the properties of solution-polymerized styrene butadiene rubber (SSBR) filled with nanosilica which was surface modified by silane coupling agents such as 3-methacryloxypropyl trimethoxy silane (MEMO), [3-(2-aminoethyl)aminopropyl] trimethoxy silane (AMMO), and bis[3-(triethoxysilyl)propyl]

disulfide (TESPD). It was found that SSBR filled with silica powder modified by a silane coupling agent exhibited not only better filler-dispersion and mechanical properties but also lower internal friction loss for a selected range of strains in comparison with unfilled SSBR and SSBR filled with silica powder.

### 1.7 Thermal Stability of Polymer Nanocomposites

Thermal properties are the properties of materials that change with temperature. Among thermal analysis techniques, which include DSC, TGA, DTA, DMA/DMTA, etc. TGA/DTA and DSC are the two most widely used methods to determine the thermal properties of polymer nanocomposites. TGA can describe the thermal stability, the onset of degradation, and the percent silica incorporated in the polymer matrix. DSC can be efficiently used to determine the thermal transition behavior of polymer/silica nanocomposites. Generally, the incorporation of nanosized inorganic particles into the polymer matrix will enhance the thermal stability by acting as a superior insulator and mass transport barrier to the volatile products generated during decomposition [90]. Shang et al. [91] studied the compatibility of soluble polyimide (PI)/SiO<sub>2</sub> composites induced by the coupling agent  $\gamma$ -glycidyloxypropyl trimethoxysilane (GOTMS). It was found that the PI/SiO<sub>2</sub> composites exhibit higher thermal stabilities in comparison with pure PI. The thermal decomposition temperature ( $T_d$ ) of a composite increased with its silica content and they were higher than that of the unfilled PI. For  $T_g$ , the  $T_g$  of the composites increased with increasing silica content. These phenomena could be explained as follows: First, the coupling agent strengthened the interaction between the organic polymer matrix and the inorganic mineral particles, which caused an increased restricting strength of SiO<sub>2</sub> on the PI molecules. Second, the coupling agent reduced the agglomeration of the SiO<sub>2</sub> particles and thereby greatly increased the interfacial area at a given silica content. Additionally, the reduced agglomeration of the SiO<sub>2</sub> particles resulted in an increase in the cross-linking density. All of these effects led to a higher  $T_g$  for the PI/SiO<sub>2</sub> composites with a coupling agent than for pure PI.

Li et al. [92] studied the thermal degradation kinetics and morphology of NR/SiO<sub>2</sub> nanocomposites. A natural rubber/silica (NR/SiO<sub>2</sub>) nanocomposite with a SiO<sub>2</sub> loading of 4 wt% was prepared by incorporating latex compounding with self-assembly techniques. The SiO<sub>2</sub> nanoparticles are homogeneously dispersed throughout the NR matrix as spherical nanoclusters with an average size of 75 nm. In comparison to pure NR, the thermal stability of the nanocomposite is significantly improved. The initial, peak and final degradation temperatures of the nanocomposite increased 17.9 °C, 17.0 °C, and 14.9 °C, respectively, over the host NR. At a given degradation temperature, the degradation rate and frequency factor of the nanocomposite are lower than those of pure NR due to a significant retarding effect of the SiO<sub>2</sub> nanoparticles. The significantly improved thermal stability of the nanocomposite is attributed to the introduction of SiO<sub>2</sub> nanoparticles into the NR matrix, where the SiO<sub>2</sub> and NR molecular chains strongly interact through various effects such as branching effect, nucleation effect, size effect, and surface effect. Therefore, the diffusion of degradation products from the NR matrix to the gas phase is slowed down. Consequently, the nanocomposite has a more complex degradation and better thermal stability than those of pure NR.

Moreover, the thermal stability of the polymer nanocomposite can be investigated by the effect of heat ageing on the mechanical properties. Since thermal resistance of the rubber would be improved, a filler having high thermal stability could be used for providing the desirable properties. The thermal ageing resistance of the rubber vulcanizates was greatly improved by the presence of the silica filler resulting in a high resistance to heat degradation.

Kongsinlark et al. [72] reported on the preparation of a natural rubber nanocomposite filled with polyisoprene (PIP)-SiO<sub>2</sub> core-shell spherical nanoparticles. The NR filled with the PIP-SiO<sub>2</sub> pre-vulcanizate clearly showed an improvement in the storage modulus, tensile strength, tensile modulus, and anti-ageing properties as compared with unfilled NR. For thermal resistance, the tensile stress of unfilled NR after heat ageing was greatly decreased indicating that the NR containing mainly the unsaturated carbon double bonds had poorer properties due to accelerated thermal ageing. On the other hand, the properties of NR filled with PIP-VTS-SiO<sub>2</sub> and PIP-MPS-

SiO<sub>2</sub> did not change and retained high stress values after ageing. The percentage retention in tensile strength of unfilled NR (52.8%) was much lower than that of PIP-VTS-SiO<sub>2</sub> filled NR (89.9%) and PIP-MPS-SiO<sub>2</sub> filled NR (90.7%), respectively. This indicated that aged NR exhibited a reduction in NR crystallization and degradation of the polymer chains by high temperature treatment. The SiO<sub>2</sub> nanoparticles cause a reduction in the flexibility of the NR chains by restriction of molecular chain slipping along the filler surface [31]. These results clearly demonstrated that the addition of PIP-VTS-SiO<sub>2</sub> and PIP-MPS-SiO<sub>2</sub> could increase the anti-ageing properties of NR products.

## 1.8 Membrane Separation

Since the polymer/silica nanocomposites not only improve the physical properties such as the mechanical properties and thermal properties of the materials, but also exhibit some unique properties, which has attracted strong interest in many industries. Besides common plastic and rubber reinforcement, one potential and practical application of this nanocomposite is membrane separation.

Pervaporation is one of the most active areas in membrane research, and the pervaporation process has been shown to be a necessary component for chemical separations. It is a relatively new membrane separation process that has elements in common with reverse osmosis and membrane gas separation. In the pervaporation process as shown in Figure 1.9, the liquid mixture to be separated (feed) is placed in contact with one side of a membrane and the permeated product (permeate) is removed as a low pressure vapor from the other side. The permeate vapor can be condensed and collected or released as desired. The chemical potential gradient across the membrane is the driving force for the mass transport. The driving force can be created by applying either a vacuum pump or an inert purge (normally air or steam) on the permeate side to maintain the permeate vapor pressure lower than the partial pressure of the feed liquid. However, vacuum pervaporation, which is customarily referred to as the standard pervaporation, is the most widely utilized mode of operation [93].

Because of the complicated penetrants-membrane interactions, it is difficult to formulate a single explanation for the complex transport process. There are principally two approaches to describing mass transport in pervaporation: (i) the solution-diffusion model [94, 95] and (ii) the pore flow model [96-98]. The solution-diffusion model (Figure 1.10a) is accepted by the majority of membrane researchers. According to this mechanism, pervaporation consists of three consecutive steps: (i) sorption of the permeant from the feed liquid to the membrane, (ii) diffusion of the permeant in the membrane, and (iii) desorption of the permeant to the vapor phase on the downstream side of the membrane. For the pore flow model (Figure 1.10b), it is assumed that there are a bundle of straight cylindrical pores on the membrane surface. The mass transport by the pore flow mechanism also consists of three steps: (i) liquid transport from the pore inlet to a liquid-vapor phase boundary, (ii) evaporation at the phase boundary, and (iii) vapor transport from the boundary to the pore outlet.

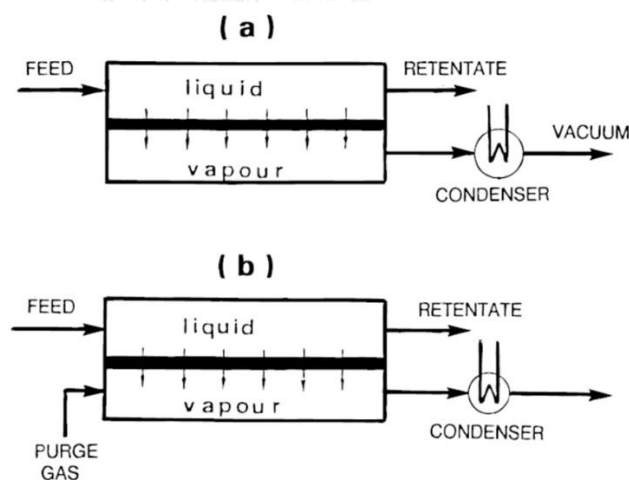


**Figure 1. 9** Schematic diagram of the pervaporation process. (a) Vacuum pervaporation, (b) purge gas pervaporation [93].



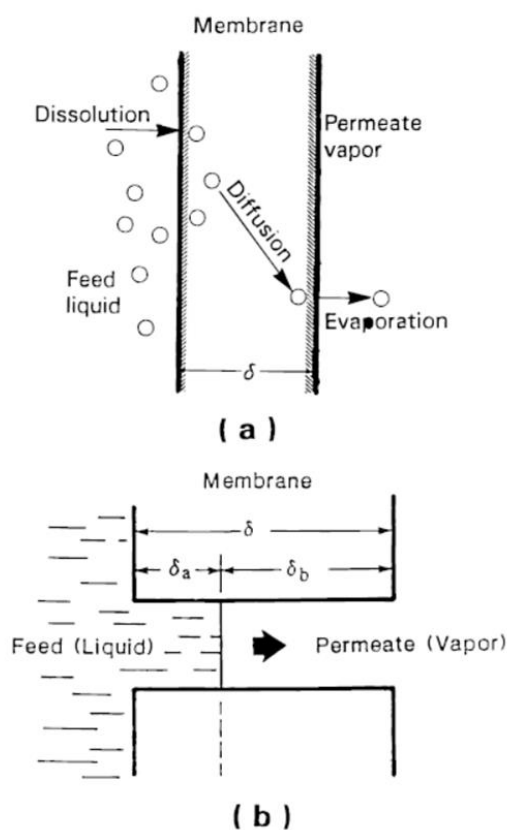


**Figure 1. 10** Schematic representation of the pervaporation transport mechanism. (a) Solution-diffusion model, (b) pore flow model [93].

Nowadays, many research activities have been associated with organic-inorganic nanocomposites for membrane preparation for separation processes. According to Liu et al. [99], silica nanoparticles in chitosan-silica complex membranes used in pervaporation dehydration of ethanol-water mixtures served as spacers between the polymer chains to provide extra space for water permeation, so as to bring about high permeation rates within the complex membranes. Khayet et al. [100] studied the effect of silica and silane modified silica fillers on the pervaporation properties of poly(phenylene oxide) (PPO). Pervaporation separation of methanol/methyl tert-butyl ether (MTBE) mixtures was carried out using both filled and unfilled membranes. Compared with the unfilled PPO membrane, the filled PPO membranes exhibited higher methanol selectivity and lower permeability. Methanol selectivity of the filled PPO membranes with silane-modified silica was better than that of the silica filled and

unfilled PPO membranes. The modified silica nanoparticles had stronger affinity and enhanced compatibility with PPO polymer than the unmodified silica nanoparticles. This generated more tortuous pathways in the PPO dense membrane matrix, and consequently the pervaporation permeation selectivity increased. Guo et al. [101] studied pervaporative dehydration of an ethylene glycol (EG) aqueous solution. A poly(vinyl alcohol) (PVA)-SiO<sub>2</sub> nanocomposite membrane with the incorporation of silica particles into PVA exhibited desirable changes in the morphology and crystalline structure of the membranes, and the thermal stability and stability of the membranes in EG aqueous solution was significantly enhanced.

Recently, Zhao et al. [102] reported that the polyelectrolyte complex (PEC)/SiO<sub>2</sub> nanohybrid membranes showed very high performance in for isopropanol dehydration as compared with other polymeric nanohybrid membranes. The selectivity of these membranes is slightly higher than that of pristine PEC membranes due to the fine dispersion of SiO<sub>2</sub>. Moreover, the incorporation of SiO<sub>2</sub> also improves the processability and mechanical properties of PEC. Sun et al. [103] studied the pervaporation of ethanol-water mixtures using organophilic nano-silica filled polydimethylsiloxane (PDMS) composite membranes. The solubility selectivity and the diffusion selectivity increased with increasing organophilic nano-silica concentration. In addition, the composite membranes exhibited striking advantages in the total flux and separation factor as compared with unfilled PDMS membrane.

## 1.9 Objective and Scope of Dissertation

The principle objective of this research is to investigate the synthesis of monodispersed styrene butadiene copolymer (SBR)-SiO<sub>2</sub>, polybutadiene (PB)-SiO<sub>2</sub> and polystyrene (PS)-SiO<sub>2</sub> nanocomposites via differential microemulsion polymerization and hydrogenated polybutadiene (HPB)-SiO<sub>2</sub> nanocomposites by diimide reduction. One approach is to improve the compatibility and dispersion of silica particles in the polymer matrix. Additionally, the mechanical properties and thermal stability of rubber filled with these nanocomposites (SBR-SiO<sub>2</sub>, PB-SiO<sub>2</sub>, HPB-SiO<sub>2</sub> and PS-SiO<sub>2</sub>) are also included.

In Chapter I, the concepts of microemulsion polymerization are reviewed. The different techniques for silica surface modification and synthesis of polymer/silica nanocomposites with historical and tutorial approaches are described. The fundamentals of diimide hydrogenation of diene-based rubber and the overview of principal concepts of nanocomposites for different applications are also described.

In Chapter II, the experimental procedures for the synthesis of polymer-silica nanocomposites SBR-SiO<sub>2</sub>, PB-SiO<sub>2</sub> and PS-SiO<sub>2</sub> with good dispersion and high efficiency as well as the preparation of SBR-SiO<sub>2</sub> filled NR, HPB-SiO<sub>2</sub> filled NR and PS-SiO<sub>2</sub> filled SBR are presented. The various techniques used for characterization of nanocomposites product are also given.

In Chapter III, the synthesis of SBR nanoparticles via differential microemulsion polymerization is carried out for the preliminary study and the effect of process parameters on monomer conversion, polymer content and particle size are reported. The morphology of SBR nanoparticles are also presented.

In Chapter IV, the results for the preparation of SBR-SiO<sub>2</sub> nanocomposites via differential microemulsion polymerization are reported. The effect of process variables on the encapsulation is investigated. The mechanical properties, thermal properties and water-ethanol mixture pervaporation of NR/SBR-SiO<sub>2</sub> are also reported.

In Chapter V, the synthesis of PB-SiO<sub>2</sub> via differential microemulsion polymerization and their hydrogenated nanoparticles by diimide reduction using hydrazine and hydrogen peroxide with boric acid as promoter are reported. The effect of process variables on encapsulation and hydrogenation degree are investigated. The thermal stability, mechanical properties and ozone resistance of NR/PB-SiO<sub>2</sub> and NR/HPB-SiO<sub>2</sub> nanocomposites are also presented in order to compare the improved properties of the rubber composites with unfilled NR.

In Chapter VI, the results of the effect of process variables on the synthesis of PS-SiO<sub>2</sub> via differential microemulsion polymerization are presented. The mechanical properties, thermal stability, gas permeability as well as water vapor permeability of SBR/PS-SiO<sub>2</sub> composites are studied. The morphology of PS-SiO<sub>2</sub> and SBR/PS-SiO<sub>2</sub> are also investigated.

In Chapter VII, the conclusions resulting from this study and recommendations for future work are summarized



## CHAPTER II

### EXPERIMENTAL AND CHARACTERIZATION

#### 2.1 Materials

##### 2.1.1 Preliminary Experiments on Synthesis of Styrene Butadiene Copolymer Nanoparticles

Styrene (ST,  $\geq 99\%$ ) was purchased from Sigma Aldrich and the inhibitor was removed before polymerization by washing the monomer with 5 wt% aqueous sodium hydroxide (NaOH,  $\geq 98\%$ , Sigma Aldrich) and drying over anhydrous magnesium sulfate ( $\text{MgSO}_4$ ,  $\geq 98\%$ , EMD). 1,3-butadiene (BD) was provided by Air Liquide and used as received. Potassium persulfate (KPS,  $\geq 99\%$ , Sigma Aldrich), sodium dodecyl sulfate (SDS,  $\geq 99\%$ , Fisher Scientific), sodium bicarbonate ( $\text{NaHCO}_3$ ,  $\geq 99\%$ , EMD) were used without further purification. Deionized water was used in all polymerization. Methyl ethyl ketone (MEK,  $\geq 95\%$ , Fisher Scientific) was used to precipitate the SBR nanoparticles.

##### 2.1.2 Synthesis of Styrene Butadiene Copolymer-SiO<sub>2</sub> Nanocomposites

For pretreatment of nano-silica, nano-SiO<sub>2</sub> (Aerosil 200, hydrophilic fumed silica, 12 nm) was supplied by Degussa. Vinyl trimethoxysilane (VTS,  $\geq 98\%$ ) was purchased from Sigma Aldrich. Ammonia solution (25 wt%  $\text{NH}_4\text{OH}$ ) was obtained from Fisher Scientific. For synthesis of the styrene butadiene copolymer (SBR)-SiO<sub>2</sub> nanoparticles, styrene (ST,  $\geq 99\%$ ) was purchased from Sigma Aldrich and the inhibitor was removed before polymerization by washing the monomer with 5 wt% aqueous sodium hydroxide (NaOH,  $\geq 98\%$ , Sigma Aldrich) and drying over anhydrous magnesium sulfate ( $\text{MgSO}_4$ ,  $\geq 98\%$ , EMD). 1,3-butadiene (BD) was provided by Air Liquide and used as received. Potassium persulfate (KPS,  $\geq 99\%$ , Sigma Aldrich), sodium dodecyl sulfate (SDS,  $\geq 99\%$ , Fisher Scientific), sodium bicarbonate ( $\text{NaHCO}_3$ ,  $\geq 99\%$ , EMD) were used

without further purification. Deionized water was used in all polymerizations. Methyl ethyl ketone (MEK,  $\geq 95\%$ , Fisher Scientific) was used to precipitate the SBR-SiO<sub>2</sub> nanoparticle.

### 2.1.3 Synthesis of Polybutadiene-SiO<sub>2</sub> Nanocomposites

Nano-SiO<sub>2</sub> (Aerosil 200, hydrophilic fumed silica, 12 nm) was supplied by Degussa. Vinyl trimethoxysilane (VTS,  $\geq 98\%$ , Sigma Aldrich) as a coupling agent and ammonia solution (25 wt% NH<sub>4</sub>OH, Fisher Scientific) as a catalyst were used for surface modification of nano-silica. 1,3-butadiene (BD,  $\geq 99.5\%$ , Air Liquide), potassium persulfate (KPS,  $\geq 99\%$ , Sigma Aldrich), sodium dodecyl sulfate (SDS,  $\geq 99\%$ , Fisher Scientific), sodium bicarbonate (NaHCO<sub>3</sub>,  $\geq 99\%$ , EMD) were used without further purification for synthesis of polybutadiene (PB)-SiO<sub>2</sub> nanoparticles. Deionized water was used in all polymerization. Methyl ethyl ketone (MEK,  $\geq 95\%$ , Fisher Scientific) was used to precipitate the PB-SiO<sub>2</sub> nanoparticle.

### 2.1.4 Hydrogenation of Polybutadiene-SiO<sub>2</sub> Nanocomposites

The PB-SiO<sub>2</sub> latex as prepared at the optimal condition (SiO<sub>2</sub> loading of 10 wt%, SDS concentration of 5 wt%, monomer to water ratio of 0.2 and KPS concentration of 3 wt%) was selected to be hydrogenated via diimide reduction. Hydrazine hydrate (N<sub>2</sub>H<sub>4</sub>,  $\geq 99\%$ , Sigma Aldrich), hydrogen peroxide solution (30 wt% H<sub>2</sub>O<sub>2</sub>, Sigma Aldrich) and boric acid as promotor (H<sub>3</sub>BO<sub>3</sub>,  $\geq 99.5\%$ , EMD) were used as received for diimide reduction.

### 2.1.5 Synthesis of Polystyrene- SiO<sub>2</sub> nanocomposites

Nano-SiO<sub>2</sub> (Aerosil 200) with an average size of 12 nm was supplied by Degussa. Vinyl trimethoxysilane (VTS,  $\geq 98\%$ , Sigma Aldrich) as a coupling agent and ammonia solution (25 wt% NH<sub>4</sub>OH, Fisher Scientific) as a catalyst were used for surface modification of nano-silica. Styrene (ST,  $\geq 99\%$ , Sigma Aldrich) was washed with 5 wt%

aqueous sodium hydroxide (NaOH,  $\geq 98\%$ , Sigma Aldrich) to remove the inhibitor and dried over anhydrous magnesium sulfate ( $\text{MgSO}_4$ ,  $\geq 98\%$ , EMD). Potassium persulfate (KPS,  $\geq 99\%$ , Sigma Aldrich), sodium dodecyl sulfate (SDS,  $\geq 99\%$ , Fisher Scientific), sodium bicarbonate ( $\text{NaHCO}_3$ ,  $\geq 99\%$ , EMD) were used as received. Deionized water was used in all polymerization. Methanol ( $\text{CH}_3\text{OH}$ ,  $\geq 95\%$ , Fisher Scientific) was used to precipitate the PS-SiO<sub>2</sub> nanoparticle.

### 2.1.6 Pre-Vulcanization of Natural Rubber Composites

Styrene butadiene copolymer (SBR)-SiO<sub>2</sub>, polybutadiene (PB)-SiO<sub>2</sub> and hydrogenated polybutadiene (HPB)-SiO<sub>2</sub> nanoparticles were used to prepare prevulcanized natural rubber (NR) composites. NR latex with approximately 60 wt% dry rubber content (DRC), sulfur as vulcanizing agent, zinc oxide (ZnO) as activator and zincdiethyl dithiocarbamate (ZDEC) as vulcanization accelerators were purchased from the Rubber Research Institute of Thailand.

## 2.2 Surface Modification of Nanosilica

Modified nano-SiO<sub>2</sub> was prepared according to the literature [72]. Firstly, 5 g of nano-SiO<sub>2</sub> was dispersed in 150 mL of deionized water with sonication in an ultrasonic bath for 1 h after that the SiO<sub>2</sub> aqueous dispersion was stirred at 550 rpm for 30 min. Then, 0.15 g of VTS was added dropwise into the dispersion and 25 wt% NH<sub>4</sub>OH was fed to adjust the pH of the dispersion to around 10. The dispersion was stirred for 30 min at room temperature, and then heated up to the reaction temperature at 90 °C, while stirring was maintained at 550 rpm. The reaction was allowed to proceed for an additional 24 h. After that the suspension was dried at 110 °C until constant weight to obtain the modified nano-SiO<sub>2</sub>. Then, the modified nano-SiO<sub>2</sub> was extracted with acetone for 24 h to remove the free VTS. Finally, VTS-SiO<sub>2</sub> was dried in an oven at 55 °C until constant weight was reached. The schematic diagram of silica surface modification is shown in Figure 2.1.

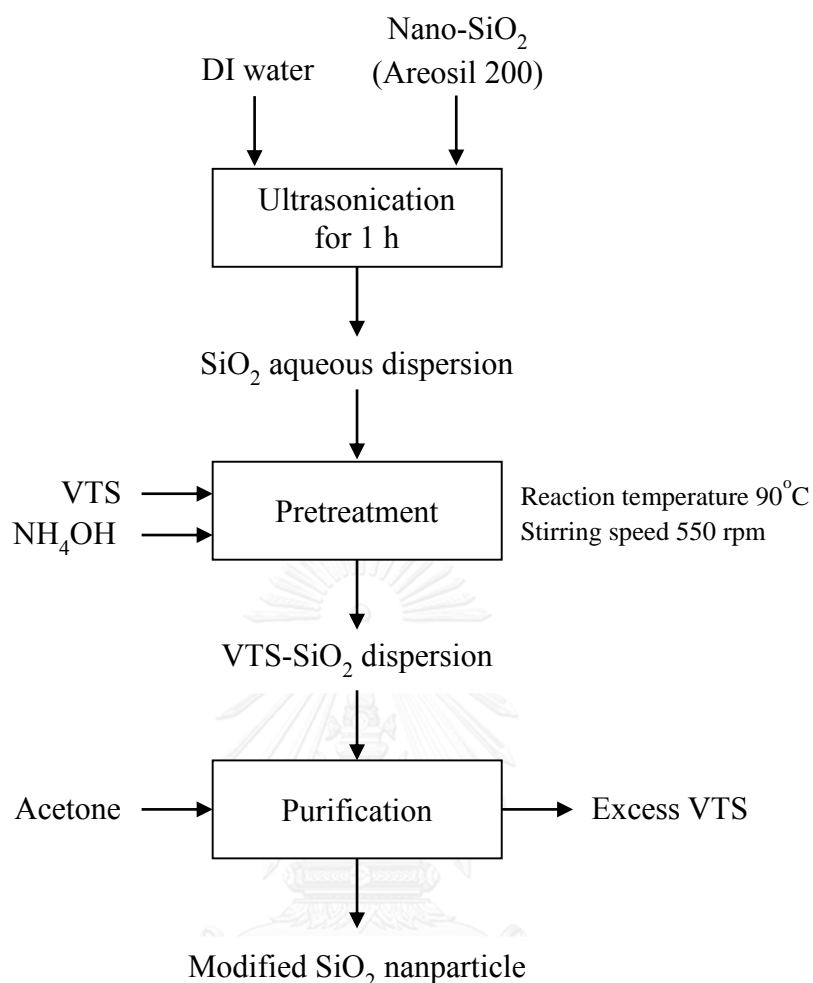


Figure 2. 1 The schematic diagram of silica surface modification.

### 2.3 Preliminary Experiments on Synthesis of Styrene Butadiene Copolymer Nanoparticles

Styrene butadiene copolymer (SBR) nanoparticles were synthesized by differential microemulsion polymerization. The polymerization of styrene and butadiene were carried out in a 300 mL Parr stainless steel reactor equipped with a feeding tube, a thermocouple and an impeller stirrer and the apparatus is shown in Figure 2.2. To obtain SBR nanoparticle latex, typically the KPS as initiator was dissolved in deionized water and then a small amount of NaHCO<sub>3</sub> as buffer and SDS as surfactant were added. The nitrogen gas was charged for degassing the reaction system while



stirring was maintained at 350 rpm. After that the pressure was increased to 80 psig using nitrogen gas and the system was heated up to 50 °C. The monomer mixture of ST and BD (liquid under 22 psig at room temperature) was continuously fed dropwise to the reactor using a designed feeding tube at a given rate of 0.3 mL/min. When the addition of monomer was completed, the reaction system was maintained at 50 °C with constant stirring rate and the polymerization was aged for a given time to reach a proper conversion. Then, the system was cooled down to room temperature.

For precipitation of SBR latex, the latex was precipitated with an excess of methyl ethyl ketone to produce the coagulated rubber. The coagulated rubber was filtered and dried in a vacuum oven at room temperature until constant weight was reached. Solid content and monomer conversion were determined by a gravimetric method. The polymer content was calculated using Eq. 1:

$$\text{Polymer content (\%)} = M_R / M_L \times 100\% \quad (1)$$

where  $M_R$  and  $M_L$  is the total mass of rubber formed and latex, respectively.

The monomer conversion was calculated using Eq. 2:

$$\text{Monomer Conversion (\%)} = M_R / M_m \times 100\% \quad (2)$$

where  $M_R$  and  $M_m$  are the total mass of rubber formed and mass of monomers, respectively.

The effect of the monomer to water ratio over the range of 0.1-0.3, surfactant concentration over the range of 1-10 wt% and initiator concentration over the range of 0.5-3 wt% on particle size, solid content and monomer conversion were investigated. The schematic diagram of SBR synthesis is shown in Figure 2.3.

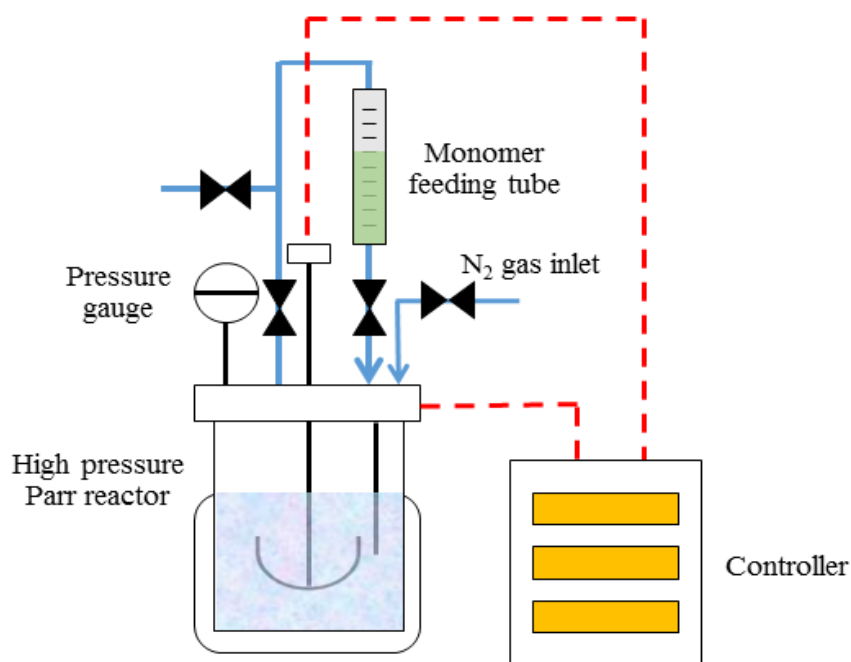


Figure 2. 2 Schematic drawing of nanosized SBR polymerization apparatus.

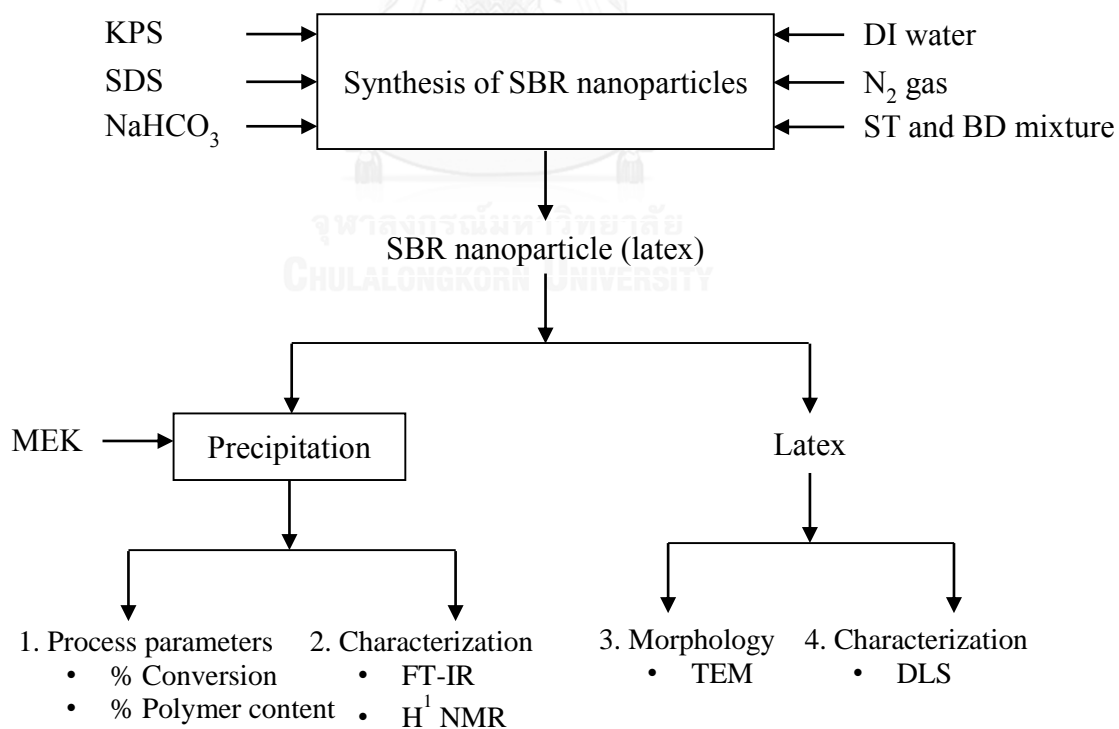


Figure 2. 3 The schematic diagram of SBR synthesis.

## 2.4 Synthesis of Styrene Butadiene Copolymer-SiO<sub>2</sub> Nanocomposites

SBR-SiO<sub>2</sub> nanoparticles were prepared by differential microemulsion polymerization in a 300 mL Parr stainless steel reactor. Typically, VTS-SiO<sub>2</sub> was dispersed in deionized water with sonication in an ultrasonic bath for 1 h. Afterwards, different amounts of VTS-SiO<sub>2</sub>, SDS, KPS, NaHCO<sub>3</sub> and deionized water were charged into a reactor equipped with a feeding tube, a thermocouple and an impeller stirrer. After subsequent addition, the mixture solution was degassed by a slow stream of nitrogen gas for 45 min at room temperature, while stirring was maintained at 350 rpm and then the system was heated up to 50 °C and the pressure was increased to 80 psig using nitrogen gas. The feeding tube was filled with the mixture of the monomers ST (5 g) and BD (5 g, liquid under 22 psig at room temperature) and then, the tube was connected with the reactor. The monomer mixture was continuously fed dropwise into the reactor at a given rate of 0.3 mL/min controlled with a needle valve. When the addition of the monomers was completed, the reaction system was maintained at 50 °C at a constant stirring rate and the polymerization mixture was aged for a given time to reach a proper conversion. The schematic diagram of SBR-SiO<sub>2</sub> synthesis is shown in Figure 2.4.

The SBR-SiO<sub>2</sub> latex was precipitated using excess methyl ethyl ketone to produce the coagulated rubber. The coagulated rubber composite was filtered and dried in a vacuum oven at room temperature until constant weight was reached. Monomer conversion was determined by a gravimetric method. The monomer conversion was calculated using Eq. 3:

$$\text{Monomer Conversion (\%)} = (M_C - M_S) / M_m \times 100\% \quad (3)$$

where  $M_C$ ,  $M_S$  and  $M_m$  are the total mass of coagulated rubber composite, total mass of SiO<sub>2</sub> in system and mass of monomers, respectively.

The coagulated rubber composite was extracted using chloroform in a soxhlet apparatus to remove the free SBR, PS and PB for 24 h and then the SBR-SiO<sub>2</sub> was dried to a constant weight. Grafting efficiency was determined by a gravimetric method. The grafting efficiency was calculated using Eq. 4:

$$\text{Grafting Efficiency} = M_G / M_R \times 100\% \quad (4)$$

where  $M_G$  and  $M_R$  are the mass of grafted rubber in the composite sample and total mass of rubber formed, respectively.

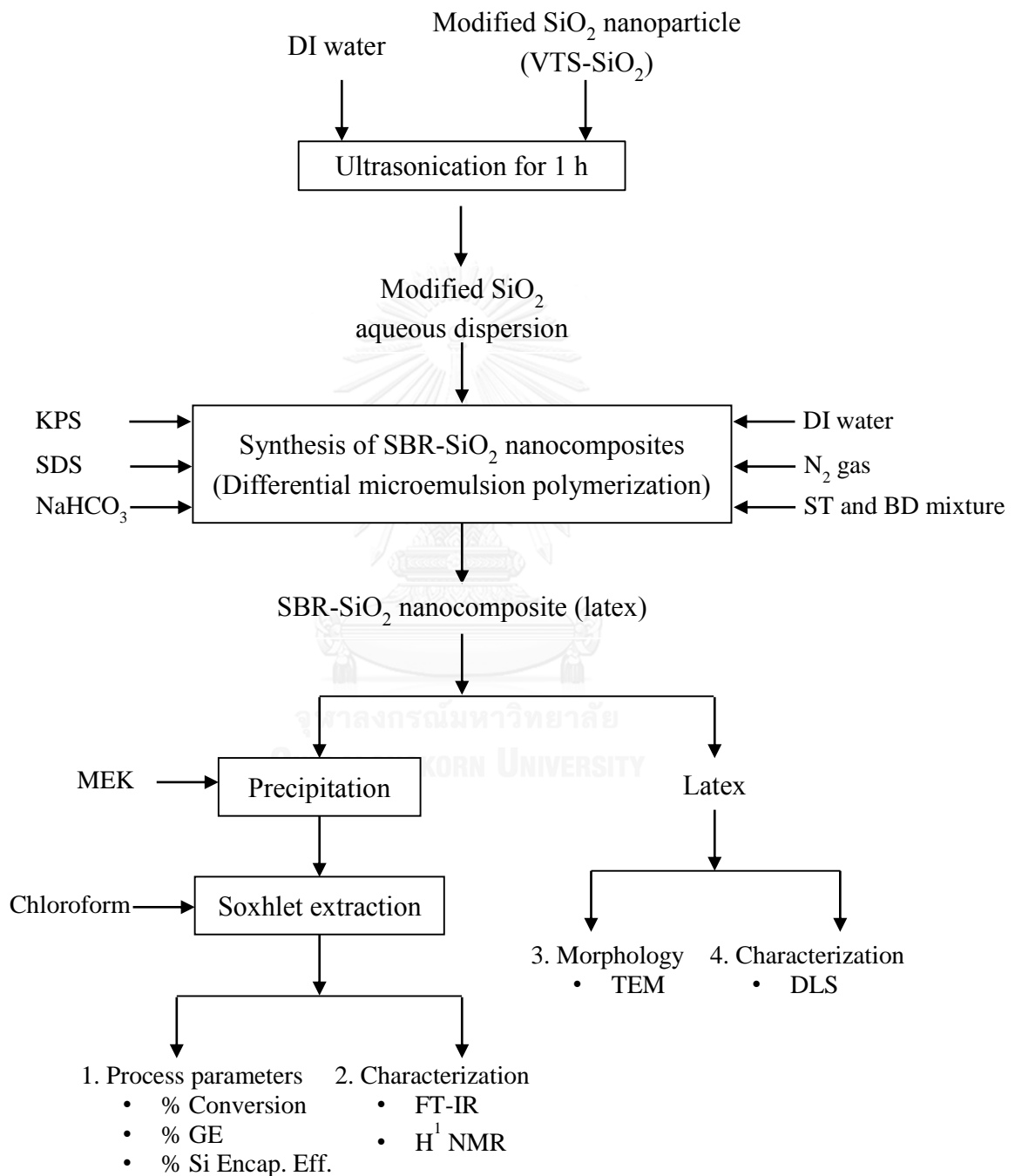


**Figure 2. 4** The schematic diagram of SBR-SiO<sub>2</sub> synthesis.

An acid etching method was used to determine the silica encapsulation efficiency [69, 72]. The composite latex was slowly added to an excess HF solution. The resulting dispersion was dried and the weight percent of the residue was determined gravimetrically. The silica encapsulation efficiency was calculated using Eq. 5:

$$\text{Silica Encapsulation Efficiency} = M_{ES} / M_S \times 100\% \quad (5)$$

where  $M_{ES}$  and  $M_S$  are the mass of encapsulated silica and total mass of  $\text{SiO}_2$  in system, respectively.

## 2.5 Synthesis of Polybutadiene- $\text{SiO}_2$ Nanocomposites

A differential microemulsion polymerization technique was used for synthesizing PB- $\text{SiO}_2$  nanoparticles. The reactions were carried out in a 300 mL Parr stainless steel reactor equipped with a feeding tube, a thermocouple and an impeller stirrer. Typically, VTS- $\text{SiO}_2$  was dispersed in deionized water with sonication in an ultrasonic bath for 1 h. Subsequently, different amounts of VTS- $\text{SiO}_2$ , SDS, KPS,  $\text{NaHCO}_3$  and deionized water were charged into the reactor. The solution was stirred at 350 rpm for 45 min under a nitrogen atmosphere at room temperature and then the system was heated up to 50 °C and the pressure was increased to 100 psig using nitrogen gas. The feeding tube was filled with BD (liquid under 22 psig at room temperature) and then, the tube was connected with the reactor. The condensed BD monomer was continuously fed dropwise into the reactor at a given rate of 0.3 mL/min as controlled by a needle valve. After the addition of the BD monomer was completed, the reaction system was maintained at 50 °C at a constant stirring rate and left to proceed for a given time to reach a desired conversion. The schematic diagram of PB- $\text{SiO}_2$  synthesis is shown in Figure 2.5.

After the polymerization was stopped, the PB- $\text{SiO}_2$  latex was precipitated using excess methyl ethyl ketone to produce the coagulated rubber. The coagulated rubber composite was dried in a vacuum oven at room temperature until constant weight was reached and was then extracted with cyclohexane using a soxhlet apparatus to

remove free PB. The monomer conversion and grafting efficiency (GE) were determined by a gravimetric method and calculated from Eq. 3 and 4, respectively.

An acid etching method was used to determine the silica encapsulation efficiency [69, 72]. The composite latex was slowly added to an excess HF solution. The resulting dispersion was dried and the weight percent of the residue was determined gravimetrically. The silica encapsulation efficiency was calculated using Eq. 5.

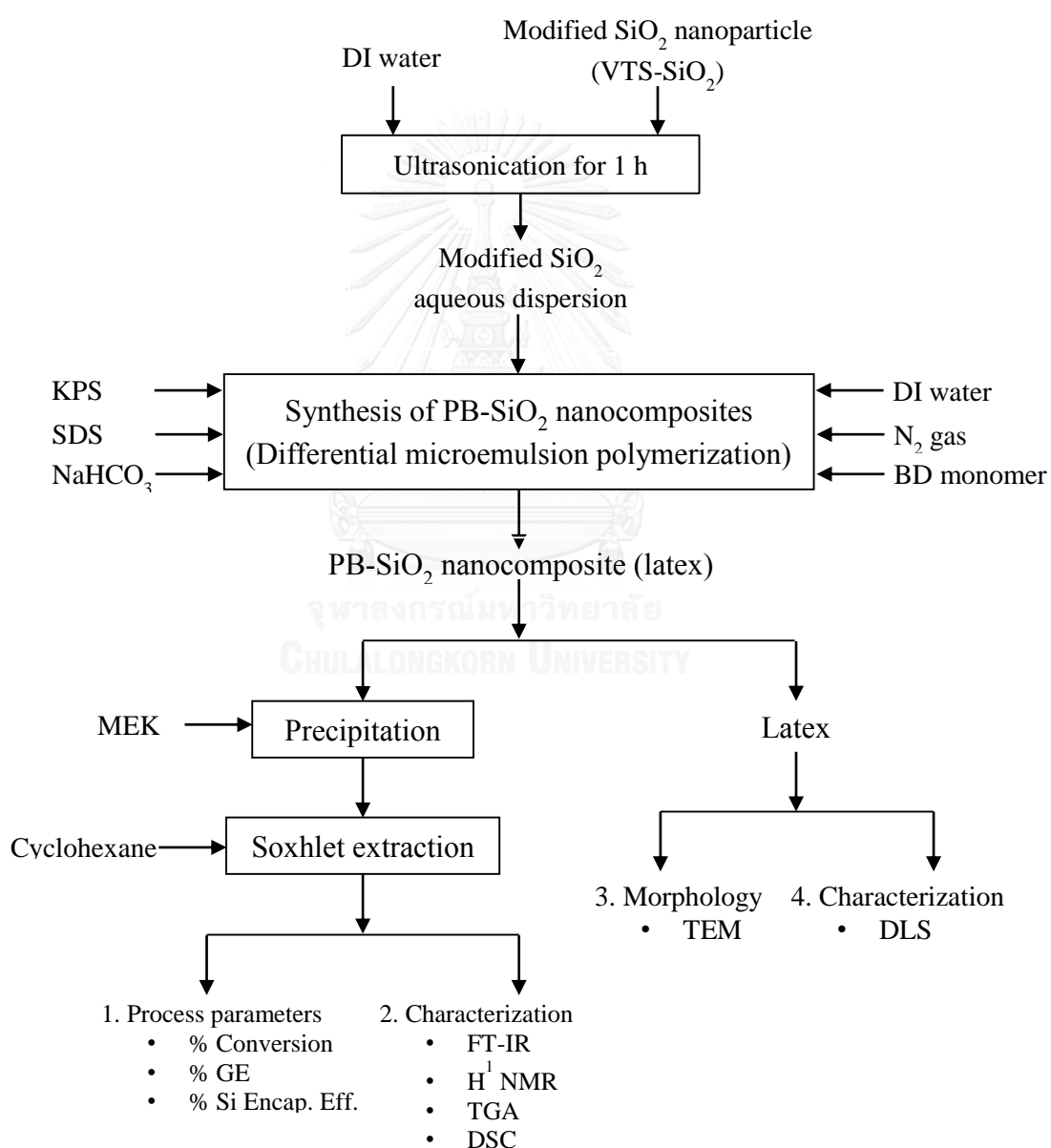


**Figure 2. 5** The schematic diagram of PB-SiO<sub>2</sub> synthesis.

## 2.6 Hydrogenation of Polybutadiene-SiO<sub>2</sub> Nanocomposites

All the hydrogenation reactions were carried out in a 500 mL glass reactor equipped with a temperature controlled oil bath and reflux condenser. In a typical run, PB-SiO<sub>2</sub> latex was charged to the glass reactor and then, hydrazine hydrate and boric acid (0.15 mol/L) were slowly added into the latex. After subsequent addition, the solution mixture was degassed with a slow stream of nitrogen gas for 30 min, while stirring was maintained at 300 rpm. Subsequently, the system was heated up to 70 °C, and then hydrogen peroxide was continuously fed into the reactor using a peristaltic pump with a feeding rate of 0.4 mL/min. After hydrogen peroxide addition was complete, the reaction was performed for 5 h at a constant temperature. After the reaction, the HPB-SiO<sub>2</sub> latex produced was then precipitated using methyl ethyl ketone to form the coagulated rubber. The schematic diagram of HPB-SiO<sub>2</sub> synthesis is shown in Figure 2.6.

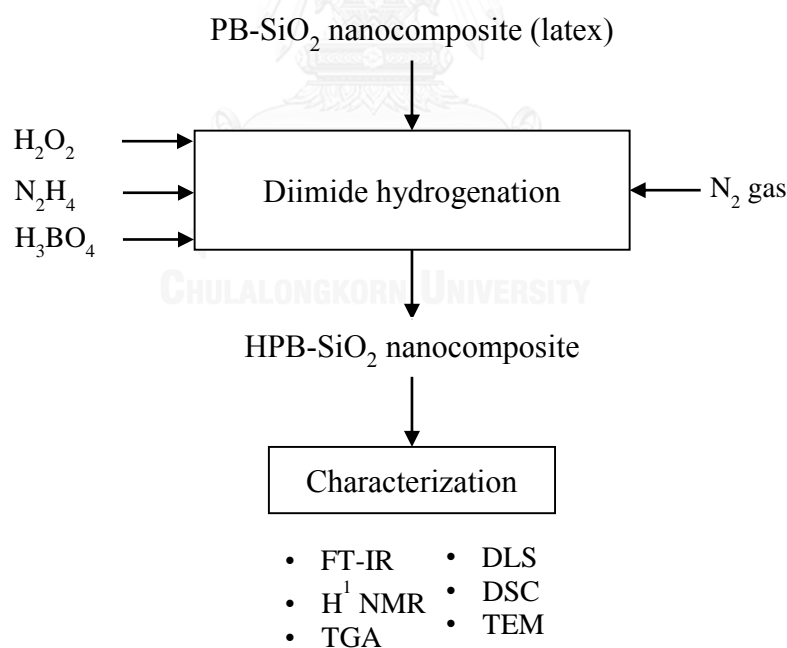


**Figure 2. 6** The schematic diagram of HPB-SiO<sub>2</sub> synthesis.

## 2.7 Synthesis of Polystyrene- SiO<sub>2</sub> Nanocomposites

Polystyrene (PS)-SiO<sub>2</sub> nanocomposites were synthesized via differential microemulsion polymerization in a 500 mL four necked round bottomed glass reactor equipped with a reflux condenser, a temperature controlled oil bath and a peristaltic pump. In a typical run, VTS-SiO<sub>2</sub> was dispersed in deionized water with sonication in an ultrasonic bath for 1 h. The specific amounts of VTS-SiO<sub>2</sub> (0.5-2 g), SDS (0.1-1 g), KPS (0.2 g), NaHCO<sub>3</sub> (0.1 g) and deionized water (33 g) were charged into a reactor and the system was then degassed by a slow stream of nitrogen gas for 45 min at room temperature under stirring at 350 rpm to prevent probable inhibition. After that the system was heated up to 70 °C and the ST monomer was fed dropwise into reactor by using a peristaltic pump at the feed rate of 0.3 mL/min. When the addition of monomer was completed, the reaction system was left to proceed for a given time to reach a desired conversion.

The PS-SiO<sub>2</sub> nanocomposite was precipitated with excess methanol to produce the coagulated solid and the precipitated solid was dried in a vacuum oven at room temperature until constant weight. Monomer conversion was determined by a gravimetric method. The monomer conversion was calculated using Eq. 3 Then the precipitated solid was extracted with petroleum ether using a soxhlet apparatus for 24 h to remove free PS. The grafting efficiency was calculated using Eq. 4. An acid etching method was used to determine the silica encapsulation efficiency [69, 72]. The silica encapsulation efficiency was calculated using Eq. 5. The schematic diagram of PS-SiO<sub>2</sub> synthesis is shown in Figure 2.7.



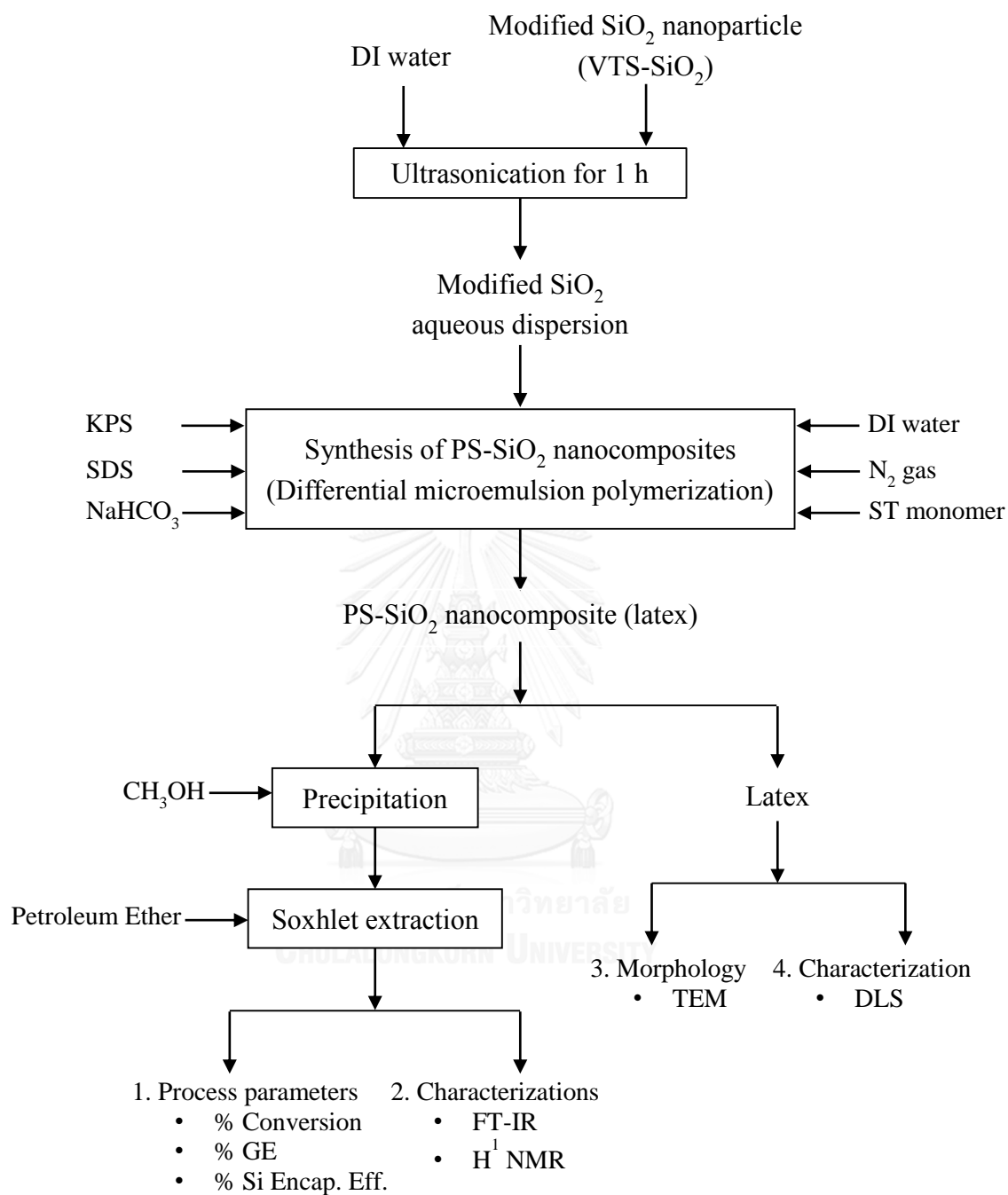


Figure 2. 7 The schematic diagram of PS-SiO<sub>2</sub> synthesis.

## 2.8 Preparation of NR/SBR-SiO<sub>2</sub> and NR/HPB-SiO<sub>2</sub> Composites

### i) Preparation of NR/SBR-SiO<sub>2</sub> Composites

For NR/SBR-SiO<sub>2</sub> composite membrane preparation, the SBR-SiO<sub>2</sub> nanoparticle latex at 10 wt% of silica loading (polymerization condition: monomer to water ratio of 0.2, SDS concentration of 3 wt% and KPS concentration of 2 wt% based on monomer amount) was selected to blend with NR latex at various weight ratios (NR: SBR-SiO<sub>2</sub> = 100:0, 90:10, 80:20, 70:30, 60:40) under a stirring rate of 450 rpm for 30 min at room temperature to form a good dispersion. After that sulfur (1.5 phr), ZnO (2 phr) and ZDEC (1 phr) were dropped into the mixture and the system was heated up to 60 °C while stirring was maintained at 350 rpm for 2 h. Then, the NR/SBR-SiO<sub>2</sub> nanocomposite latex was cast on a glass plate of a dimensions of 9 cm × 9 cm × 3 mm. The cast membrane was dried at 70 °C for 5 h in an oven. The membrane thickness was approximately 0.2 mm measured at five different points using a micrometer.

### ii) Preparation of NR/PB-SiO<sub>2</sub> and NR/HPB-SiO<sub>2</sub> Composites

The PB-SiO<sub>2</sub> latex (polymerization condition: monomer to water ratio of 0.2, SDS concentration of 5 wt%, KPS concentration of 3 wt% and SiO<sub>2</sub> loading of 10 wt% based on BD monomer amount) or HPB-SiO<sub>2</sub> latex (hydrogenation condition: N<sub>2</sub>H<sub>4</sub> concentration of 3 mol/L, H<sub>2</sub>O<sub>2</sub> concentration of 4 mol/L and H<sub>3</sub>BO<sub>3</sub> concentration of 0.15 mol/L at C=C concentration of 1 mol/L) was dropped into the NR latex at various weight ratios (NR:PB-SiO<sub>2</sub> or NR:HPB-SiO<sub>2</sub> = 100:0, 95:5, 90:10, 80:20, 70:30) under a stirring rate of 450 rpm for 30 min at room temperature to form a good dispersion. After that sulfur (1.5 phr) as vulcanizing agent, ZnO (2 phr) as activator and ZDEC (1 phr) as accelerators were dropped into the latex mixture and the system was heated up to 60 °C while stirring was maintained at 350 rpm for 2 h. Then, the NR/PB-SiO<sub>2</sub> or NR/HPB-SiO<sub>2</sub> latex was cast on a glass plate having dimensions of 13 cm × 13 cm × 3 mm. The cast sheet was dried at 70 °C for 5 h in an oven. The composite sheet

thickness was approximately 2.0 mm measured at five different points using a micrometer.

## 2.9 Preparation of SBR/PS-SiO<sub>2</sub> Composites

The PS-SiO<sub>2</sub> latex (polymerization condition: monomer to water ratio of 0.2, SDS concentration of 3 wt%, KPS concentration of 2 wt% and SiO<sub>2</sub> loading of 10 wt% based on ST monomer amount) was dropped into the SBR latex at various weight ratios (SBR:PS-SiO<sub>2</sub> = 100:0, 95:5, 90:10, 80:20, 70:30) under a stirring rate of 450 rpm for 30 min at room temperature to form a good dispersion. Then, the SBR/PS-SiO<sub>2</sub> composite latex was cast on a glass plate of a dimensions of 15 cm × 15 cm × 3 mm. The film thickness was approximately 0.1 mm measured at five different points using a micrometer. The appearance SBR/PS-SiO<sub>2</sub> composite film was shown in Figure 2.8.

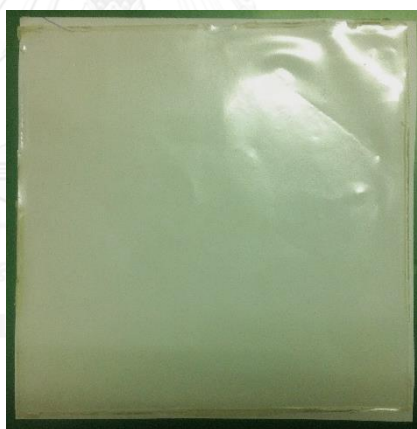


**Figure 2. 8** Appearance of SBR/PS-SiO<sub>2</sub> composite film.

## 2.10 Characterization

### 2.10.1 Fourier Transform Infrared Spectroscopy

The SiO<sub>2</sub>, VTS-SiO<sub>2</sub>, SBR-SiO<sub>2</sub>, PB-SiO<sub>2</sub>, HPB-SiO<sub>2</sub> and PS-SiO<sub>2</sub> were characterized by FTIR analysis (Thermo Nicolet 6700 spectrometer). Before analysis, the samples

were extracted to remove free VTS and ungrafted SBR, PB, HPB and PS. The samples SiO<sub>2</sub>, grafted VTS-SiO<sub>2</sub>, SBR-SiO<sub>2</sub>, PB-SiO<sub>2</sub>, HPB-SiO<sub>2</sub> and PS-SiO<sub>2</sub> were ground with KBr powder and compressed to form a pellet for FTIR analysis.

### 2.10.2 <sup>1</sup>H NMR Spectroscopy

The molar compositions (ST:BD) and microstructure of the grafted SBR-SiO<sub>2</sub> were determined by <sup>1</sup>H Nuclear Magnetic Resonance (NMR) spectroscopy (Bruker 300 MHz spectrometer). The sample solution was prepared by dissolving 20 mg dried SBR-SiO<sub>2</sub> in 1 mL of deuterated chloroform (CDCl<sub>3</sub>) at room temperature.

The hydrogenation degree (HD) of HPB-SiO<sub>2</sub> was determined by proton nuclear magnetic resonance (<sup>1</sup>H NMR) spectroscopy (Bruker 300 MHz spectrometer). The sample solution was prepared by dissolving 20 mg dried HPB-SiO<sub>2</sub> in 1 mL of deuterated chloroform (CDCl<sub>3</sub>) at room temperature, and the spectra were analyzed using an Advance Bruker 300 MHz spectrometer. The hydrogenation degree (HD) was calculated by using Eq. 6:

$$\text{Hydrogenation degree (\%HD)} = (A - 4B) / (A + 4B) \times 100\% \quad (6)$$

where A and B are the peak areas of saturated protons (in the range of 0.7-2.0 ppm) and the unsaturated protons (in the range of 5.0-6.0 ppm), respectively.

### 2.10.3 Particle Diameter Measurement

The particle size, in term of the number-average diameter (D<sub>n</sub>), and particle size distribution of the SBR-SiO<sub>2</sub>, PB-SiO<sub>2</sub>, HPB-SiO<sub>2</sub> and PS-SiO<sub>2</sub> were determined by a dynamic light scattering technique (DLS, Nanotracc 150 particle size analyzer).

### 2.10.4 Morphological Study

The morphology and core-shell structure of the SBR-SiO<sub>2</sub>, PB-SiO<sub>2</sub>, HPB-SiO<sub>2</sub> and PS-SiO<sub>2</sub> nanoparticles were observed using a LEO 912 AB 100kV Energy Filtered

Transmission Electron Microscope (EFTEM). The nanosized composite latex was first diluted 20 times with deionized water. Then, 10  $\mu\text{L}$  of the diluted solution was dropped on a 400-mesh copper grid at room temperature and the excess solution was drawn off the grid with tissue paper. After that the grid was stained with 1%  $\text{OsO}_4$  for 2 min and the excess  $\text{OsO}_4$  was drawn off with tissue paper.

#### **2.10.5 Thermogravimetric Analysis (TGA)**

Thermogravimetric analysis (TGA) was performed with a thermal analysis instrument (Perkin-Elmer Pyris Diamond) to obtain the decomposition temperature ( $T_{\text{id}}$  and  $T_{\text{max}}$ ). 10 mg of the samples were placed into a platinum pan. The temperature was raised under a nitrogen atmosphere from room temperature to 800  $^{\circ}\text{C}$  at a constant heating rate of 10  $^{\circ}\text{C}/\text{min}$  with a flow rate of nitrogen gas of 50 mL/min.

#### **2.10.6 Differential Scanning Calorimetry (DSC)**

Differential scanning calorimetry (DSC, Mettler Toledo 822e) was used to obtain the glass transition temperature ( $T_g$ ). The NR composite and SBR composite samples were cooled to -100  $^{\circ}\text{C}$  with liquid nitrogen and then heated to 25  $^{\circ}\text{C}$  at a constant rate of 10  $^{\circ}\text{C}/\text{min}$ . The glass transition temperature ( $T_g$ ) of all samples was calculated from the midpoint of the base-line shift of the DSC thermogram.

#### **2.10.7 Contact Angle Measurement**

The contact angle of water was measured using a Standard Goniometer (Ramé-Hart Model 200-F1). Water droplets were placed on the NR/SBR- $\text{SiO}_2$  and SBR/PS- $\text{SiO}_2$  composites and then, the dimensions of the droplets were examined using the software system. Each measurement was repeated three times and then averaged for the final results.

### 2.10.8 Gas Permeability

Oxygen permeability measurements of SBR/PS-SiO<sub>2</sub> composite films were carried out at 23 °C, 0% RH, atmospheric pressure using an oxygen permeation analyzer (Illinois model 8000). According to ASTM D 3985-05, the amounts of oxygen that permeated through the films were detected in units of cc/m<sup>2</sup>·day.

Water vapor permeability of SBR/PS-SiO<sub>2</sub> composite films was determined using water vapor permeation tester (MOCON PERMATRAN-W @3/33) at 38 °C, 90% RH, using ASTM E96-00 procedure. The test film was sealed to a glass dish containing anhydrous calcium chloride and the dish was placed in a desiccator maintained at with saturated magnesium nitrate. The water vapor transferred through the film and absorbed by the desiccant was determined by measuring the weight gain. WVP was calculated from the following equation:

$$WVP = (C \times x) / A \Delta P \quad (7)$$

where WVP is in g/m·s·Pa, C is the slope of the weight gain of the dish versus time, x is the film thickness (m), A is area of the exposed film (m<sup>2</sup>) and  $\Delta P$  is the water vapor pressure differential across the film (Pa).

### 2.11 Mechanical Properties of NR and SBR Composites

The mechanical properties of composite rubbers (NR/SBR-SiO<sub>2</sub>, NR/PB-SiO<sub>2</sub>, NR/HPB-SiO<sub>2</sub> and SBR/PS-SiO<sub>2</sub>) in terms of tensile strength, % elongation at break and modulus were evaluated using a Universal Testing Machine (INSTRON 5566) at 500 mm/min of the cross-head speed according to ASTM-412. All samples were cut into dumbbell-type specimens using a Wallace die cutter, and the average of three measurements of the five specimens was considered as the representative value.

## 2.12 Thermal Resistance of Vulcanized Rubber

The thermal resistance of NR/PB-SiO<sub>2</sub> and NR/HPB-SiO<sub>2</sub> were measured from the change of their mechanical properties after aging. All tensile specimens were aged at 100 °C for 24 h in an oven and the mechanical properties of the samples before and after aging were measured to study the thermal resistance. The %Retention (%Re) was calculated by using Eq. 8:

$$\% \text{Retention (\%Re)} = (\text{Properties after ageing}) / (\text{Properties before ageing}) \times 100\% \quad (8)$$

## 2.13 Ozone Resistance of Vulcanized Rubber

Ozone resistance of NR/PB-SiO<sub>2</sub> and NR/HPB-SiO<sub>2</sub> nanocomposites were studied using an ozone test chamber (HAMPDEN, Northampton, England) according to ISO 1431-1:2004. Before exposure to ozone, all samples were stretched by 20% elongation for 48 h in the absence of light under an ozone-free atmosphere. After that the samples were placed into an ozone test chamber for 72 h under an ozone concentration of 50 parts per hundred million (pphm) and a temperature of 40 °C. Photographs of the samples after 24 h, 48 h and 72 h testing were taken to investigate the cracks on the rubber surface.

## 2.14 Pervaporation of Water-Ethanol Mixture

The pervaporation process was performed using a plate and frame module as shown in Figure 2.9. The effective membrane area was 11.34 cm<sup>2</sup>. The membrane (NR: SBR-SiO<sub>2</sub> = 90:10, 80:20, 70:30, 60:40) was put on a stainless steel porous support and then, it was allowed to come in contact with the feed solution for 2 h by circulating the solution from a feed reservoir kept at room temperature. After that the vacuum was applied to permeate side and the pervaporation process was operated for an additional 3 h. Permeate was collected in cold traps cooled with liquid nitrogen. The

composition of the permeate was determined using the calibration curve of the solution compositions versus their absorbance number.

The performance of the membrane for pervaporation was characterized from the total permeate flux,  $J$  ( $\text{g}/\text{m}^2\text{h}$ ) and selectivity. Total permeate flux was calculated using Eq. 9:

$$J = W / (A \cdot t) \quad (9)$$

where  $W$ ,  $A$  and  $t$  represent the total weight of permeate (g), the effective membrane area ( $\text{m}^2$ ) and the operating time (h), respectively. The selectivity was calculated using Eq. 10:

$$S = (Y_W \cdot X_E) / (Y_E \cdot X_W) \quad (10)$$

where  $Y_W$  and  $Y_E$  represent the weight fraction of water and ethanol in the permeate and  $X_W$  and  $X_E$ , those of water and ethanol in the feed, respectively.

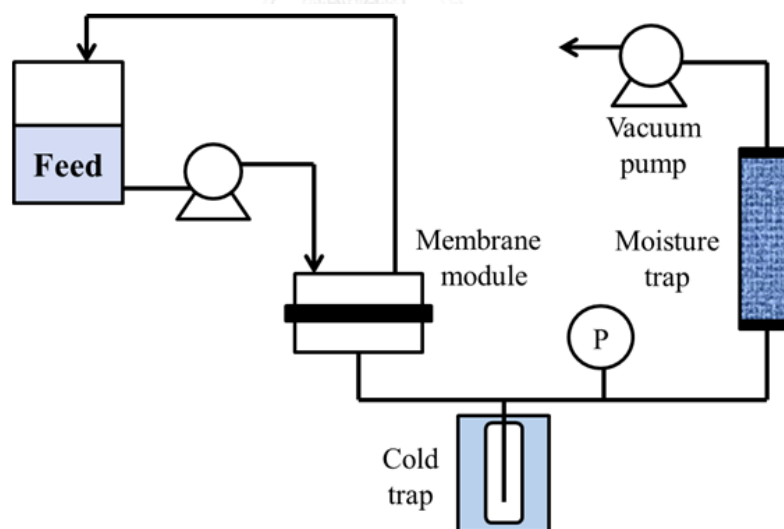


**Figure 2. 9** Schematics of pervaporation equipment.



## CHAPTER III

### PRELIMINARY STUDY ON SYNTHESIS OF STYRENE BUTADIENE COPOLYMER NANOPARTICLES VIA DIFFERENTIAL MICROEMULSION POLYMERIZATION

#### 3.1 Introduction

Differential microemulsion polymerization (DMP) as an environmental friendly process was developed to obtain nanosized polymer latex at an extremely low surfactant concentration. The surfactants are not only expensive but also have significant negative impact on the physical properties of polymers. This technique is desirable to reduce the surfactant concentration under mild reaction conditions and also yield nanosized particles with high conversion. For the mechanism of DMP, the initiator first decomposes in the water phase to generate primary radicals and some of the primary radicals could attack monomers to form polymer radicals. These polymer radicals propagated in the water phase reaching a critical chain length and precipitate to form polymer particles (homogeneous nucleation) or enter into monomer-swollen micelles to generate polymer particles (heterogeneous nucleation). However, the synthesis of polymer via differential microemulsion polymerization has not been widely reported. Most of the research has focused on miniemulsion and microemulsion polymerization.

This study aims to prepare styrene butadiene copolymer (SBR) nanoparticles by differential microemulsion polymerization, and to clarify the effects of process variables consisting of monomer to water ratio, surfactant concentration and initiator concentration on monomer conversion, polymer content and particle size. The SBR nanoparticles were characterized by FTIR analysis and  $^1\text{H}$  NMR spectroscopy to confirm the structure. In addition, TEM was also used to determine the morphology and size distribution of the SBR nanoparticle.

### 3.2 Characterization of SBR Nanoparticles

The FTIR spectrum of SBR nanoparticles is shown in Figure 3.1. The common vibration absorption peaks of C-H asymmetric stretching, C-H symmetric stretching and C-H in-plane bending for the CH<sub>2</sub> groups are apparent at 2916, 2843 and 1447 cm<sup>-1</sup>, respectively. For polystyrene units, the peaks at 1942 and 1695 cm<sup>-1</sup> are attributed to overtone C-H out of plane bending in the aromatic ring. Moreover, the peaks at 1598 and 1489 cm<sup>-1</sup> are related to C=C skeletal in the aromatic ring. The C-H in-plane bending in the aromatic monosubstituted ring is apparent at 1153 and 1027 cm<sup>-1</sup>. The peak at 838 cm<sup>-1</sup> corresponds to polystyrene unit vibrations. Additionally, C-H out of plane bending in the aromatic monosubstituted ring is apparent at 756 and 697 cm<sup>-1</sup>. For 1,2 polybutadiene units, a strong C=C stretching in CH<sub>2</sub>=CH- group is evident at 1636 cm<sup>-1</sup>. =CH<sub>2</sub> symmetric stretching, =CH- out of plane bending and =CH<sub>2</sub> out of plane bending in the CH<sub>2</sub>=CH- group appear at 3081, 991 and 912 cm<sup>-1</sup>, respectively. For 1,4 polybutadiene units, a =C-H stretching and C-H out of plane bending in trans-RCH=CHR were obvious at 3022 and 965 cm<sup>-1</sup>, respectively. The peak at 1350 cm<sup>-1</sup> corresponds to C-H in-plane bending in the CH<sub>2</sub> groups of trans- and cis-polybutadiene units. Moreover, =CH-H stretching and =C-H in plane bending in cis-RCH=CHR are apparent at 2999 and 1311 cm<sup>-1</sup>, respectively [104]. A strong C-H in plane bending in cis-polybutadiene unit is evident at 1221 cm<sup>-1</sup>. In addition, a match of 94.18% was obtained on comparing with the spectrum of standard SBR. These results indicate that styrene butadiene copolymer has been successfully synthesized via differential microemulsion polymerization.

<sup>1</sup>H NMR spectroscopy was used to identify the copolymer composition and microstructure. From spectrum of SBR-SiO<sub>2</sub> as shown in Figure 3.2, the peak in the 6.7-7.3 ppm range corresponded only to the protons of styrene (2 ortho-H, 1 para-H and 2 meta-H, -C<sub>6</sub>H<sub>5</sub>), and the peak at 5.5 ppm indicated the protons of 1,2-butadiene double bond (1H, -CH=CH<sub>2</sub>). Moreover, the peak in the 5-5.44 ppm range represented the 1,4-butadiene double bond (2 cis-H and 2 trans-H, -CH=CH-), and the peak in the 4.6-5 ppm range which is related to protons of the 1,2-butadiene double bond (2H, -CH=CH<sub>2</sub>), while peaks in the 1.2-2.5 ppm range belong to the protons of methyl and

methylene groups. The molar composition of polybutadiene units and polystyrene units in the copolymer calculated by the ratio of the summation of H signals of  $-\text{CH}=\text{CH}-$  of the 1,4 polybutadiene (5.3 ppm) and H of  $-\text{CH}=\text{CH}_2$  of the vinyl-1,2 polybutadiene (4.94 ppm) and meta-H signals of  $-\text{C}_6\text{H}_5$  of polystyrene (6.88 ppm), is around 0.6 and 0.4, respectively [105].

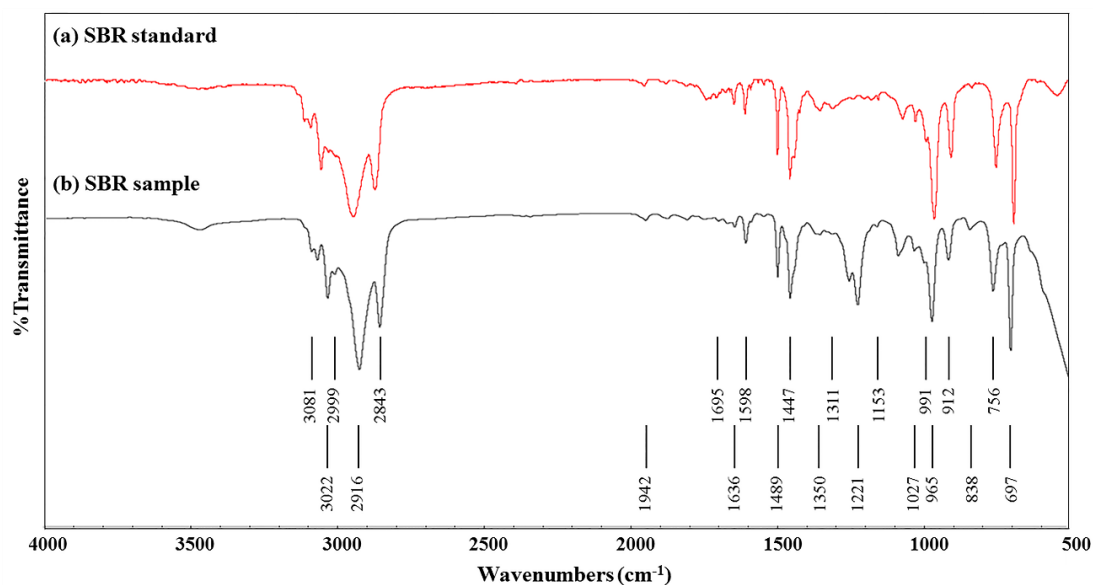


Figure 3. 1 FTIR spectrum of SBR nanoparticles.

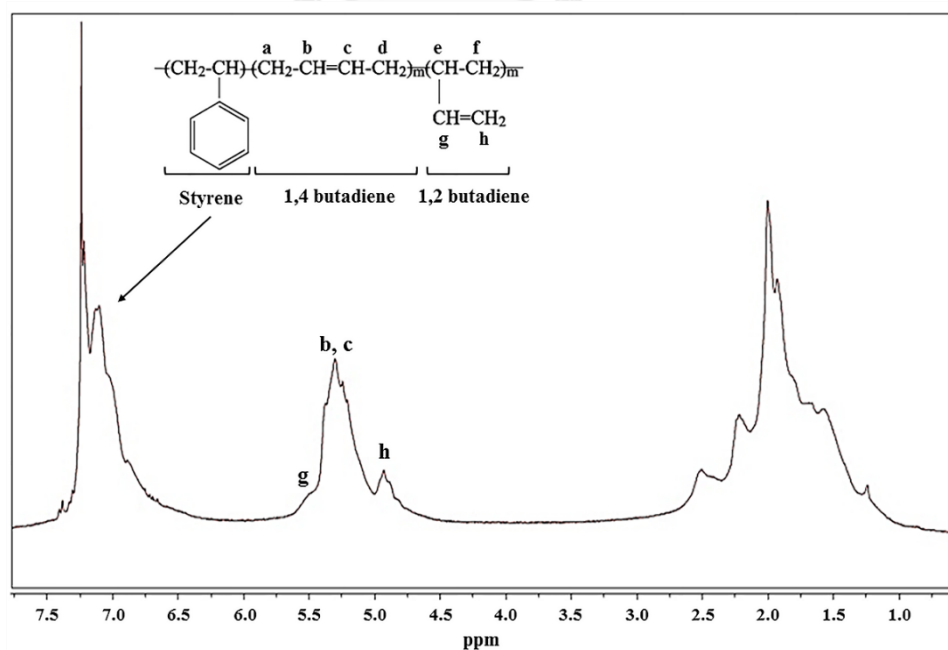
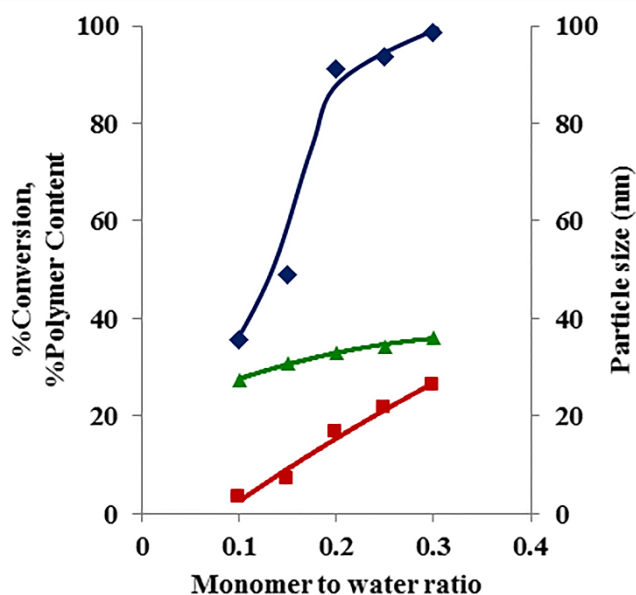


Figure 3. 2  $^1\text{H}$ -NMR spectrum of SBR nanoparticle in  $\text{CDCl}_3$ .

### 3.3 Effect of Process Parameters

#### 3.3.1 Effect of Monomer to Water Ratio

The effect of monomer to water ratio on monomer conversion, polymer content and particle size of SBR nanoparticles is shown in Figure 3.3. The monomer conversion and polymer content increased with increasing monomer to water ratio and reached a maximum at a monomer to water ratio of 0.3. The particle size increased from 27 nm to 36 nm with an increase in the monomer to water ratio from 0.1 to 0.3, indicating that the particle size at a lower monomer to water ratio is smaller than that at a higher monomer to water ratio. This phenomenon could be explained by the particle nucleation mechanism. KPS as a water soluble initiator was used in this system; thus the nucleation mainly occurred in the water phase. More water would provide a higher probability of homogeneous nucleation in the water phase and then each particle would share less monomer amount resulting in a smaller particle size at a lower monomer to water ratio [14]. Additionally, more collisions and aggregation of the nanoparticles occurred at a high monomer to water ratio and thus the monomer conversion and polymer content increased resulting in a larger particle size than that obtained at a low monomer to water ratio [12]. The monomer conversion (98%) and polymer content (26%) were maximized at a monomer to water ratio of 0.3 via DMP at which a small particle size (36 nm) was achieved.



**Figure 3.3** Effect of monomer to water ratio ( $M/H_2O$ ) on; (◆) %Conversion, (■) %Polymer content, (▲) Particle size. Condition: SDS = 5 wt%, KPS = 2 wt% based on monomer.

### 3.3.2 Effect of Surfactant Concentration

In this study, SDS was used as surfactant at a concentration above the critical micelle concentration (CMC). The effects of the surfactant concentration on monomer conversion, polymer content and particle size of SBR nanoparticles are shown in Figure 3.4a. It indicates that the monomer conversion increased from 68% to 97% and the polymer content increased from 12.7% to 17.7% with an increase in the surfactant concentration from 1 to 10 wt% based on monomer. This phenomenon can be explained in that in an emulsion polymerization system, a certain amount of surfactant can form numerous compact micelles while the inner space of each micelle can be used as a reaction domain [106, 107]. A high level of surfactant concentration could provide more micelles resulting in more reaction domains in the system. Thus, a higher surfactant concentration would result in the higher monomer conversion and polymer content. Moreover, the particle size was greatly decreased from 69 nm to 22 nm with an increase in the surfactant concentration from 1 to 10 wt% based on monomer. This

can be explained in that at a high surfactant concentration (above the CMC), more micelles were generated and micellar nucleation could dominate over homogeneous nucleation while coagulative nucleation was neglected [107-109]. Thus, more homogeneous latex particles were produced resulting in a smaller particle size.

The surfactant concentration has a significant effect on the characteristics of the SBR nanoparticle latex as shown in Fig. 3.4b. This indicated that the diameter of latex particles showed a trend of decreasing and the latex became more transparent with an increase in surfactant concentration.

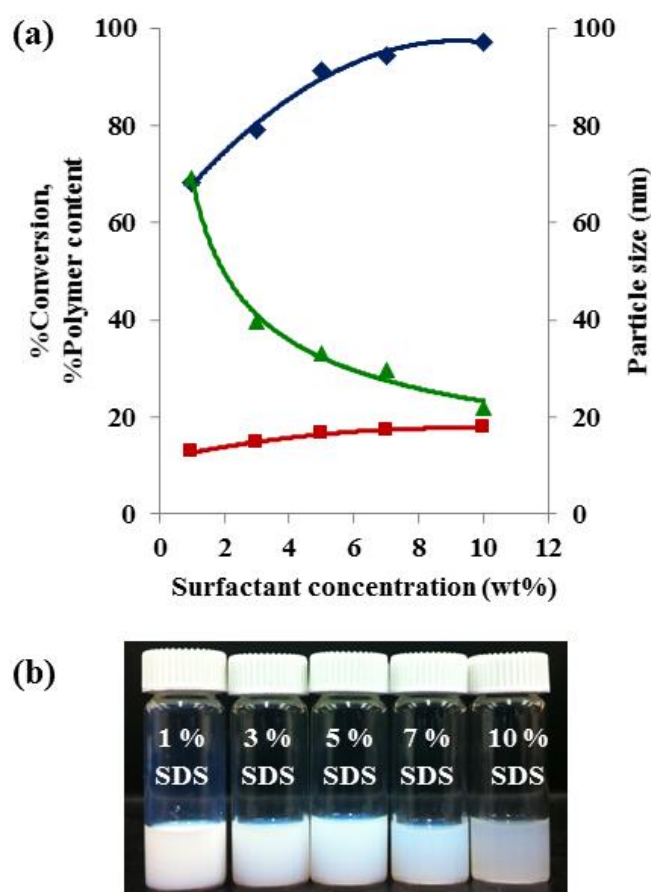


**Figure 3. 4** Effect of surfactant concentration on; (a) (◆) %Conversion, (■) %Polymer content, (▲) Particle size and (b) characteristic of the latex. Condition:  $M/H_2O = 0.2$ , KPS = 2 wt% based on monomer.

### 3.3.3 Effect of Initiator Concentration

From Figure 3.5a, the effects of the initiator concentration on the monomer conversion, polymer content and particle size of SBR nanoparticles could also be observed. It indicated that the particle size significantly increased from 15 nm to 53 nm with an increase in the initiator concentration from 0.5 to 3 wt% based on monomer. This can be explained in that at high level of the initiator concentration, more free radicals were generated [14, 110]. Thus, some dead polymer which occurred from combination of two radicals having carbon double bonds in the polymer chains could be initiated and propagated again resulting in a larger particle size. The monomer conversion increased from 14% to 88% and polymer content increased from 2.6% to 16% with an increase in the initiator concentration from 0.5 to 3 wt% based on monomer. This result could be explained in that increasing the initiator concentration resulted in more nucleation in the water phase. Moreover, more free radicals were generated and reacted with monomer to produce primary radicals and then the growing polymer chains increased resulting in an increase in monomer conversion and polymer content [108, 111]. Therefore, the appropriate condition for SBR nanoparticle synthesis via DMP was at a 0.2 M/H<sub>2</sub>O ratio, 3 wt% SDS and 2 wt% KPS providing high monomer conversion (80%) and small particle size (39 nm)

The effect of initiator concentration on the characteristic of the SBR nanoparticle latex is shown in Figure 3.5b which indicated that with a decrease in the particle size, the emulsion became more transparent.

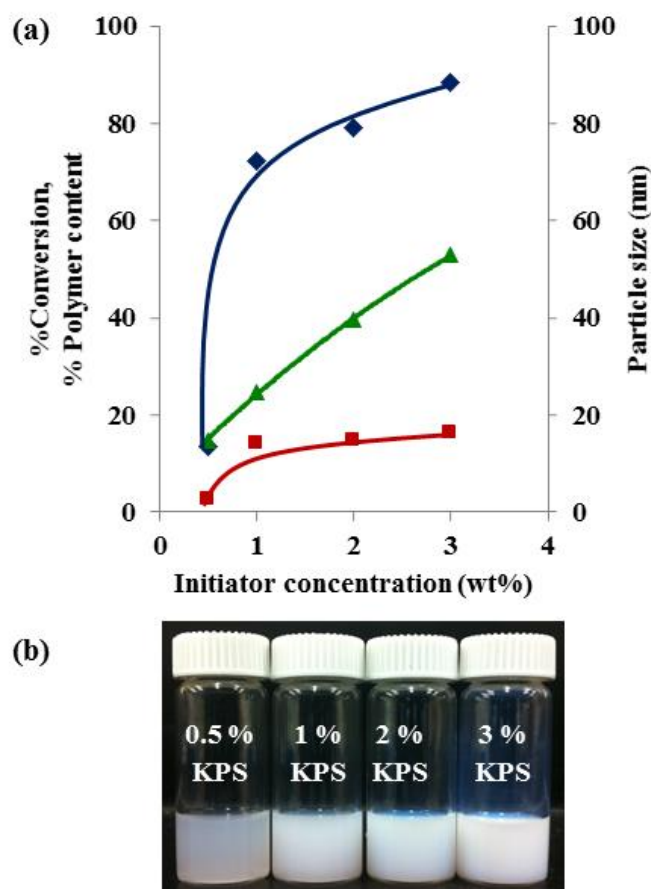


**Figure 3.5** Effect of initiator concentration on; (a) (◆) %Conversion, (■) %Polymer content, (▲) Particle size and (b) characteristic of the latex. Condition:  $M/H_2O = 0.2$ ,  $SDS = 3$  wt% based on monomer.

### 3.4 Morphology of SBR Nanoparticles

Morphology of SBR nanoparticles characterized by TEM is illustrated in Figure 3.6. It can be seen that the SBR nanoparticles with uniform size were spherical with a smooth surface and no agglomeration morphology of SBR nanoparticles was observed. The average particle size of SBR nanoparticle as seen from TEM photograph was about 35 nm in good agreement with the DLS characterization. From the particle size distribution of the SBR nanoparticles analyzed by the DLS technique as shown in Figure 3.8, a narrow size distribution ( $PDI = 1.19$ ) and homogeneous dispersion of nanosized SBR with an average particle size of 36 nm was observed.



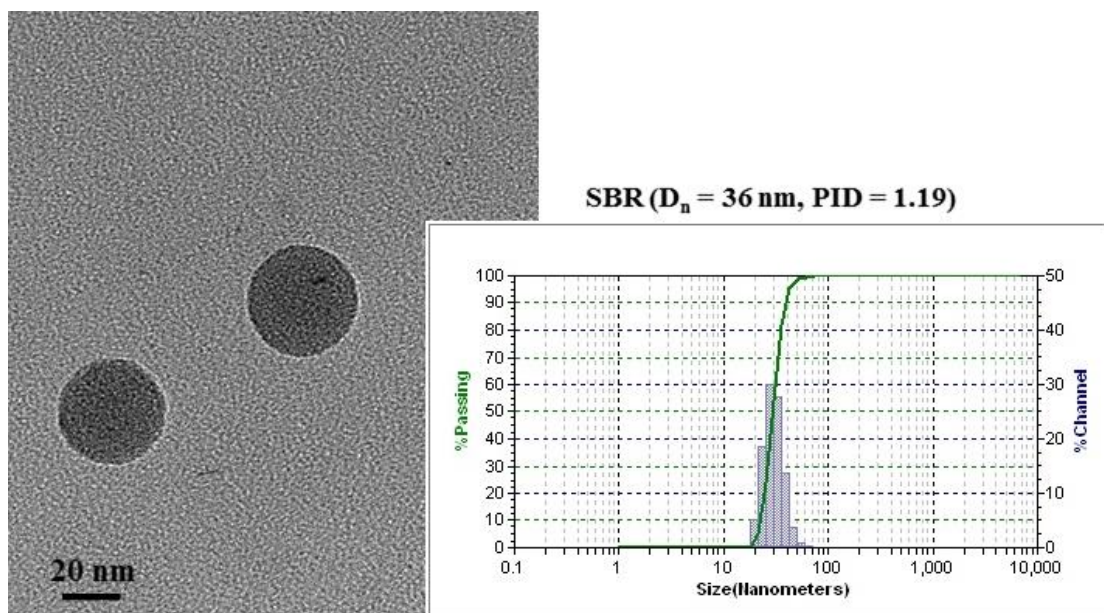


Figure 3. 6 TEM micrograph and particle size distribution of SBR nanoparticles. Condition: M/H<sub>2</sub>O = 0.3, SDS = 5 wt%, KPS = 2 wt% based on monomer.

## CHAPTER IV

### PREPARATION OF STYRENE BUTADIENE COPOLYMER-SILICA NANOCOMPOSITES VIA DIFFERENTIAL MICROEMULSION POLYMERIZATION AND NR/SBR-SiO<sub>2</sub> MEMBRANE FOR PERVAPORATION OF A WATER-ETHANOL MIXTURE

#### 4.1 Introduction

Polymer nanocomposites have attracted a great deal of interest because these materials possess high potential to achieve great property improvement by the addition of a small amount of nanoparticles into the polymer matrices. A critical challenge in the design of these hybrid inorganic-organic species is the control of the mixing between the two dissimilar phases. One method of achieving this is by differential microemulsion polymerization in which nanocomposites are formed by polymerization in the presence of inorganic component. Organic-inorganic nanocomposites were developed to form membranes for separation processes. In this research work, NR as a green polymer was used as the matrix for the NR/styrene butadiene copolymer (SBR)-SiO<sub>2</sub> nanocomposite membranes due to their low glass transition temperature ( $T_g$ ) and availability in latex form. Furthermore, NR can suppress the swelling of the polymeric structure and maintain the integrity of the membrane.

The purpose of the present work was to synthesize monodispersed SBR-SiO<sub>2</sub> nanocomposites via differential emulsion polymerization. The effect of silica loading, monomer to water ratio, surfactant concentration and initiator concentration on monomer conversion, grafting efficiency, silica encapsulation efficiency and particle size were studied. The prevulcanized blend of a natural rubber latex and SBR-SiO<sub>2</sub> nanoparticle was expected to possess good nanocomposite membrane properties for pervaporation.

## 4.2 Characterization of SBR-SiO<sub>2</sub> Nanocomposites

From the FTIR spectrum of modified SiO<sub>2</sub> (VTS-SiO<sub>2</sub>) as shown in Figure 4.1(a), the intensive absorption band at 1097, 800 and 473 cm<sup>-1</sup> are assigned to the vibration absorption of the Si-O-Si groups. A strong surface hydroxyl group (O-H) of silica is apparent at 3428 cm<sup>-1</sup>. Moreover, the peaks at 3061, 2957, 1612 and 1409 cm<sup>-1</sup> are attributed to C-H stretching, =CH<sub>2</sub> stretching, C=C stretching and C-H out of plain bending of the VTS group, respectively, which indicates the incorporation of VTS onto the silica surface [72].

From the spectrum of SBR-SiO<sub>2</sub> as shown in Figure 4.1(b), the new peaks at 2849 and 2916 cm<sup>-1</sup> correspond to C-H stretching in the CH<sub>2</sub> group of the styrene butadiene copolymer. For polystyrene units, the peaks at 1450, 1495 and 1695 cm<sup>-1</sup> are attributed to C-H in plain bending, C=C stretching and overtone C-H out of plain bending in the aromatic ring, respectively. Moreover, a C-H out of plain bending in the aromatic monosubstituted ring is apparent at 700 cm<sup>-1</sup>. For 1,2 polybutadiene units, a strong C=C stretching in CH<sub>2</sub>=CH- group is evident at 1639 cm<sup>-1</sup>. For 1,4 polybutadiene units, a =C-H stretching and C-H out of plain bending in RCH=CHR were obvious at 3025 and 971 cm<sup>-1</sup>, respectively [104]. These results indicate that the styrene butadiene copolymer has been successfully grafted onto the silica surface via differential microemulsion polymerization.

<sup>1</sup>H NMR was used to identify the copolymer composition and microstructure. A spectrum of SBR-SiO<sub>2</sub> is shown in Figure 4.2. As seen from the figure, the peak in the 6.7-7.3 ppm range corresponded only to the protons of styrene (2 ortho-H, 1 para-H and 2 meta-H, -C<sub>6</sub>H<sub>5</sub>), and the peak in the 5-5.75 ppm range represented the combined protons of 1,2-butadiene double bond (1H, -CH=CH<sub>2</sub>) and 1,4-butadiene double bond (2 cis-H and 2 trans-H, -CH=CH-), and the peak in the 4.6-5 ppm range was related to protons of 1,2-butadiene double bond (2H, -CH=CH<sub>2</sub>), while in the 1.2-2.5 ppm range the peaks are attributed to the protons of methyl and methylene. The molar ratio of butadiene to styrene in the nanocomposite, calculated from the area ratios as obtained by integration from the peak intensities, is around 1.5 [105].

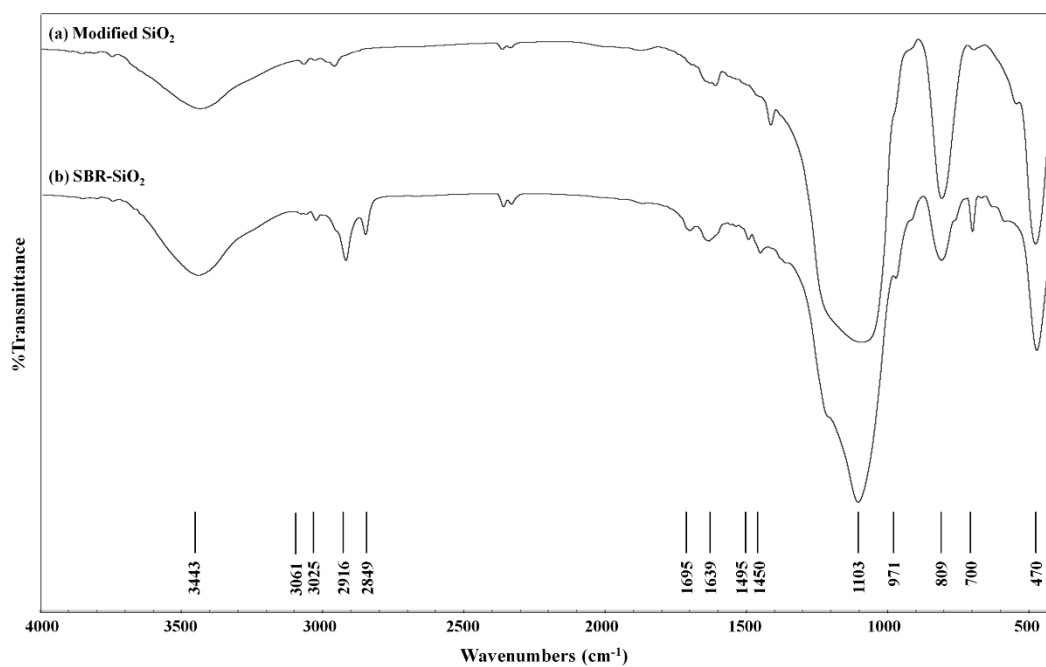


Figure 4.1 FTIR spectrum of (a) Modified SiO<sub>2</sub> and (b) SBR-SiO<sub>2</sub>.

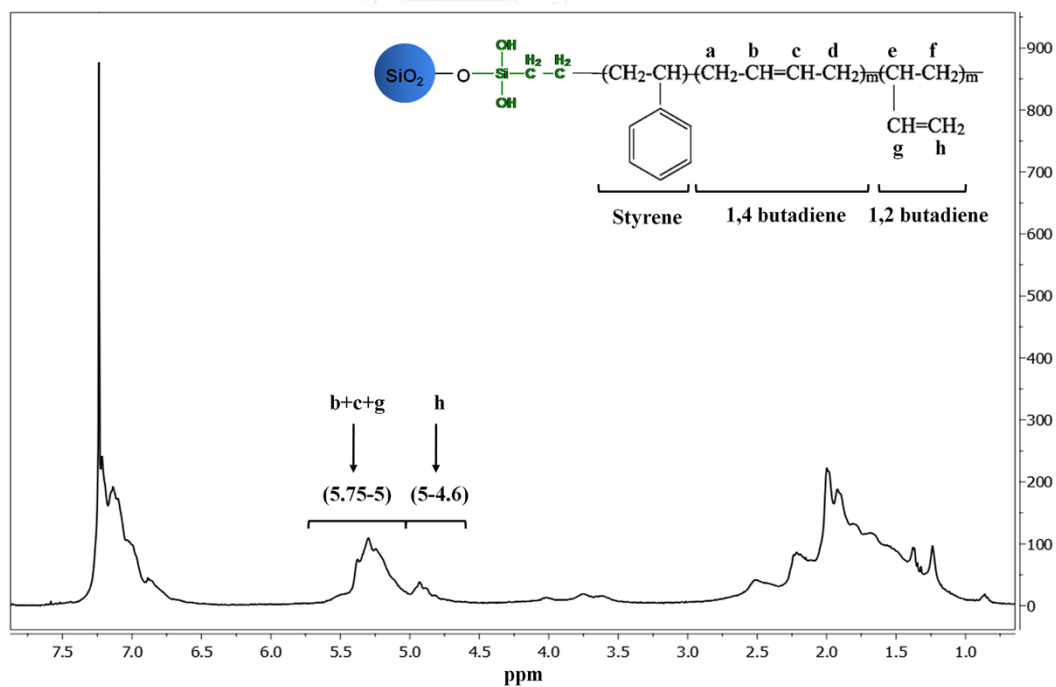


Figure 4.2 <sup>1</sup>H-NMR spectrum of SBR-SiO<sub>2</sub> in CDCl<sub>3</sub>.

### 4.3 Effect of Process Parameters

#### 4.3.1 Effect of Silica Loading

The effect of silica loading (5-20 wt% based on monomer) on SiO<sub>2</sub> encapsulation with SBR is shown in Figure 4.3. The monomer conversion and silica encapsulation efficiency decreased and particle size increased from 30 nm to 45 nm with an increase in silica loading from 5 to 20 wt%. These results indicated that the high level of silica loading tended to increase the aggregation of silica particles and decreased the encapsulated silica content resulting in a low silica encapsulation efficiency and large particle size. Moreover, the higher aggregation of silica particles may be the reason for the decrease in particle stability and monomer-swollen micelles and thus, the monomer conversion decreased [72]. Therefore, the appropriate silica loading in the system was in the range from 5 to 10 wt% providing a high monomer conversion (90-85%), high silica encapsulation efficiency (90-80%) and small particle size (30-35nm) via differential microemulsion polymerization.

From the effect of silica loading on the characteristics of the SBR-SiO<sub>2</sub> nanoparticles as shown in Figure 4.4a, the latex became more opaque with an increase in silica loading. However, the differential emulsion polymerization of ST and BD on modified SiO<sub>2</sub> could provide SBR-SiO<sub>2</sub> nanoparticles with a monodispersion of silica in the SBR latex resulting in a homogeneous composite latex. For the physical mixing of modified SiO<sub>2</sub> with the SBR latex (Figure 4.4b), it is clearly observed that the system has a two-phase dispersion of modified SiO<sub>2</sub> and SBR latex due to the hydrophilic surface of the silica particle. The hydrophilic surface caused a heterogeneity, free polymer formation and silica agglomeration which cannot be broken down with high speed shearing or milling via mechanical mixing. Therefore, the encapsulation of silica with SBR could enhance the compatibility and dispersion of silica in the SBR matrix, reduce the silica-silica interaction and achieve homogeneity of silica in the SBR latex.

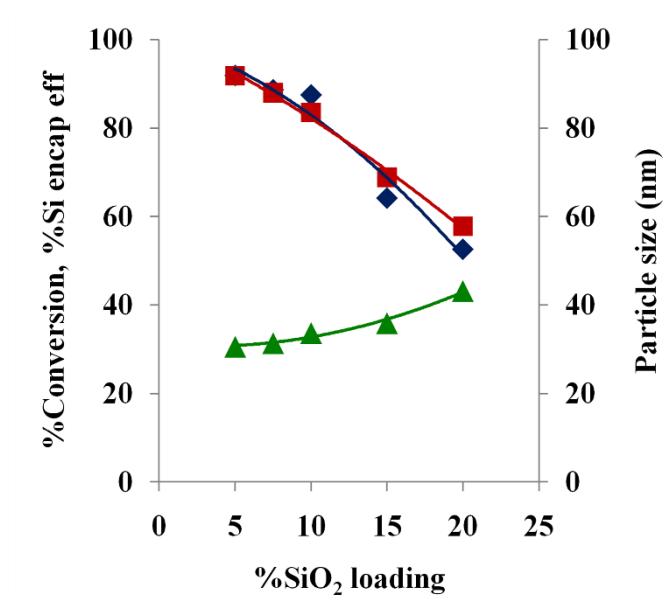


Figure 4. 3 Effect of silica loading on; (◆) %Conversion, (■) %Si encapsulation eff, (▲) Particle size. Condition: M/H<sub>2</sub>O = 0.2, SDS = 5 wt%, KPS = 2 wt% based on monomer.

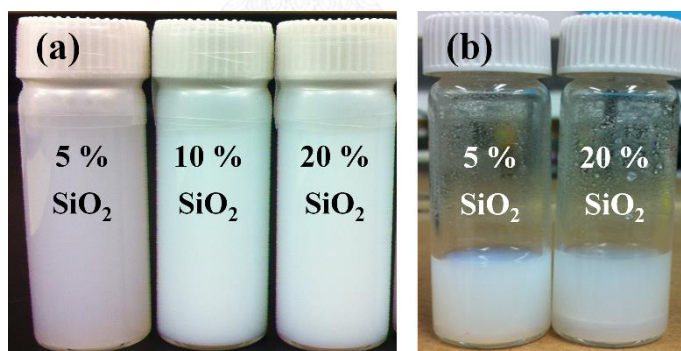
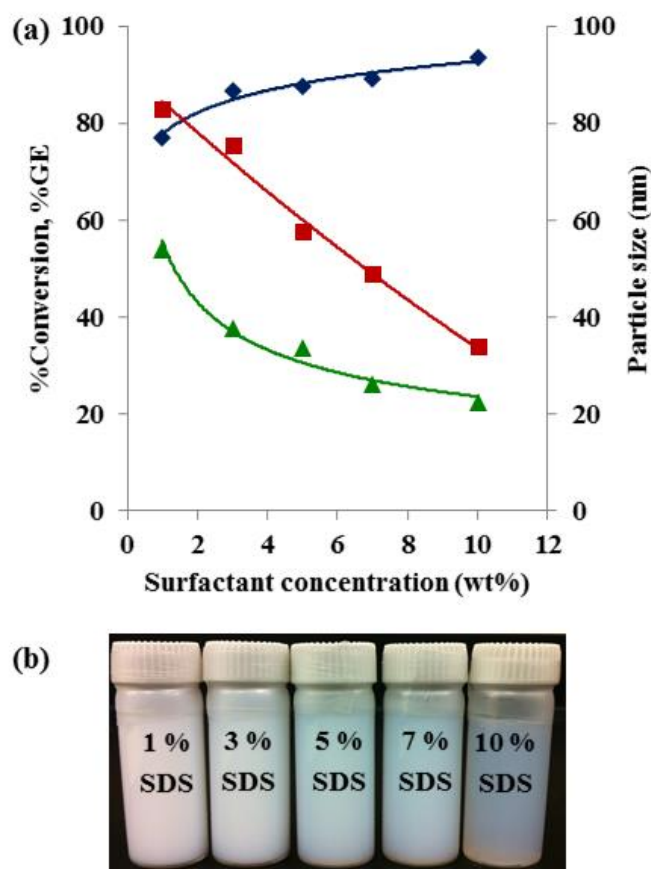


Figure 4. 4 Effect of (a) Silica encapsulated (b) Silica mixed with SBR on characteristic of the latex.

### 4.3.2 Effect of Surfactant Concentration

In this study, SDS was used as surfactant at a concentration above the critical micelle concentration (CMC). The surfactant concentration has a significant effect on monomer conversion, grafting efficiency and particle size as shown in Figure 4.5a. It can be seen that the particle size smoothly decreased from 54 nm to 22 nm with an increase in the surfactant concentration from 1 to 10 wt% based on monomer. This phenomenon can be explained in that when the SDS concentration reached the CMC, more surfactant generated more micelles. Therefore, more latex particles were produced resulting in a smaller particle size [14, 112]. Moreover, the monomer conversion increased with an increase in surfactant concentration. This can be explained in that a higher surfactant concentration may generate more micelles which give more reaction domains in the system resulting in a higher polymerization rate and monomer conversion [106, 107]. However, the grafting efficiency was decreased from 83% to 34% on increasing the surfactant concentration from 1 to 10 wt% based on monomer due to the fact that at the high surfactant concentration, free SBR (homopolymer) occurred rather than the encapsulation of SiO<sub>2</sub> within the SBR. This result can be explained in that when the surfactant concentration increased, the monomer was polymerized progressively faster and its chance to react with macroradicals was reduced resulting in limiting the graft copolymerization and favoring the homopolymerization [113].

The effect of surfactant concentration on the characteristics of the SBR-SiO<sub>2</sub> nanoparticle latex is shown in Figure 4.5b, which also indicates that with an increase in surfactant concentration, the diameter of latex particles shows a trend of decreasing and the latex becomes more transparent.



**Figure 4. 5** Effect of surfactant concentration on; (a) (◆) %Conversion, (■) %GE, (▲) Particle size. Condition and (b) characteristic of latex:  $\text{SiO}_2 = 10$  wt%,  $M/\text{H}_2\text{O} = 0.2$ , KPS = 2 wt% based on monomer.

### 4.3.3 Effects of Monomer to Water Ratio

The monomer to water ratio has an influence on the monomer conversion, grafting efficiency and particle size of SBR- $\text{SiO}_2$  encapsulation as illustrated in Figure 4.6. Particle size increased from 25 nm to 45 nm with an increase in the monomer to water ratio from 0.1 to 0.5. This is due to the fact that when the monomer to water ratio was high, resulting in significant collisions, aggregation of nanoparticles occurred [12, 107]. As the monomer to water ratio increased, the monomer conversion and grafting efficiency increased and reached a maximum at a monomer to water ratio of 0.3. Beyond the maximum point, the monomer conversion and grafting efficiency



decreased slightly. This implied that at higher monomer to water ratio, copolymerization of ST and BD to form SBR is more pronounced than graft copolymerization of ST and BD onto SiO<sub>2</sub>. Hence, at high monomer to water ratio, the grafting has a lower active surface area at the reaction site resulting in a lower grafting efficiency. Moreover, most of the further added monomer molecules could diffuse into the existing polymer particles, which were larger than the newly nucleated particles, and monomer diffusion into the polymer particles required more time resulting in a decrease in monomer conversion [114]. Thus, the decreasing monomer conversion at the high monomer to water ratio showed a similar trend on grafting efficiency. The monomer conversion (98%) and grafting efficiency (78%) were maximized at a monomer to water ratio of 0.3 at which a small particle size (39 nm) was achieved.

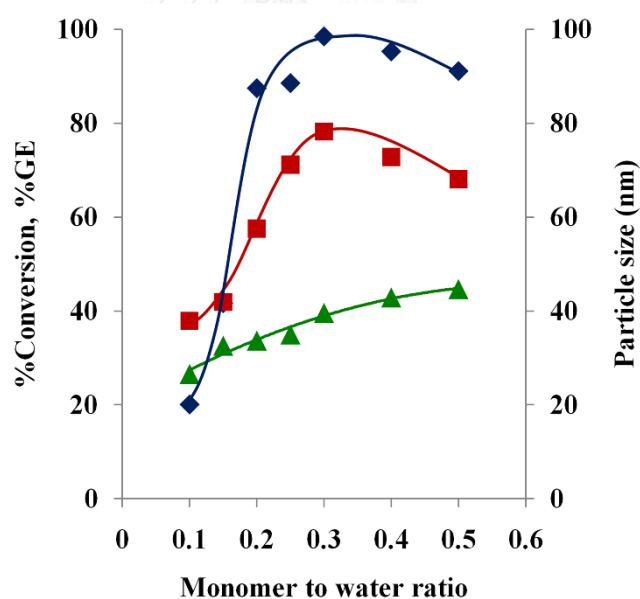


**Figure 4. 6** Effect of monomer to water ratio ( $M/H_2O$ ) on; (◆) %Conversion, (■) %GE, (▲) Particle size. Condition: SiO<sub>2</sub> = 10 wt%, SDS = 5 wt%, KPS = 2 wt% based on monomer.

#### 4.3.4 Effect of Initiator Concentration

The initiator concentration significantly affected the encapsulation of SiO<sub>2</sub> with SBR as shown in Figure 4.7. It indicated that as the initiator concentration was increased over the range of 0.5-4 wt% based on monomer; the particle size increased. This can be explained in that at high initiator concentration, the formation of more active sites caused an increase in the number of free radicals that one particle could share and then some dead polymer particles were initiated resulting in the larger particle size [14]. Monomer conversion increased from 5 to 90% with an increase in the initiator concentration. This can be explained in that, the higher KPS concentration generated more free radicals and the radicals reacted with monomer to produce primary radicals and then the growing polymer chains increased; thus the monomer conversion increased rapidly [108, 111]. Moreover, the grafting efficiency decreased slightly with an increase in initiator concentration due to the fact that more free SBR resulted than grafting of SBR onto the silica surface.

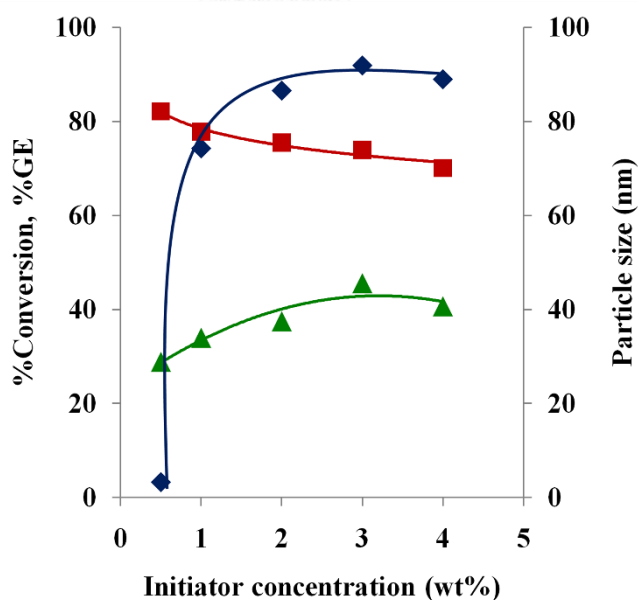


**Figure 4. 7** Effect of initiator concentration on; (◆) %Conversion, (■) %GE, (▲) Particle size. Condition: SiO<sub>2</sub> = 10 wt%, M/H<sub>2</sub>O = 0.2, SDS = 3 wt% based on monomer.

#### 4.4 Morphology of SBR-SiO<sub>2</sub> Nanocomposites

The morphology of SBR-SiO<sub>2</sub> nanocomposites from TEM is shown in Figure 4.8. From Figure 4.8a-c, representative TEM images of SBR-SiO<sub>2</sub> core-shell nanocomposites at different surfactant concentrations, 1 wt%, 3 wt% and 10 wt%, respectively, were obtained. The darker areas represent the silica core regions and the lighter areas illustrate the SBR encapsulated onto the silica surface as the shell. The modified SiO<sub>2</sub> was completely encapsulated with SBR. In addition, the thickness of the SBR shell decreased with increasing surfactant concentration. This implies that the grafting efficiency decreased with an increasing surfactant concentration resulting in a reduction in the SBR shell thickness. However, the silica nanoparticles were well dispersed in the SBR latex. A uniform size and core-shell spherical morphology of the SBR-SiO<sub>2</sub> nanocomposite was produced and no agglomeration morphology of composite particles was observed. For SBR/untreated SiO<sub>2</sub> (Figure 4.8d), morphology of silica agglomeration and free SBR were predominantly observed. This can be explained in that the silica surface with hydroxyl groups (-OH) have the highest polarity which leads to agglomeration of the nanoparticles causing poor dispersion capacity, inferior compatibility and a lower stability in the polymer matrix. Thus, the monodispersed SBR-SiO<sub>2</sub> nanocomposites with core-shell morphology have been successfully synthesized via differential microemulsion polymerization.

Table 4.1 presents a comparison of the SBR-SiO<sub>2</sub> size and shell thickness measured by the DLS technique and TEM images. From the effect of surfactant and initiator concentration, the difference of SBR-SiO<sub>2</sub> diameter ( $\Delta D_n$ ) and SBR shell thickness ( $\Delta S$ ) measured by the DLS technique and TEM images are 0.1 – 0.6 nm and 0.2 – 0.5 nm, respectively. This clearly confirms that the sizes of SBR-SiO<sub>2</sub> nanoparticles, SiO<sub>2</sub> core and SBR shell determined by the TEM images are consistent with those obtained using the DLS technique.

The formation mechanism of SBR-SiO<sub>2</sub> core-shell nanoparticles is illustrated in Figure 4.9. The modified SiO<sub>2</sub>, SDS surfactant and KPS initiator were dispersed in deionized water to form a homogeneous solution (Figure 4.9a). The SDS surfactant creates micelles in the system, where the hydrophobic tails form the core of organic

phase and the hydrophilic heads turn towards the aqueous phase, and could stabilize the colloidal particles. For differential microemulsion polymerization, small amounts of ST and BD monomers diffused through the water to the micelle and the KPS initiator decomposed in the aqueous phase generating free radicals that produce reactive monomer radicals on the monomer molecule and silica surface for the initiation stage (Figure 4.9b). The monomer radicals were reacted with other monomer molecules to produce the oligomeric radicals to produce growing chains in the propagation stage (Figure 4.9c). Hence, the styrene butadiene copolymer could graft onto the silica surface via encapsulation with a  $\text{SiO}_2$  core and SBR shell.

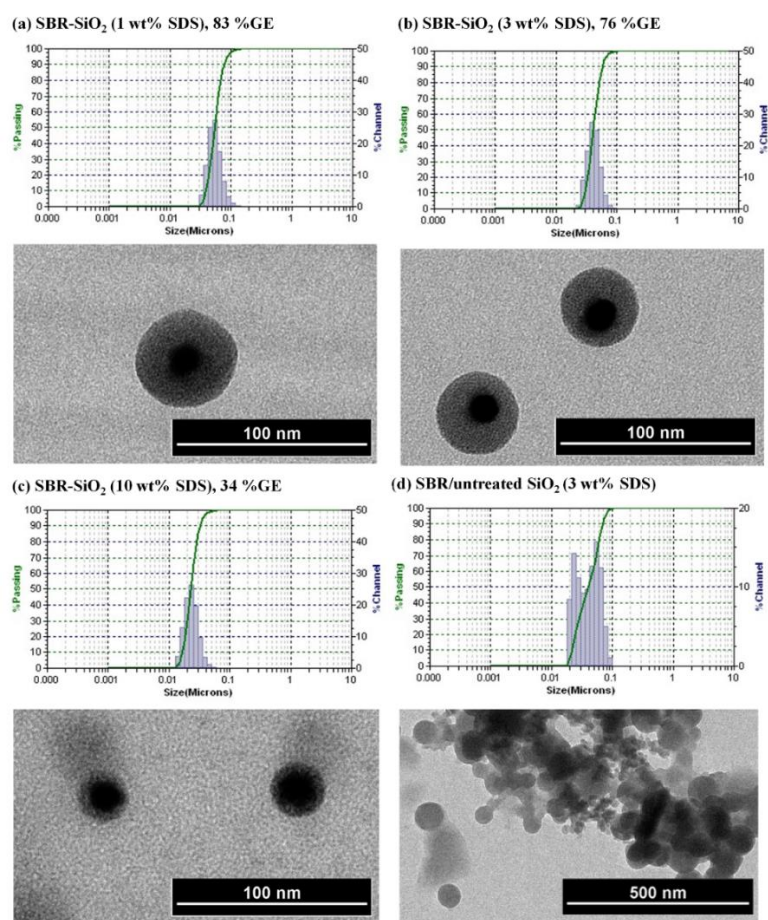


**Figure 4. 8** TEM imaging of composite samples (a) SBR- $\text{SiO}_2$  (1 wt% SDS), (b) SBR- $\text{SiO}_2$  (3 wt% SDS), (c) SBR- $\text{SiO}_2$  (10 wt% SDS) and (d) SBR/untreated  $\text{SiO}_2$  (3 wt% SDS) at 10 wt% silica loading. Condition:  $\text{SiO}_2$  = 10 wt%, M/ $\text{H}_2\text{O}$  = 0.2, KPS = 2 wt% based on monomer.

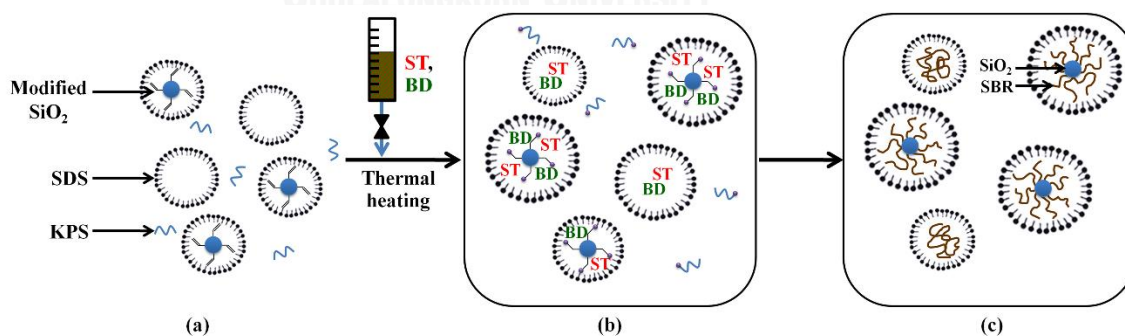
**Table 4. 1** The sizes of SBR-SiO<sub>2</sub> nanoparticle, SiO<sub>2</sub> core and SBR shell.

Effects	Measured by DLS		Measured by TEM		
	SBR-SiO <sub>2</sub> diameter (nm) <sup>a</sup>	SBR shell thickness (nm) <sup>b</sup>	SBR-SiO <sub>2</sub> diameter (nm)	SiO <sub>2</sub> core diameter (nm)	SBR shell thickness (nm) <sup>b</sup>
	<b>Effect of surfactant concentration</b>				
1 %SDS	54.0	21.0	54.1	13.0	20.6
3 %SDS	37.5	12.8	37.8	13.3	12.3
7 %SDS	26.0	7.0	25.5	12.5	6.5
10 %SDS	22.5	5.3	23.0	13.3	4.9
<b>Effect of initiator concentration</b>					
1 %KPS	34.0	11.0	34.4	12.8	10.8
2 %KPS	37.5	12.8	37.1	12.5	12.3
3 %KPS	45.6	16.8	46.2	13.0	16.6
4 %KPS	40.7	14.4	40.2	12.3	14.0

<sup>a</sup> SBR-SiO<sub>2</sub> size is based on the number-average size measured by DLS technique.

<sup>b</sup>  $S_{DLS} = (D_{n, DLS} - D_{c, DLS})/2$ ,  $D_{c, DLS} = 12$  nm and  $S_{TEM} = (D_{n, TEM} - D_{c, TEM})/2$

$D_n$  = SBR-SiO<sub>2</sub> diameter,  $D_c$  = SiO<sub>2</sub> diameter,  $S$  = SBR shell thickness

**Figure 4. 9** A schematic of formation mechanism of SBR-SiO<sub>2</sub> core-shell nanoparticles.

#### 4.5 Thermal Properties of NR/SBR-SiO<sub>2</sub> Nanocomposite Membranes

For preparation of NR/SBR-SiO<sub>2</sub> nanocomposite membranes, SBR-SiO<sub>2</sub> at 10 wt% of silica loading was selected to blend with the NR latex. DSC was used to determine the glass transition temperature ( $T_g$ ) of the nanocomposites. The  $T_g$  of the nanocomposite membranes with different NR to SBR-SiO<sub>2</sub> ratio and amount of SiO<sub>2</sub> are presented in Table 4.2. From the DSC thermograms, the NR/SBR-SiO<sub>2</sub> membranes exhibit a single  $T_g$  due to the good dispersion of SBR-SiO<sub>2</sub> in the NR matrix. The encapsulation of the SiO<sub>2</sub> core by the SBR shell enhanced the good compatibility and dispersion of SiO<sub>2</sub> in the NR matrix resulting in the homogeneity of the NR/SBR-SiO<sub>2</sub> composite. The  $T_g$  of nanocomposites shifted to a higher temperature with the addition of SBR-SiO<sub>2</sub> into the NR matrix. This can be explained in that the nanosized SiO<sub>2</sub> can move easier than the polymer chain and this movement of SiO<sub>2</sub> would limit that of the polymer chain (chain restriction). Thus, the  $T_g$  was increased with increasing SBR-SiO<sub>2</sub> in the NR matrix. The nanosized SiO<sub>2</sub> has a great influence on the  $T_g$  of the NR/SBR-SiO<sub>2</sub> composite and the high level of SiO<sub>2</sub> (4 wt% SiO<sub>2</sub>) in the composite tended to decrease the chain segment movement resulting in a high  $T_g$  (-57.3°C) compared with NR (-63.6 °C). Moreover, the  $T_g$  of NR/SBR-SiO<sub>2</sub> nanocomposite membranes were higher than that of unfilled NR ( $\Delta T_g = 2.4 - 6.3$  °C), which indicated a lower mobility and flexibility of the polymer chains by the addition of rigid particles [72].

TGA was used to measure the initial decomposition temperature ( $T_{id}$ ) and the maximum decomposition temperature ( $T_{max}$ ). The NR and NR/SBR-SiO<sub>2</sub> nanocomposite membranes showed one-step polymer degradation and provided smooth weight loss curves. The  $T_{id}$  and  $T_{max}$  of all nanocomposite membrane samples are summarized in Table 4.2. The  $T_{max}$  increased from 381.5 °C to 395.2 °C with an increasing SBR-SiO<sub>2</sub> loading in the membrane from 0 to 40 wt% (SiO<sub>2</sub> content = 0 – 4 wt%). The  $T_{max}$  of NR/SBR-SiO<sub>2</sub> nanocomposite membranes were higher than that of unfilled NR. This result implies that SBR-SiO<sub>2</sub> could be uniformly dispersed in the NR matrix resulting in the high thermal stability of nanocomposite membrane.

**Table 4. 2** Thermal properties of NR/SBR-SiO<sub>2</sub> nanocomposites membranes.

NR/SBR-SiO <sub>2</sub> <sup>a</sup> (wt/wt)	SiO <sub>2</sub> content <sup>b</sup> (wt%)	T <sub>g</sub> (°C)	T <sub>id</sub> (°C)	T <sub>max</sub> (°C)
100/0	-	-63.6	354.0	381.5
90/10	1.0	-61.2	353.9	383.4
80/20	2.0	-60.0	353.6	388.2
70/30	3.0	-58.6	355.6	391.9
60/40	4.0	-57.3	353.6	395.2

<sup>a</sup> SBR-SiO<sub>2</sub> preparation condition: M/H<sub>2</sub>O = 0.2, SiO<sub>2</sub> = 10 wt%, SDS = 5 wt%, KPS = 2 wt% based on monomer.

<sup>b</sup> Silica content based on total rubber.

#### 4.6 Mechanical Properties of NR/SBR-SiO<sub>2</sub> Nanocomposite Membranes

The effect of SBR-SiO<sub>2</sub> loading on the ratio of NR to SBR-SiO<sub>2</sub> of 100/0, 90/10, 80/20 70/30 and 60/40 (equivalent to 0%, 1%, 2%, 3% and 4% silica content in all membranes, respectively) on mechanical properties of nanocomposite membranes are illustrated in Table 4.3. The tensile strength, modulus and elongation at break of NR/SBR-SiO<sub>2</sub> nanocomposite membranes were significantly affected by the addition of SBR-SiO<sub>2</sub>. From Table 4.3, the tensile strength and modulus at 300% strain of all NR/SBR-SiO<sub>2</sub> nanocomposite membranes were higher than that of unfilled NR. The tensile strength was increased from 17.6 MPa to 25.6 MPa and the modulus at 300% strain was increased from 1.35 MPa to 1.58 MPa with an increase in SBR-SiO<sub>2</sub> loading from 0 to 40 wt% (SiO<sub>2</sub> content = 0 – 4 wt%). This indicated that SBR-SiO<sub>2</sub> nanoparticles could increase the external force resistance due to the high interaction between the silica nanoparticle and the NR matrix, well dispersed SBR-SiO<sub>2</sub> nanoparticles and reduction of silica agglomeration resulting in improvement in the tensile strength and modulus of the nanocomposite membrane [115]. Furthermore, the elongation at break was decreased from 842% to 798% with increasing SBR-SiO<sub>2</sub> loading from 0 to 40 wt% due to the hard and stiff nature of the silica particles [72].

**Table 4. 3** Mechanical properties of NR/SBR-SiO<sub>2</sub> nanocomposites membranes.

NR/SBR-SiO <sub>2</sub> <sup>a</sup> (wt/wt)	SiO <sub>2</sub> content <sup>b</sup> (wt%)	Tensile strength (MPa)	300% Modulus (MPa)	Elongation at break (%)
100/0	-	17.6 ± 1.2	1.35 ± 0.1	842 ± 11
90/10	1.0	19.8 ± 1.1	1.42 ± 0.09	829 ± 15
80/20	2.0	22.1 ± 1.6	1.49 ± 0.07	820 ± 22
70/30	3.0	24.9 ± 1.3	1.55 ± 0.07	812 ± 18
60/40	4.0	25.6 ± 2.8	1.58 ± 0.05	798 ± 31

<sup>a</sup> SBR-SiO<sub>2</sub> preparation condition: M/H<sub>2</sub>O = 0.2, SiO<sub>2</sub> = 10 wt%, SDS = 5 wt%, KPS = 2 wt% based on monomer.

<sup>b</sup> Silica content based on total rubber.

## 4.7. Pervaporation

### 4.7.1. Effect of SBR-SiO<sub>2</sub> Loading

The separation of a water-ethanol mixture via pervaporation through a NR/SBR-SiO<sub>2</sub> nanocomposite membrane was investigated. For the pervaporation of a water-ethanol mixture (5 vol% water), the effect of SBR-SiO<sub>2</sub> loading on the permeate flux is illustrated in Figure 4.10a. It can be seen that the permeate flux was significantly affected by SBR-SiO<sub>2</sub> loading in the membrane. The total permeate flux increased from 80 to 425 g/m<sup>2</sup>h with increasing SBR-SiO<sub>2</sub> loading from 10 wt% to 40 wt%. Additionally, the partial water flux had a similar trend to the total permeate flux. The diffusion of water molecules became faster due to the fact that a higher SBR-SiO<sub>2</sub> loading would provide more reactive hydroxyl groups in the membrane resulting in a stronger interaction between the membrane and water. Thus, more water molecules can be adsorbed and diffuse through the membrane [116]. This also implies that the reactive hydroxyl groups are more pronounced than chain restriction in the membrane ( $T_g$  increment). Moreover, SBR-SiO<sub>2</sub> is uniformly dispersed in the NR matrix in both the surface and bulk membrane. Nevertheless, the emulsion (Si encap. eff. = 78%) consisted of completely encapsulated SiO<sub>2</sub> by the SBR shell (78%) and incompletely








encapsulated and free SiO<sub>2</sub> (22%) resulting in the hydrophilicity of the NR/SBR-SiO<sub>2</sub> membrane. These results are consistent with contact angle measurements as illustrated in Table 4.4. The water contact angle decreased with an increasing SBR-SiO<sub>2</sub> loading in the membrane. This result indicated that the reactive hydroxyl groups of the SBR-SiO<sub>2</sub> nanoparticle exhibited an enhanced effect on the hydrophilic surface of the membrane. In addition, the highly dispersed silica nanoparticle in the membrane could interfere with the tight packing of polymer chains, which makes the diffusion of water molecules through the membranes easier [103, 116]. Moreover, the total permeate fluxes and partial water fluxes overlap each other due to the small difference of total permeate fluxes and partial water fluxes of about 2-3 g/m<sup>2</sup>h and both were significantly greater than the partial ethanol fluxes suggesting that the membranes are highly water selective [117]. The effect of SBR-SiO<sub>2</sub> loading on the pervaporation selectivity at 5 vol% water in the feed water-ethanol mixture is shown in Figure 4.10b. The increasing SBR-SiO<sub>2</sub> loading in the membrane strongly affected the pervaporation efficiency. It is obviously seen that the pervaporation selectivity increased with increasing SBR-SiO<sub>2</sub> loading. The selectivity and water flux of the NR/SBR-SiO<sub>2</sub> membranes increased due to the fact that hydrophilicity of nanosized SiO<sub>2</sub> is favorable to the adsorption, diffusion and permeation of water molecules. Moreover, the highly dispersed SBR-SiO<sub>2</sub> has an active surface, which could change the membrane structure, resulting in easier permeation of water molecules [116].

Our results for selective pervaporation of water-ethanol mixtures could be compared with works reported earlier in terms of a flux dependence on filler loading. Aside from the silica filled membrane, the NR/PVA semi-IPN membrane incorporating a zeolite was also prepared for pervaporation dehydration of water-ethanol mixtures. The permeation flux and separation factor were improved by increasing the zeolite loading and a high permeation flux of 2,350 g/m<sup>2</sup>h with a high separation factor of 2,100 was provided at high zeolite loading of 10 wt% [117]. However, research on pervaporation using a silica filled membrane at low silica loading gave similar results. Liu et al. reported a high permeation flux of 410 g/m<sup>2</sup>h with a separation factor of 919 for pervaporation dehydration of an ethanol-water solution using chitosan-silica complex membranes with 5 wt% SiO<sub>2</sub> loading [99]. Recently, Sun et al. reported a

permeation flux of 114 g/m<sup>2</sup>h for separation of ethanol from water via pervaporation using hydrophobic silica filled PDMS composite membranes with 5 wt% silica loading [103]. From the present research work on pervaporation of a water-ethanol solution, a high permeation flux of 425 g/m<sup>2</sup>h and a high separation factor of 2,976 could be obtained by using NR/SBR-SiO<sub>2</sub> membranes at a low SiO<sub>2</sub> loading of 4 wt%. Thus, it can be concluded that the permeation flux is also strongly dependent on the polymer and filler types providing hydrophilicity to the membrane.

**Table 4. 4** Contact angle of NR/SBR-SiO<sub>2</sub> nanocomposite membranes.

NR/SBR-SiO <sub>2</sub> <sup>a</sup> (wt/wt)	SiO <sub>2</sub> content <sup>b</sup> (wt%)	Contact angle in degree	Water droplet
100/0	-	110.1±0.3	
90/10	1.0	100.5±1.0	
80/20	2.0	92.3±0.2	
70/30	3.0	85.5±0.6	
60/40	4.0	77.4±2.6	

<sup>a</sup> SBR-SiO<sub>2</sub> preparation condition: M/H<sub>2</sub>O = 0.2, SiO<sub>2</sub> = 10 wt%, SDS = 5 wt%, KPS = 2 wt% based on monomer.

<sup>b</sup> Silica content based on total rubber.

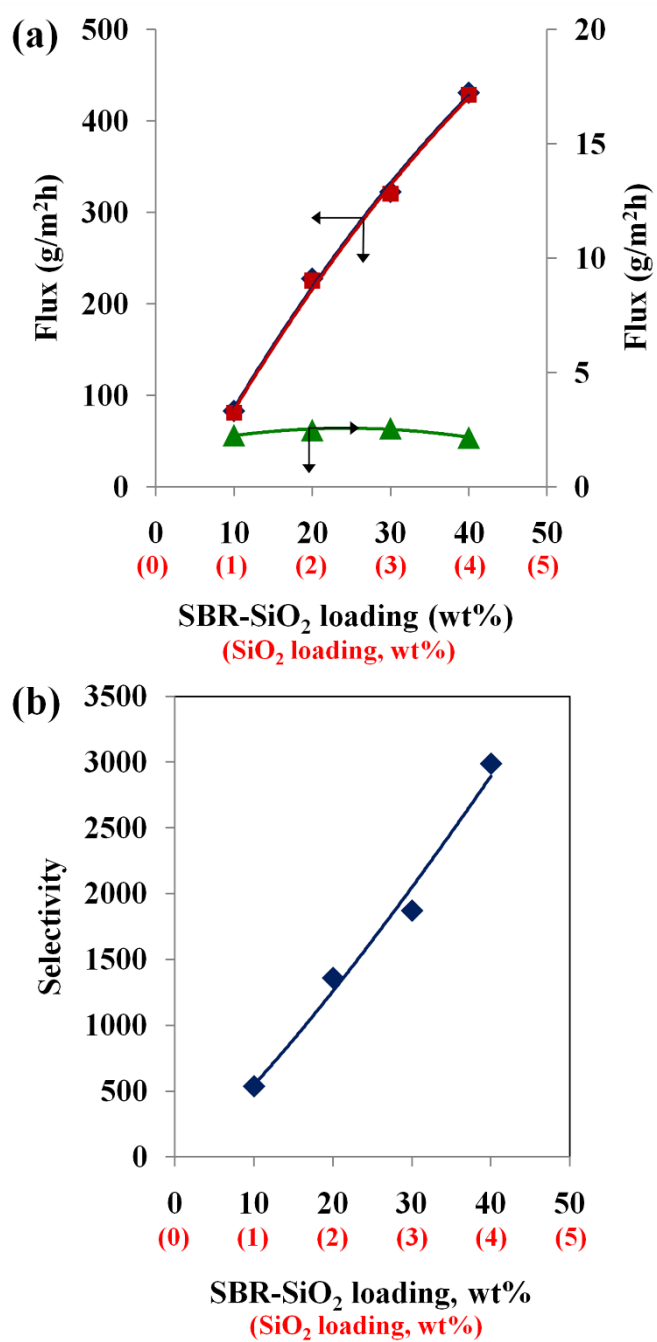
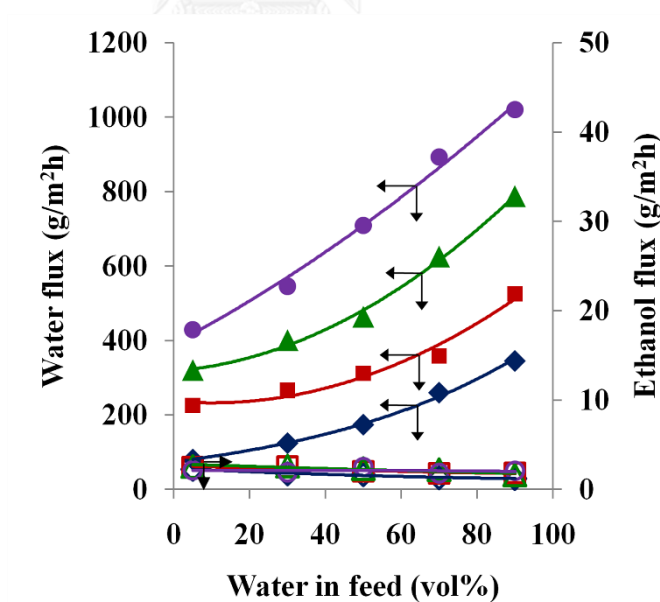


Figure 4. 10 Effect of SBR-SiO<sub>2</sub> loading (wt%) in membrane on; (a) total permeate fluxes (◆), partial water flux (■) and partial ethanol flux (▲) and (b) pervaporation selectivity at 5 vol% water concentration in feed.

#### 4.7.2 Effect of Feed Composition

The effect of feed water concentration on the partial fluxes of water and ethanol through the NR/SBR-SiO<sub>2</sub> nanocomposite membrane are shown in Figure 4.11. Obviously, the partial water fluxes increased on increasing the feed water concentration as well as the SBR-SiO<sub>2</sub> loading. On the opposite side, the partial ethanol flux was slightly decreased when increasing the feed water concentration. This result implies that with more reactive hydroxyl groups in the membrane, water molecules pass through the membrane faster, leading to a higher permeation flux. Furthermore, with an increase in feed water concentration, the free volume in the membrane was increased, which led to an increase in the partial water flux. The water molecules can permeate easily because the volume of the water molecule is smaller than that of ethanol, and SiO<sub>2</sub> nanoparticles in the membrane cause water molecules to permeate more easily [99, 116]. Thus, the composite membrane yields a higher water flux and a lower ethanol flux.



**Figure 4. 11** Effect of water concentration (vol%) in feed on partial water and partial ethanol fluxes for NR/SBR-SiO<sub>2</sub> nanocomposite membranes with SBR-SiO<sub>2</sub> loading of 10 wt% (◆, ◇), 20 wt% (■, □), 30 wt% (▲, △) and 40 wt% (●, ○).

## CHAPTER V

### SYNTHESIS OF POLYBUTADIENE-SILICA NANOPARTICLES VIA DIFFERENTIAL MICROEMULSION POLYMERIZATION AND THEIR HYDROGENATED NANOPARTICLES BY DIIMIDE REDUCTION

#### 5.1 Introduction

Encapsulation is regarded as being of major importance since it offers interesting potential applications of nanocomposite materials in different fields. Thus, encapsulation of nanosilica with polymers can improve the compatibility of nanosilica in the rubber matrix resulting in an improvement of filler dispersion and performance of the rubber composite. However, rubbers such as polybutadiene (PB) suffer from a drawback in their thermal and ozone stability due to the C=C in their polymer backbones. The C=C of the rubber are sensitive to oxygen, ozone and heat resulting in rubber degradation and the reduction of mechanical and thermal properties. Hydrogenation of diene-based rubbers is an important process to obtain hydrogenated rubber and improve their thermal properties and oxidative.

In the present study, we propose to synthesize monodispersed PB-SiO<sub>2</sub> nanocomposites via differential microemulsion polymerization (DMP) and hydrogenated polybutadiene (HPB)-SiO<sub>2</sub> nanocomposites by diimide reduction. For DMP, the effect of silica loading, surfactant concentration, monomer to water ratio and initiator concentration on monomer conversion, grafting efficiency, silica encapsulation efficiency and particle size were studied. For diimide reduction as a green process of hydrogenation, the influence of hydrazine hydrate and hydrogen peroxide concentration on the hydrogenation degree and particle size were also investigated. For rubber application, the mechanical properties of tensile strength, modulus and elongation at break, the thermal properties of glass transition temperature and decomposition temperature, and ozone resistance of NR/PB-SiO<sub>2</sub> and NR/HPB-SiO<sub>2</sub> composites were studied.

## 5.2 Characteristics of PB-SiO<sub>2</sub> and HPB-SiO<sub>2</sub>

The spectra of SiO<sub>2</sub> and modified SiO<sub>2</sub> are shown in Figure 5.1a. For SiO<sub>2</sub>, the intensive absorption bands at 1097, 800 and 473 cm<sup>-1</sup> are assigned to the vibration absorption of the Si-O-Si groups and the peak at 3428 cm<sup>-1</sup> is attributed to the strong surface hydroxyl group (O-H) of silica. For modified SiO<sub>2</sub>, the new peaks at 3061, 2957, 1612 and 1409 cm<sup>-1</sup> relate to C-H stretching, =CH<sub>2</sub> stretching, C=C stretching and C-H out of plane bending of the VTS group, respectively. These results indicate that VTS could be bound on the silica surface [118].

The spectrum of PB-SiO<sub>2</sub> and HPB-SiO<sub>2</sub> are shown in Figure 5.1b. For the PB-SiO<sub>2</sub> composite particles, new peaks at 2846 and 2952 cm<sup>-1</sup> correspond to CH<sub>2</sub> stretching of PB. In addition, the peaks at 679, 1636 and 3064 cm<sup>-1</sup> relate to =CH out of plane deformation, C=C stretching and C-H stretching, respectively. The CH<sub>2</sub> twisting, CH<sub>2</sub> wagging and CH<sub>2</sub> in plane deformation are apparent at 909, 968, and 1410 cm<sup>-1</sup>, respectively [119]. These results imply that PB has been successfully grafted onto the silica surface via differential microemulsion polymerization. For the HPB-SiO<sub>2</sub> nanocomposite, peaks at 2923 and 2846 cm<sup>-1</sup> are related to the CH<sub>2</sub> asymmetrical stretching and CH<sub>2</sub> symmetrical stretching, respectively. The intensity bands at 1469, 1377 and 724 cm<sup>-1</sup> correspond to bending deformation, CH<sub>3</sub> symmetric deformation and rocking deformation of HPB, respectively. Moreover, the peak for C=C stretching at 1633cm<sup>-1</sup> was decreased. These results confirm that PB-SiO<sub>2</sub> was successfully hydrogenated via diimide reduction.

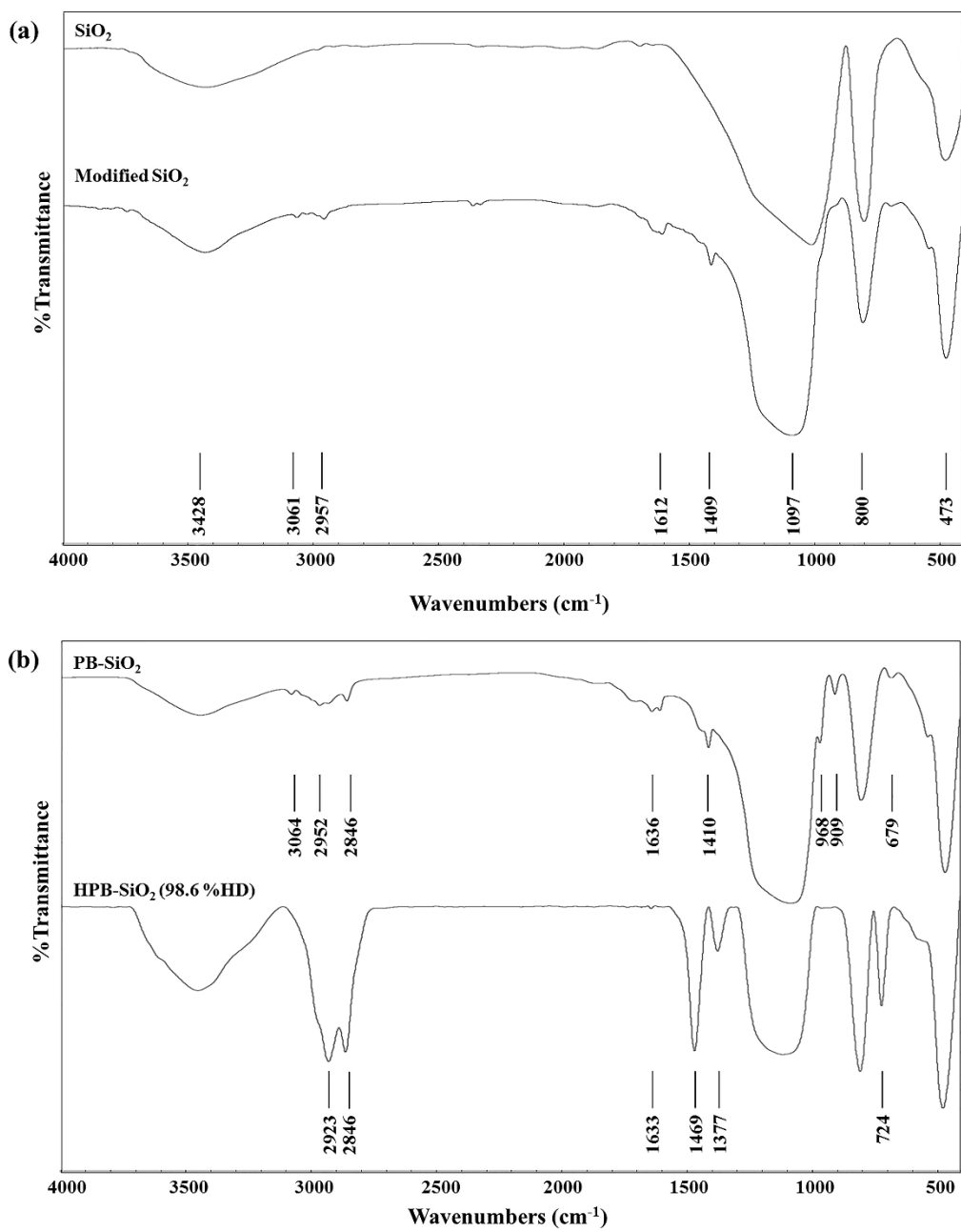


Figure 5. 1 FTIR spectrum of (a) SiO<sub>2</sub>, Modified SiO<sub>2</sub> and (b) PB-SiO<sub>2</sub>, HPB-SiO<sub>2</sub>.

### 5.3 Differential Microemulsion Polymerization (DMP)

#### 5.3.1 Effect of Silica Loading

Silica loading had a significant effect on monomer conversion, silica encapsulation efficiency and particle size as shown in Figure 5.2a. As the silica loading was increased from 5 to 20 wt% based on monomer, the monomer conversion and silica encapsulation efficiency decreased and particle size increased from 24 nm to 32 nm. These results imply that at a high level of silica loading, more aggregation of silica particles was produced resulting in an increase in particle size and a decrease in particle stability and number of monomer-swollen micelles; hence, the monomer conversion was decreased. In addition, some silica particles were not encapsulated at high silica loading resulting in a low silica encapsulation efficiency [72, 118]. Therefore, the appropriate silica loading in the system was in the range of 5 to 10 wt% providing a high monomer conversion (96-82%), high silica encapsulation efficiency (92-79%) and small particle size (24-27 nm) via DMP. The effect of silica loading on the characteristics of PB-SiO<sub>2</sub> nanoparticles as shown in Figure 5.2b, illustrated that the latex became more transparent with a decrease in silica loading; however, nano-SiO<sub>2</sub> particles were well dispersed in the PB latex resulting in a homogeneous composite latex. Therefore, the encapsulation of silica with PB via DMP could enhance the compatibility and dispersion of silica in the PB matrix, reduce the silica-silica interaction and yield homogeneity of silica in the PB latex.



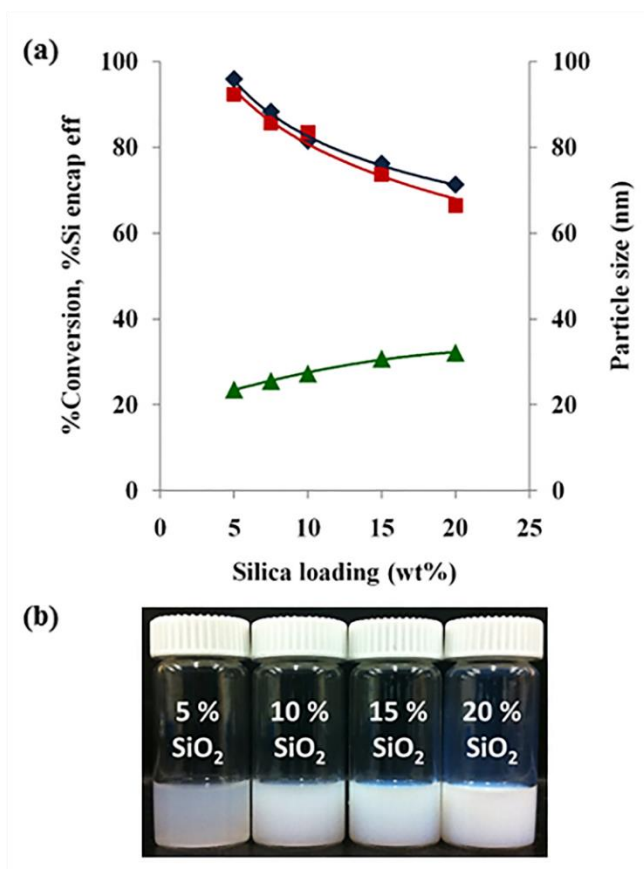


**Figure 5. 2** Effect of silica loading on; (a) (◆) %Conversion, (■) %Si encapsulation eff, (▲) Particle size and (b) characteristics of the latex. Condition:  $M/H_2O = 0.2$ , SDS = 5 wt%, KPS = 3 wt% based on monomer.

### 5.3.2 Effect of Surfactant Concentration

The effect of SDS concentration (1–10 wt% based on monomer) on the monomer conversion, grafting efficiency and particle size is presented in Figure 5.3a. The particle size decreased from 28 nm to 19 nm with an increase in the surfactant concentration from 1 to 10 wt% based on monomer. This result implies that the PB-SiO<sub>2</sub> particle size could be controlled by the amount of surfactant [107]. The monomer conversion increased with an increase in surfactant concentration. This is due to the fact that the micelle numbers increased with increasing SDS concentration, as more reaction domains were generated [106, 120]. The high reaction domains resulted in an increase in the polymerization rate and thus, the monomer conversion was increased.

Moreover, the grafting efficiency was increased with increasing SDS concentration, reaching a maximum grafting efficiency of 83% at a SDS amount of 7 wt% and then it decreased. Surfactant could provide monomer swollen micelles favouring the diffusion of hydrophobic monomer onto the silica surface and the stability of PB-SiO<sub>2</sub> nanocomposite resulted in an increase in grafting efficiency [121]. However, the grafting efficiency decreased at a high surfactant concentration due to the fact that the free PB (homopolymer) occurred rather than the encapsulation of SiO<sub>2</sub> within PB. At a high SDS concentration, the polymerization rate was increased and the chance to react with macroradicals was reduced resulting in limiting the graft copolymerization [113]. The surfactant concentration significantly affected the characteristics of the PB-SiO<sub>2</sub> nanoparticle latex as shown in Figure 5.3b. It can be seen that at a high surfactant level, more transparent latex was produced.

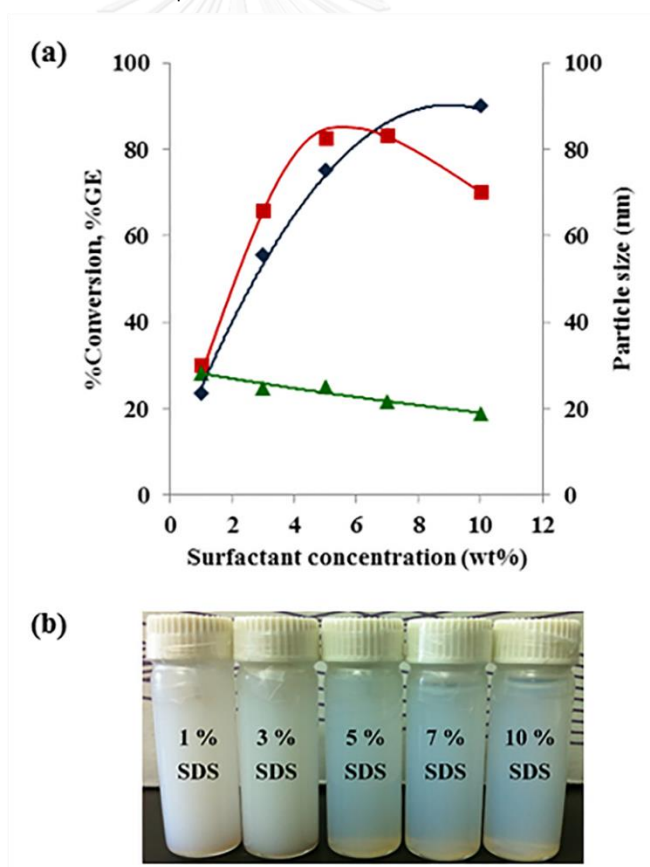


**Figure 5.3** Effect of surfactant concentration on; (a) (◆) %Conversion, (■) %GE, (▲) Particle size and (b) characteristics of the latex. Condition: SiO<sub>2</sub> = 10 wt%, M/H<sub>2</sub>O = 0.2, KPS = 2 wt% based on monomer.

### 5.3.3 Effects of Monomer to Water Ratio

From Figure 5.4, the effect of monomer to water ratio on the monomer conversion, grafting efficiency and particle size of PB-SiO<sub>2</sub> could also be observed. The particle sizes are found to increase from 19 nm to 23 nm with an increase in the monomer to water ratio from 0.1 to 0.5. At a high monomer to water ratio, more collisions and aggregation of the nanoparticles occurred and thus the monomer conversion increased which resulted in a larger particle size than that obtained at a low monomer to water ratio [12, 107]. The monomer conversion and grafting efficiency increased with increasing monomer to water ratio and reached a maximum at a monomer to water ratio of 0.2. At a high monomer to water ratio (above 0.2), the monomer conversion and grafting efficiency decreased dramatically. This implied that at higher monomer to water ratio, polymerization of BD is more pronounced than graft polymerization onto SiO<sub>2</sub> since the grafting has a lower active surface area at the reaction site [122]. Moreover, most of the additional added monomer molecules could diffuse into the existing polymer particles, which were larger than the newly nucleated particles, and monomer diffusion into the polymer particles required more time resulting in a decrease in monomer conversion [114]. A high monomer conversion (83%) and grafting efficiency (83%) were obtained via DMP at a low monomer to water ratio of 0.2 at which a small particle size (22 nm) was achieved.

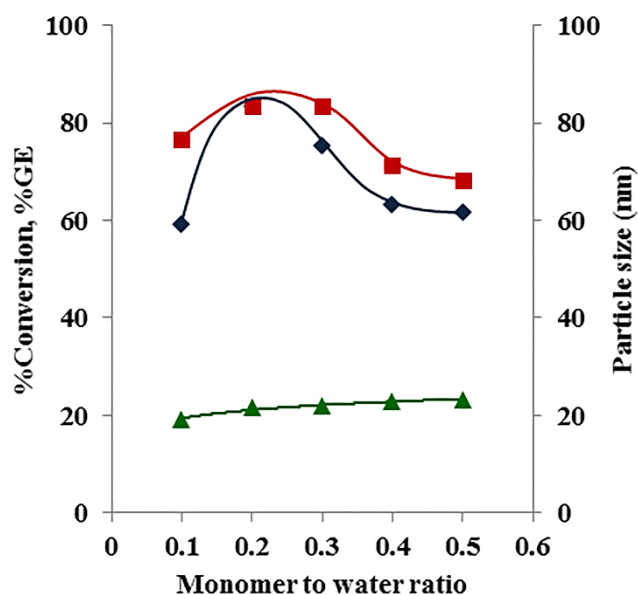


**Figure 5. 4** Effect of monomer to water ratio (M/H<sub>2</sub>O) on; (◆) %Conversion, (■) %GE, (▲) Particle size. Condition: SiO<sub>2</sub> = 10 wt%, SDS = 7 wt%, KPS = 2 wt% based on monomer.

#### 5.3.4 Effect of Initiator Concentration

The dependence of the monomer conversion, grafting efficiency and particle size on initiator concentration are illustrated in Figure 5.5. The results indicated that with an increase in the initiator concentration from 1 to 5 wt% based on monomer, the monomer conversion increased from 75 to 98%. The particle size increased slightly with an increase in the initiator concentration. This phenomenon can be explained in that increasing the initiator concentration results in more nucleation in the water phase as a result of more free radicals being formed [14]. Thus, some dead polymer occurred from combination of two radicals having carbon double bonds in the polymer chains probably have more chance to be initiated to new radicals that could play a role on the polymerization resulting in a larger particle size. Additionally, at high KPS concentration, more free radicals were generated and reacted with monomer to produce primary radicals and then the growing polymer chains increased; thus, the monomer conversion increased rapidly [108, 111]. However, the grafting efficiency

decreased with an increase in KPS concentration. This implies that at a high KPS concentration, a higher free PB resulted rather than the grafting of PB onto the silica surface. Hence, a low initiator concentration was more favorable for PB-SiO<sub>2</sub> encapsulation.

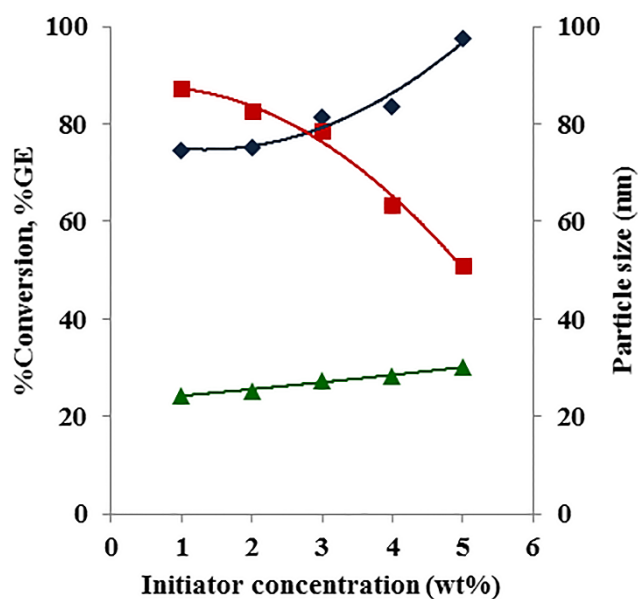


**Figure 5. 5** Effect of initiator concentration on; (◆) %Conversion, (■) %GE, (▲) Particle size. Condition: SiO<sub>2</sub> = 10 wt%, M/H<sub>2</sub>O = 0.2, SDS = 5 wt% based on monomer.

#### 5.4 Diimide Hydrogenation: Effect of N<sub>2</sub>H<sub>4</sub> and H<sub>2</sub>O<sub>2</sub> Concentration

The PB-SiO<sub>2</sub> latex as prepared at the optimum condition: SiO<sub>2</sub> loading of 10 wt%, surfactant concentration of 5 wt%, monomer to water ratio of 0.2 and initiator concentration of 3 wt%, was selected to be hydrogenated via diimide reduction. Figure 5.6 shows the <sup>1</sup>H NMR spectra of PB-SiO<sub>2</sub> and HPB-SiO<sub>2</sub> nanoparticles (98.6 %HD). For PB-SiO<sub>2</sub>, signals were attributed to 1,4 olefinic protons at 5.39 ppm, 1,2 terminal vinyl protons at 4.94 ppm, 1,2 nonterminal vinyl protons at 5.54 ppm, 1,2 methylene at 1.41 ppm and 1,4 methylene at 2.01 ppm [123]. For HPB-SiO<sub>2</sub>, the signals in the range of 4.8 - 5.6 ppm attributable to olefinic protons show nearly-complete reduction and the

new signals for the saturated carbon centered at 0.7 – 1.6 ppm were detected. The hydrogenation degree (HD) calculated from the peak area of olefinic protons and saturated protons was 98.6 %. PB-SiO<sub>2</sub> was completely hydrogenated under the optimal condition (hydrogenation condition: [C=C] = 1 mol/L, [N<sub>2</sub>H<sub>4</sub>] = 3 mol/L, [H<sub>2</sub>O<sub>2</sub>] = 4 mol/L, H<sub>3</sub>BO<sub>3</sub> = 0.15 mol/L).

Diimide reduction is suitable for the hydrogenation of diene-based rubber in latex form. In this study, the diimide reduction technique for PB-SiO<sub>2</sub> latex was performed by using hydrazine hydrate (N<sub>2</sub>H<sub>4</sub>) and hydrogen peroxide (H<sub>2</sub>O<sub>2</sub>). The reactions for diimide hydrogenation can be divided into two steps, as presented by the following equations:



The effect of N<sub>2</sub>H<sub>4</sub> and H<sub>2</sub>O<sub>2</sub> concentration on diimide hydrogenation of PB-SiO<sub>2</sub> are shown in Figure 5.7. The HD increased from 74.8 to 98.6 % with increasing N<sub>2</sub>H<sub>4</sub> concentration from 1 to 3 mol/L (Figure 5.7a). This can be explained in that with a higher amount of N<sub>2</sub>H<sub>4</sub>, more diimide molecules were generated according to Eq. (5.1) resulting in an increase in the hydrogenation degree [82, 83]. However, HD decreased when the N<sub>2</sub>H<sub>4</sub> concentration was higher than 3 mol/L. This result implies that the diimide molecules can self-react at a high level of N<sub>2</sub>H<sub>4</sub> resulting in decreasing the HD. Another possible explanation for the decreasing HD is that the excess diimide in the system may diffuse into the aqueous phase [78]. Moreover, the hydrogenation was also carried out by varying H<sub>2</sub>O<sub>2</sub> concentration as presented in Figure 5.7b. H<sub>2</sub>O<sub>2</sub> was used as a strong oxidizing agent to react with the N<sub>2</sub>H<sub>4</sub> molecule for producing the diimide species. It can be observed that HD increased from 73.7 to 98.6 % with an increase in H<sub>2</sub>O<sub>2</sub> concentration from 1 to 4 mol/L and then decreased at a higher concentration. At a higher H<sub>2</sub>O<sub>2</sub> concentration, a crosslinking reaction possibly occurred, which caused a decrease in the number of free carbon double bonds available for diimide reduction [124]. Thus, the HD tended to decrease at high H<sub>2</sub>O<sub>2</sub> concentration. Additionally, the N<sub>2</sub>H<sub>4</sub> and H<sub>2</sub>O<sub>2</sub> concentration did not affect the particle size of HPB-SiO<sub>2</sub>.

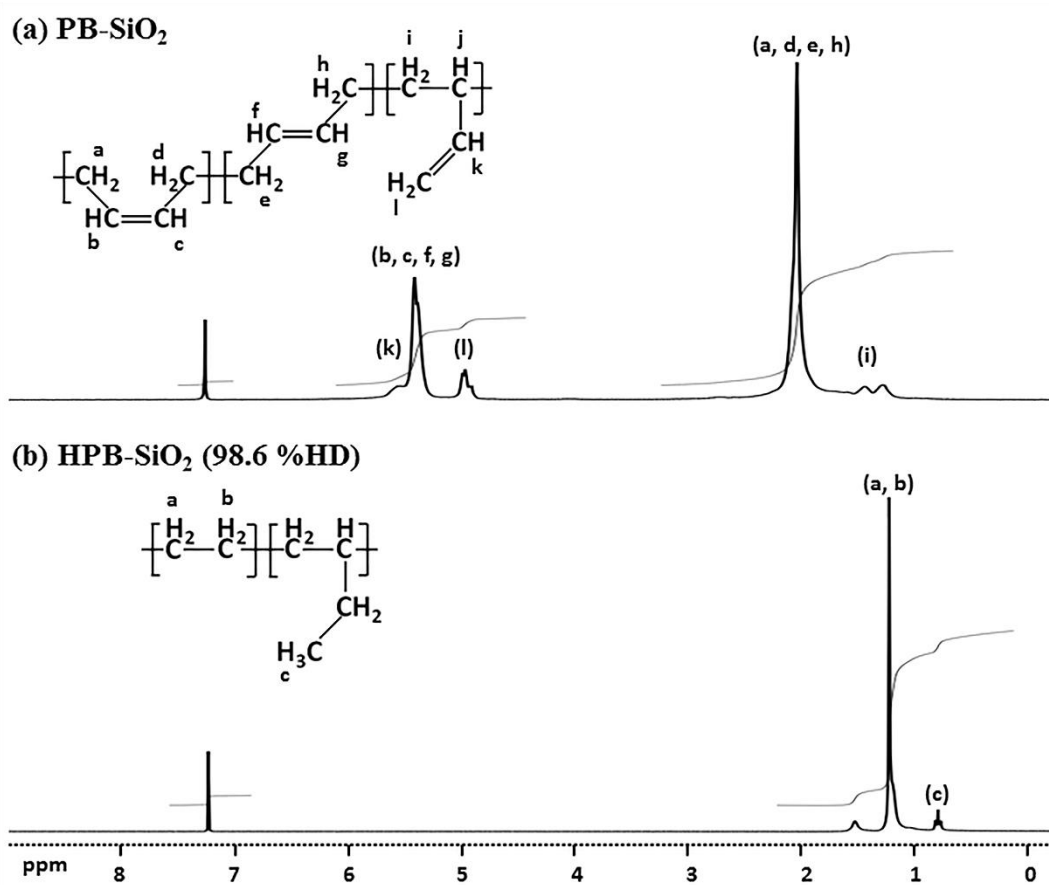
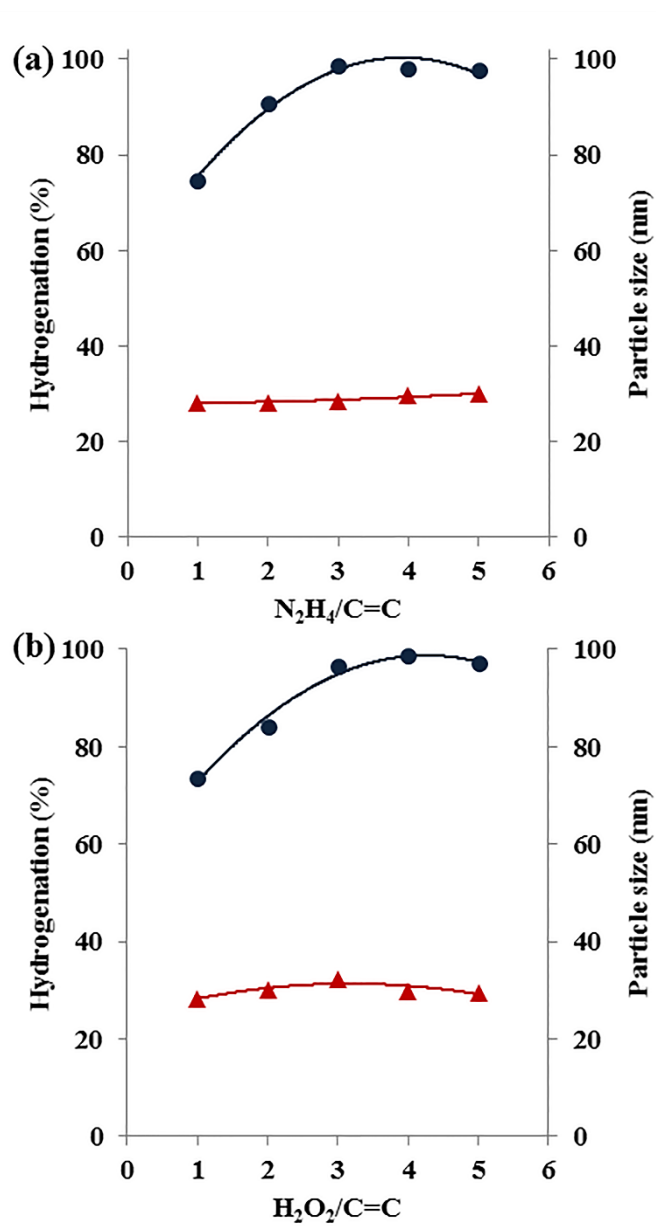


Figure 5. 6 <sup>1</sup>H-NMR spectra of (a) PB-SiO<sub>2</sub> and (b) HPB-SiO<sub>2</sub> at 98.6 %HD.



**Figure 5. 7** Hydrogenation of PB-SiO<sub>2</sub>; (a) effect of [N<sub>2</sub>H<sub>4</sub>] at [H<sub>2</sub>O<sub>2</sub>] = 4 mol/L and (b) effect of [H<sub>2</sub>O<sub>2</sub>] at [N<sub>2</sub>H<sub>4</sub>] = 3 mol/L on hydrogenation degree (●) and particle size (▲). Condition: [H<sub>3</sub>BO<sub>3</sub>] = 0.15 mol/L, [C=C] = 1 mol/L, T = 70 °C, time = 5 h.



## 5.5 Morphology of PB-SiO<sub>2</sub> and HPB-SiO<sub>2</sub>

From TEM micrographs of PB-SiO<sub>2</sub> and HPB-SiO<sub>2</sub> (98.6 %HD) nanocomposites as shown in Figure 5.8, a uniform size and core-shell spherical morphology of the PB-SiO<sub>2</sub> and HPB-SiO<sub>2</sub> nanocomposite was clearly observed and no agglomeration of composite particles occurred. From Figure 5.8b, when the hydrogenation degree increased to 98.6 %, a lightly colored domain at the outer layer of the nanoparticles appeared, suggesting a core-shell morphology. Since the OsO<sub>4</sub> agent could only stain the carbon-carbon double bonds in the polymer chain, the dark color domain indicated a high double bond concentration while the lightly colored domain indicated a region of low C=C amount. This observation confirms that C=C in the PB was hydrogenated to saturated units during diimide reduction. The non-hydrogenated PB showed relatively sharp particle edges because of the high OsO<sub>4</sub> concentration inside the particle as shown in Figure 5.8a. Moreover, the particle size distributions of PB-SiO<sub>2</sub> and HPB-SiO<sub>2</sub> showed a very similar pattern. The particle size of HPB-SiO<sub>2</sub> (29.7 nm) was slightly increased from that of the initial PB-SiO<sub>2</sub> (27.3 nm). It can be concluded that well-dispersed SiO<sub>2</sub> was successfully encapsulated by a shell of HPB.

The formation mechanism of modified SiO<sub>2</sub>, PB-SiO<sub>2</sub> and HPB-SiO<sub>2</sub> nanoparticles is illustrated in Figure 5.9. For silica surface modification, the nano-SiO<sub>2</sub> was pretreated using VTS as organo-silane coupling agent due to its unique bifunctional structure of a methoxy group and a vinyl group at the chain ends of VTS. The methoxy groups of VTS were first hydrolyzed by water in aqueous solution to form silanol groups and then, the silanol groups reacted with hydroxyl groups on the silica surface through a polycondensation reaction to form siloxane linkage between the silica surface and the VTS. Thus, the vinyl ends with carbon double bonds of the attached VTS on the silica surface could be polymerized with the BD monomer to form a silica core and PB shell structure. For differential microemulsion polymerization, modified SiO<sub>2</sub>, SDS surfactant and KPS initiator were dispersed in deionized water to form a homogeneous mixture. The small amounts of BD diffused into the micelle and the KPS initiator decomposed in the aqueous phase generating free radicals that produce reactive monomer radicals on the monomer molecule and silica surface for the initiation stage and then BD was

polymerized resulting in chain propagation. Hence, PB could graft onto the silica surface with a  $\text{SiO}_2$  core and PB shell. The PB- $\text{SiO}_2$  was then hydrogenated by diimide reduction. The C=C were reacted with the diimide molecule, generated from the redox reaction between  $\text{N}_2\text{H}_4$  and  $\text{H}_2\text{O}_2$  which is promoted by boric acid ( $\text{H}_3\text{BO}_3$ ), through a coordination process. The hydrogen was transferred to produce an alkyl complex and then HPB- $\text{SiO}_2$  was obtained.

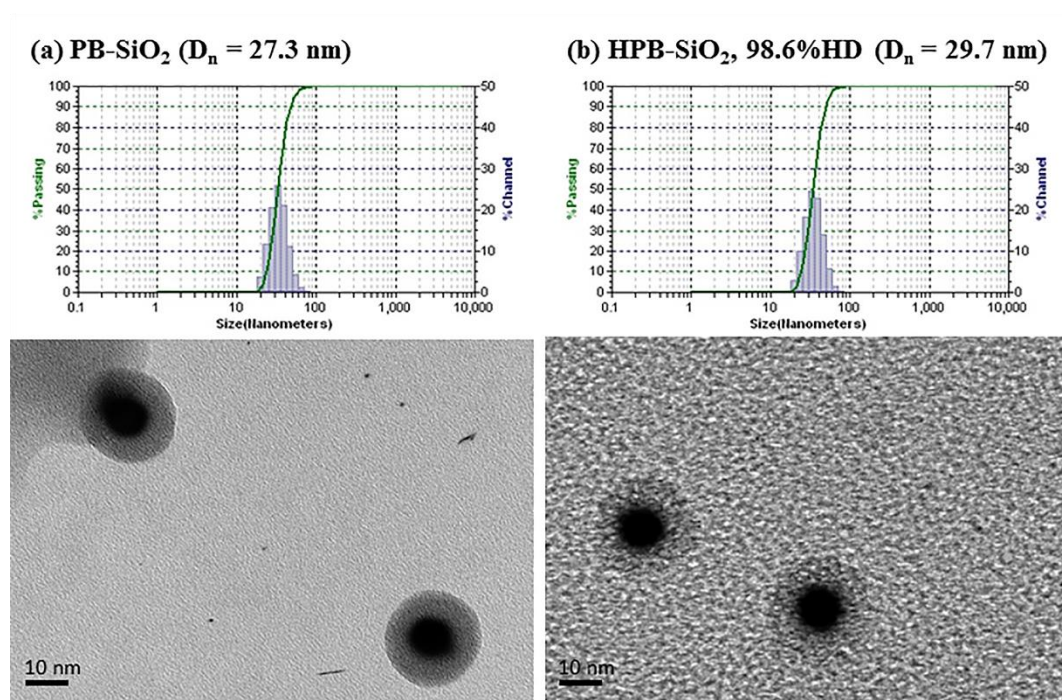


**Figure 5. 8** TEM micrographs and particle size distribution of samples (a) PB- $\text{SiO}_2$  and (b) HPB- $\text{SiO}_2$  at 98.6 %HD.



However,  $T_{id}$  and  $T_{max}$  decreased at high  $\text{SiO}_2$  loading (20 wt%) due to an agglomeration of nano- $\text{SiO}_2$  in the PB matrix resulting in a reduction of the thermal resistance. Additionally,  $T_{id}$  and  $T_{max}$  of HPB- $\text{SiO}_2$  (10 wt%  $\text{SiO}_2$ , 98.6 %HD) was higher than that of PB- $\text{SiO}_2$ . This implied that thermal stability of polybutadiene depended on the amount of C=C in the polymer chain [82, 83]. The hydrogenation could improve the thermal stability of PB- $\text{SiO}_2$  by converting the weak  $\pi$  bond in PB- $\text{SiO}_2$  to a strong  $\sigma$  bond, which leads to a higher thermal stability. Thus, the hydrogenation involves the reduction of C=C in PB resulting in an increase in thermal stability of HPB- $\text{SiO}_2$  nanoparticles. It can be concluded that the synthesis of HPB- $\text{SiO}_2$  nanocomposites shows improved thermal stability and a dramatic increase in heat resistance.

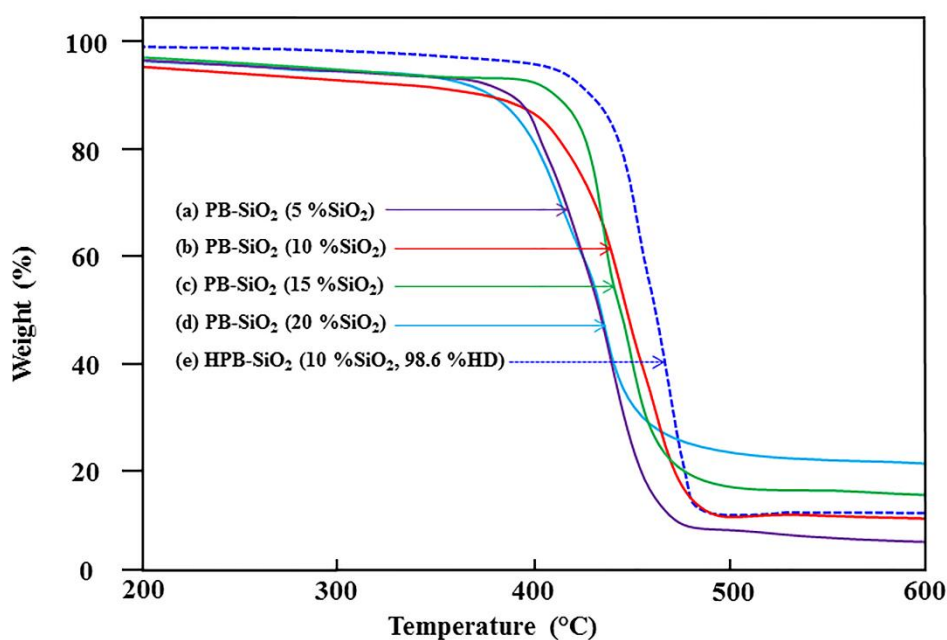


**Figure 5. 10** TGA thermograms of (a) PB- $\text{SiO}_2$  (5 % $\text{SiO}_2$ ), (b) PB- $\text{SiO}_2$  (10 % $\text{SiO}_2$ ), (c) PB- $\text{SiO}_2$  (15 % $\text{SiO}_2$ ), (d) PB- $\text{SiO}_2$  (20 % $\text{SiO}_2$ ) and (e) HPB- $\text{SiO}_2$  (10 % $\text{SiO}_2$ , 98.6 %HD).

**Table 5. 1** Decomposition temperature of PB-SiO<sub>2</sub> and HPB-SiO<sub>2</sub> nanocomposites.

Composites	SiO <sub>2</sub> loading (wt%)	T <sub>id</sub> (°C)	T <sub>max</sub> (°C)
PB-SiO <sub>2</sub> <sup>a</sup>	5	402.6	438.5
	10	406.2	441.9
	15	413.5	448.0
	20	395.7	433.6
HPB-SiO <sub>2</sub> <sup>b</sup>	10	450.7	469.6

<sup>a</sup> PB-SiO<sub>2</sub> preparation condition: M/H<sub>2</sub>O = 0.2, SDS = 5 wt%, KPS = 3 wt% based on monomer.

<sup>b</sup> HPB-SiO<sub>2</sub> at 98.6 %HD.

## 5.7 NR Nanocomposites

### 5.7.1 Thermal Properties of NR/PB-SiO<sub>2</sub> and NR/HPB-SiO<sub>2</sub> Composites

The TG and DTG curves for NR/HPB-SiO<sub>2</sub> composites are illustrated in Figure 5.11. For the TG curves (Figure 5.11a), the results indicate that decomposition of all composites showed a one-step polymer degradation and provided smooth weight loss curves. However, the DTG curve of the NR/HPB-SiO<sub>2</sub> composites (Figure 5.11b) showed two peaks at a temperature around 393 °C and 480 °C, respectively. Thus, a two-step decomposition of the composite occurred for NR/HPB-SiO<sub>2</sub> due to the effect of HPB-SiO<sub>2</sub> filled in NR [125].

The T<sub>g</sub> of the unfilled NR, NR/PB-SiO<sub>2</sub> and NR/HPB-SiO<sub>2</sub> composites at various blend ratios are presented in Table 5.2. For NR/PB-SiO<sub>2</sub>, the T<sub>g</sub> of NR/PB-SiO<sub>2</sub> were slightly lower than that of unfilled NR ( $\Delta T_g = 0.2-1.8$  °C). However, the T<sub>g</sub> of NR/HPB-SiO<sub>2</sub> were slightly higher than that of unfilled NR ( $\Delta T_g = 1.0-2.1$  °C). The decrease in T<sub>g</sub> of NR/PB-SiO<sub>2</sub> composites could be explained in that the T<sub>g</sub> of PB-SiO<sub>2</sub> was lower than that of unfilled NR.

The T<sub>id</sub> and T<sub>max</sub> of the unfilled NR, NR/PB-SiO<sub>2</sub> and NR/HPB-SiO<sub>2</sub> composites at various blend ratios are summarized in Table 5.2. The T<sub>id</sub> of NR/PB-SiO<sub>2</sub> samples

increased from 355.9 °C to 357.4 °C with an increasing PB-SiO<sub>2</sub> loading in the composite from 0 to 30 wt% (SiO<sub>2</sub> content = 0 – 3 wt%). Similarly, the T<sub>id</sub> of NR/HPB-SiO<sub>2</sub> composites increased from 355.9 °C to 361.3 °C with an increasing HPB-SiO<sub>2</sub> loading in the composite from 0 to 30 wt% (SiO<sub>2</sub> content = 0 – 3 wt%). Moreover, with an increasing PB-SiO<sub>2</sub> loading in the composite from 0 to 30 wt% (SiO<sub>2</sub> content = 0 – 3 wt%), the T<sub>max</sub> of NR/PB-SiO<sub>2</sub> composites increased from 384.0 °C to 403.5 °C and T<sub>max</sub> of NR/HPB-SiO<sub>2</sub> composites increased from 384.0 °C to 405.3 °C. The T<sub>id</sub> and T<sub>max</sub> of NR/PB-SiO<sub>2</sub> and NR/HPB-SiO<sub>2</sub> nanocomposites were higher than that of unfilled NR. This result implies that PB-SiO<sub>2</sub> and HPB-SiO<sub>2</sub> could be uniformly dispersed in the NR matrix resulting in the high thermal stability of the nanocomposite. However, according to the DTG curve (Fig. 5.11b), the NR/HPB-SiO<sub>2</sub> composites at a blend ratio of 90:10, 80:20 and 70:30 had another T<sub>max</sub> of 476.1 °C, 480.6 °C and 483.2 °C, respectively. This could be explained in that the second T<sub>max</sub> was attributed to HPB-SiO<sub>2</sub> which had a higher T<sub>max</sub> than that of NR and PB-SiO<sub>2</sub> [126, 127].

**Table 5. 2** Thermal properties of NR/PB-SiO<sub>2</sub> and NR/HPB-SiO<sub>2</sub> composites.

Samples	NR/PB-SiO <sub>2</sub> or NR/HPB-SiO <sub>2</sub> (wt/wt)	SiO <sub>2</sub> content <sup>c</sup> (wt%)	T <sub>g</sub> (°C)	T <sub>id</sub> (°C)	T <sub>max1</sub> (°C)	T <sub>max2</sub> (°C)
NR	-	-	-63.3	355.9	384.0	-
NR/PB-SiO <sub>2</sub> <sup>a</sup>	90/10	1.0	-63.5	356.4	390.3	-
	80/20	2.0	-63.9	356.9	397.3	-
	70/30	3.0	-65.1	357.4	403.5	-
NR/HPB-SiO <sub>2</sub> <sup>b</sup>	90/10	1.0	-62.3	359.6	398.5	476.1
	80/20	2.0	-61.8	360.9	402.1	480.6
	70/30	3.0	-61.2	361.3	405.3	483.2

<sup>a</sup> PB-SiO<sub>2</sub> preparation condition: M/H<sub>2</sub>O = 0.2, SiO<sub>2</sub> = 10 wt%, SDS = 5 wt%, KPS = 3 wt% based on monomer.

<sup>b</sup> HPB-SiO<sub>2</sub> at 98.6 %HD.

<sup>c</sup> Silica content based on total rubber.

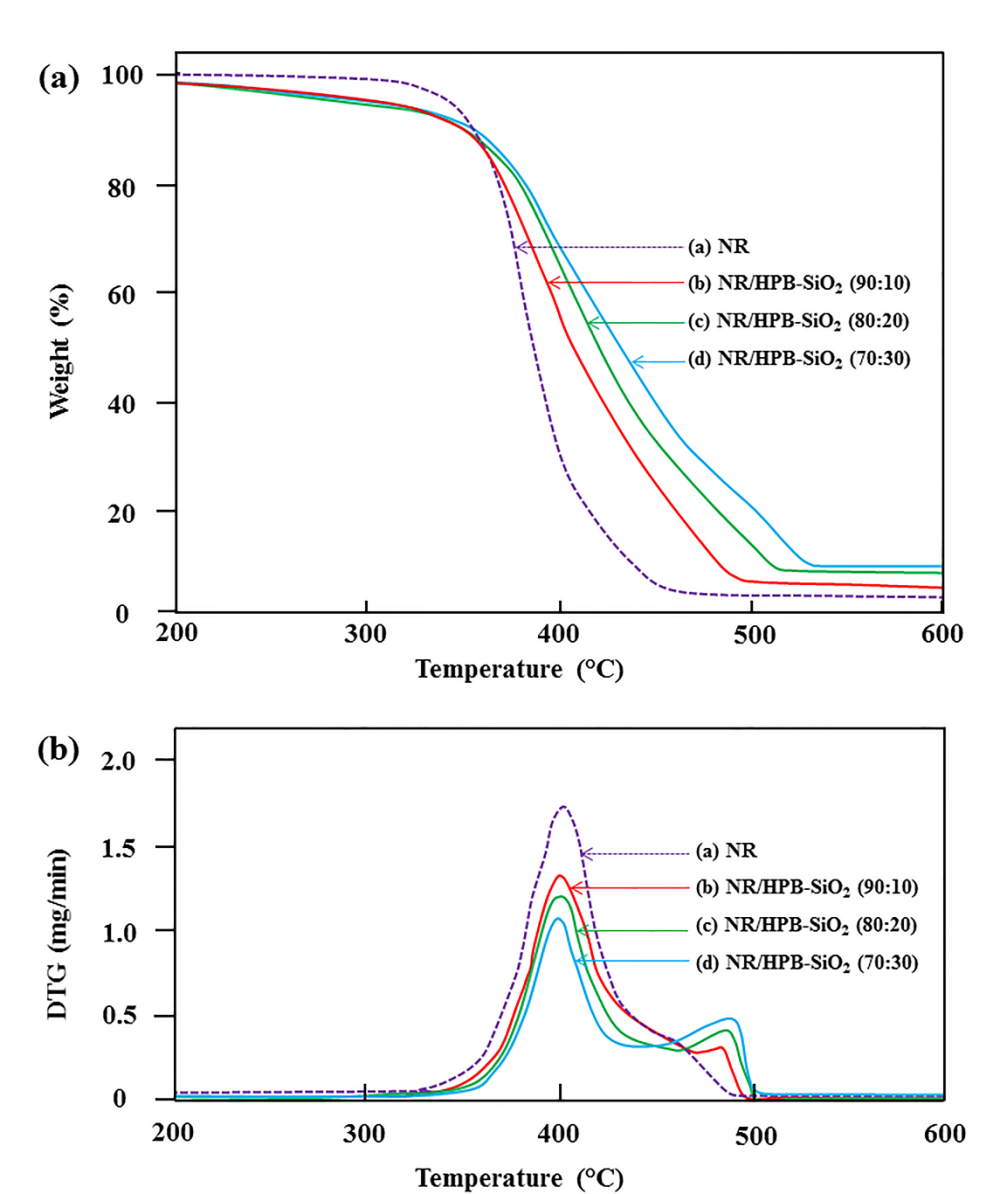


Figure 5.11 Temperature dependence of (a) weight loss and (b) DTG for NR/HPB-SiO<sub>2</sub> composites.

### 5.7.2. Mechanical Properties of NR/PB-SiO<sub>2</sub> and NR/HPB-SiO<sub>2</sub> Composites

The influence of the PB-SiO<sub>2</sub> and HPB-SiO<sub>2</sub> amount at NR/PB-SiO<sub>2</sub> or NR/HPB-SiO<sub>2</sub> ratios of 100/0, 90/10, 80/20 and 70/30 (equivalent to 0%, 1%, 2% and 3% silica content in all composites, respectively) on mechanical properties of nanocomposites are reported in Table 5.3. The tensile strength, modulus and elongation at break of the NR/PB-SiO<sub>2</sub> and NR/HPB-SiO<sub>2</sub> nanocomposites were significantly affected by the addition of PB-SiO<sub>2</sub> and HPB-SiO<sub>2</sub>, respectively. For NR/PB-SiO<sub>2</sub> composites, the tensile strength, modulus at 300% strain and elongation at break of all nanocomposites were higher than that of unfilled NR. The tensile strength was increased from 20.0 MPa to 25.3 MPa, the modulus at 300% strain was increased from 1.87 MPa to 2.29 MPa and the elongation at break was increased from 662% to 721% with an increase in PB-SiO<sub>2</sub> loading from 0 to 30 wt% (SiO<sub>2</sub> content = 0 – 3 wt%). This indicated that the PB-SiO<sub>2</sub> nanoparticles could increase the external force resistance due to the high interaction between silica nanoparticles and the NR matrix, with well dispersed PB-SiO<sub>2</sub> nanoparticles and a reduction of silica agglomeration resulting in improvement in the tensile strength and modulus of the nanocomposite [115]. Furthermore, the elongation at break was increased with increasing PB-SiO<sub>2</sub> loading due to the flexible and elastic nature of polybutadiene.

For NR/HPB-SiO<sub>2</sub> nanocomposites, HPB-SiO<sub>2</sub> latex at 98.6 %HD containing 10 wt% of silica loading was selected to blend with NR latex. The tensile strength was increased from 20.0 MPa to 28.3 MPa and modulus at 300% strain was increased from 1.87 MPa to 2.49 MPa with an increase in HPB-SiO<sub>2</sub> loading from 0 to 30 wt% (SiO<sub>2</sub> content = 0 – 3 wt%). Interestingly, the tensile strength of the NR/HPB-SiO<sub>2</sub> composite was higher than that of NR/PB-SiO<sub>2</sub> at the same silica content due to the thermoplastic properties of the ethylene segments. Moreover, the silica particle can act as a restriction site for rubber chain mobility resulting in enhancing the deformation resistance of the material which is beneficial for the improvement of the tensile strength and modulus of the composite material. However, the elongation at break decreased with an increase in HPB-SiO<sub>2</sub> loading due to the rigid and stiff nature of silica particles and ethylene segments.



**Table 5. 3** Mechanical properties of NR/PB-SiO<sub>2</sub> and NR/HPB-SiO<sub>2</sub> composites.

Samples	NR/PB-SiO <sub>2</sub> or NR/HPB-SiO <sub>2</sub> (wt/wt)	SiO <sub>2</sub> content <sup>c</sup> (wt%)	Tensile strength (MPa)	300% Modulus (MPa)	Elongation at break (%)
NR	-	-	20.0 ± 0.5	1.87 ± 0.09	662 ± 22
NR/PB-SiO <sub>2</sub> <sup>a</sup>	90/10	1.0	22.6 ± 0.8	1.95 ± 0.05	698 ± 15
	80/20	2.0	23.1 ± 2.1	2.15 ± 0.07	711 ± 4
	70/30	3.0	25.3 ± 1.0	2.29 ± 0.04	721 ± 8
NR/HPB-SiO <sub>2</sub> <sup>b</sup>	90/10	1.0	23.7 ± 0.6	2.08 ± 0.07	658 ± 9
	80/20	2.0	25.2 ± 0.9	2.27 ± 0.09	642 ± 12
	70/30	3.0	28.3 ± 0.5	2.49 ± 0.05	627 ± 8

<sup>a</sup> PB-SiO<sub>2</sub> preparation condition: M/H<sub>2</sub>O = 0.2, SiO<sub>2</sub> = 10 wt%, SDS = 5 wt%, KPS = 3 wt% based on monomer.

<sup>b</sup> HPB-SiO<sub>2</sub> at 98.6 %HD.

<sup>c</sup> Silica content based on total rubber.

### 5.7.3. Thermal Resistance of NR/PB-SiO<sub>2</sub> and NR/HPB-SiO<sub>2</sub> Composites

To investigate the thermal resistance of PB-SiO<sub>2</sub> filled NR and HPB-SiO<sub>2</sub> filled NR composites, the influence of heat aging on the mechanical properties is presented in Figure 5.12. For tensile strength as shown in Figure 5.12a, the tensile strength of unfilled NR after heat aging was greatly decreased from 20.0 MPa to 12.6 MPa (63 % retention) over the range of strain studied. This indicated that the NR containing mainly unsaturated carbon double bonds had poorer properties due to accelerated thermal aging. The tensile strength of NR/PB-SiO<sub>2</sub> composites, at all blend ratios, after heat aging were decreased with a percentage retention of 74.8-77.9%; however, they were much higher than that of unfilled NR. This result indicated that the degradation rate of the NR/PB-SiO<sub>2</sub> composite are lower than that of unfilled NR due to retarding effect of the PB-SiO<sub>2</sub> nanoparticles. For NR filled with HPB-SiO<sub>2</sub> the properties did not change and retained high stress values after aging. The percentage retention in tensile strength of NR/HPB-SiO<sub>2</sub> composites (91.1-95.1%) was much higher than that of unfilled NR (63%) and NR/PB-SiO<sub>2</sub> (74.8-77.9%). After diimide reduction, the carbon-carbon double

bonds were hydrogenated and no chain scission occurred. Moreover, good dispersion of nanosized HPB-SiO<sub>2</sub> within NR is useful for increasing tensile strength retention. This indicated that HPB-SiO<sub>2</sub> nanoparticles could function as a heat stabilizer and prevent polymer chain scission on high temperature treatment. When NR was exposed to high temperature, most of the polymer chain scission occurred and NR was degraded due to the low heat stability of the C=C in the polymer backbone. On the other hand, for the NR/HPB-SiO<sub>2</sub> composites after heat aging, HPB-SiO<sub>2</sub> as a heat stabilizer stopped the propagation of NR chain scission and retarded the degradation of the NR/HPB-SiO<sub>2</sub> composites.

The percentage retention in modulus at 300% strain after aging of NR/PB-SiO<sub>2</sub> at various blend ratios are in the range of 70.3% to 80.8% as presented in Figure 5.12b. The lowest modulus retention of unfilled NR and NR/PB-SiO<sub>2</sub> composites implied poor heat resistance. For NR/HPB-SiO<sub>2</sub> composites, the percentage retention in modulus increased up to 97.6% when the HPB-SiO<sub>2</sub> amount was increased up to 30 wt%. In addition, the elongation at break of NR/HPB-SiO<sub>2</sub> after aging slightly increased with an increase in NR/HPB-SiO<sub>2</sub> blend ratio as shown in Figure 5.12c. This can be seen in that the enhancement in aging resistance was dominated by the addition of HPB-SiO<sub>2</sub> nanoparticles into the rubber matrix.

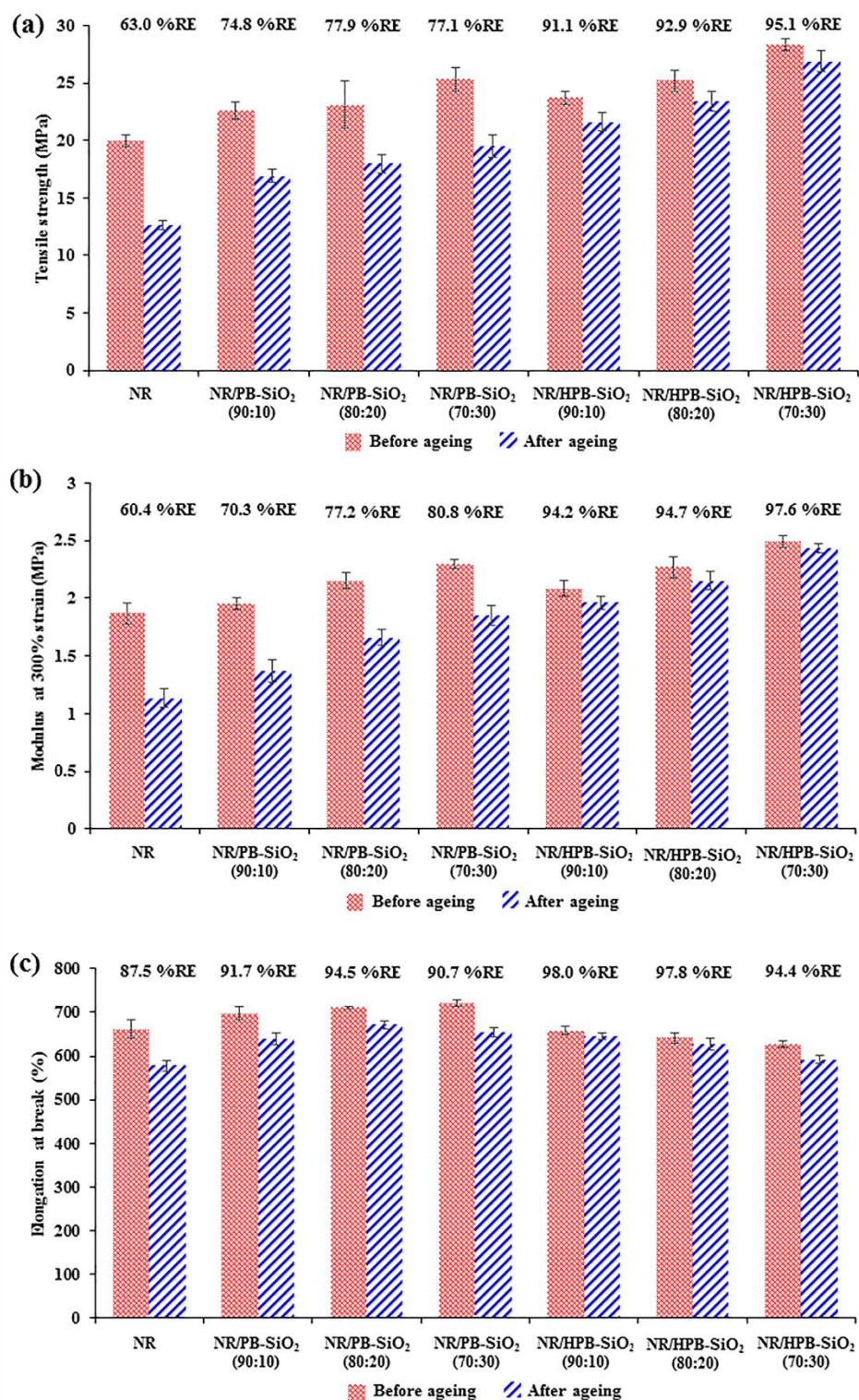


Figure 5. 12 Mechanical properties of NR, NR/PB-SiO<sub>2</sub> and NR/HPB-SiO<sub>2</sub> before and after aging: (a) tensile strength (MPa), (b) modulus at 300% strain (MPa) and (c) elongation at break (%).

#### 5.7.4. Ozone Resistance of NR/PB-SiO<sub>2</sub> and NR/HPB-SiO<sub>2</sub> Nanocomposites

Polybutadiene and natural rubber are important rubbers and are very useful in various applications. However, PB and NR are highly sensitive to the ozone degradation, due to the presence of C=C in the main chain. To improve the ozone degradation of the rubber composite, HPB/SiO<sub>2</sub> may be an effective filler for NR. The ozone resistance of unfilled NR and NR/HPB-SiO<sub>2</sub> nanocomposites at various blend ratios are presented in Table 5.4. After 24 h exposure, C-3 type cracking occurred for unfilled NR due to the strong effect of ozone aging on the surface of unfilled NR. Similarly, the C-3 type cracking after ozone exposure for 24 h also occurred for NR/PB-SiO<sub>2</sub> at all blend ratios. The NR/HPB-SiO<sub>2</sub> nanocomposites at ratios of 90:10 and 80:20 exhibited less cracking of B-2 type. However, the surface cracking of NR/HPB-SiO<sub>2</sub> at a ratio of 70:30 was not observed. This implied that increasing HPB-SiO<sub>2</sub> loading could restrain ozone-induced degradation resulting in a reduction in surface cracking. Over 48 h, the cracking number of unfilled NR significantly increased to C-4 type similar to NR/PB-SiO<sub>2</sub> composites. The NR/HPB-SiO<sub>2</sub> nanocomposites at ratios of 90:10, 80:20 and 70:30 represented low cracking of C-3, B-2 and A-2, respectively. This observation is due to the fact that the reaction between ozone and the C-H bond is much slower than that between ozone and the C=C bond. After 72 h exposure, the unfilled NR and NR/PB-SiO<sub>2</sub> were completely degraded while all NR/HPB-SiO<sub>2</sub> composites exhibited good ozone resistance. It can be concluded that at high HPB-SiO<sub>2</sub> loading the ozone resistance of composites was better than that of the unfilled NR due to the retardation of cracking; thus the incorporation of HPB-SiO<sub>2</sub> in the NR latex provides better ozone resistance.

The photographs of the surface of the NR, NR/PB-SiO<sub>2</sub> and NR/HPB-SiO<sub>2</sub> composite after exposure for 72 h are shown in Figure 5.13. The surface of unfilled NR shows long cracks and numerous cracking (Figure 5.13a). For NR/PB-SiO<sub>2</sub>, the C-4 type cracking after ozone exposure for 72 h occurred at a blend ratio of 90:10, 80:20 and 70:30, respectively as shown in Figure 5.13b-d. The appearance of ozone cracking was evident for the degradation of unfilled NR and NR/PB-SiO<sub>2</sub> composites. It can be concluded that the C=C bond in the polymer backbone of NR and NR/PB-SiO<sub>2</sub> are sensitive to ozone resulting in rubber degradation and the reduction of mechanical

and thermal properties. Moreover, ozone also attacks polymers containing hydrogen atoms in which the reaction between ozone and the C-H bond is much slower than that between ozone and the C=C bond [128]. The cracking density of NR/HPB-SiO<sub>2</sub> at 80:20 was lower than that of unfilled NR (Figure 5.13b). Moreover, NR/HPB-SiO<sub>2</sub> showed shorter and shallower cracks, indicating that the cracking was suppressed. From Figure 5.13c, the surface of NR/HPB-SiO<sub>2</sub> (80:20) represents a smaller number and shorter (below 1 mm) cracking than that of unfilled NR and NR/HPB-SiO<sub>2</sub> at 90:10 due to the presence of higher degree of saturated carbons which leads to the suppression of crack growth. For the NR/HPB-SiO<sub>2</sub> composite (70:30), the cracks generated by ozone exposure were shallow, small and discontinuous. This observation suggests that the HPB-SiO<sub>2</sub> as dispersed ozone resistant particles acted as a crack preventer for the NR matrix which could impede the rate at which the microvoids caused by ozone attacked the exposed surface and coalesced into macroscopic cracks [129]. Hence, the presence of HPB-SiO<sub>2</sub> nanoparticles could prevent the growth of cracks in the rubber.

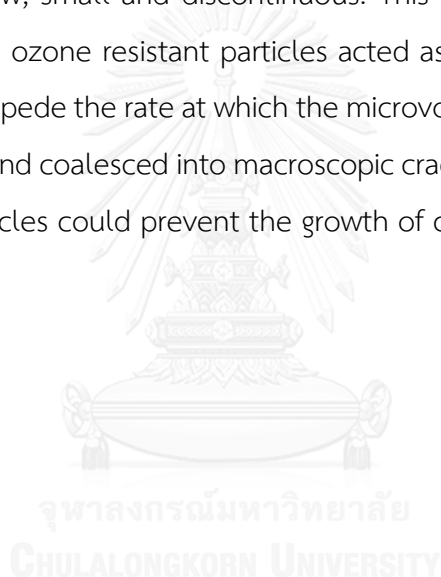


**Table 5. 4** Cracking of NR, NR/PB-SiO<sub>2</sub> and NR/HPB-SiO<sub>2</sub> nanocomposites.

Samples	NR/HPB-SiO <sub>2</sub> (wt/wt)	Type of cracking		
		24 h	48 h	78 h
NR	-	C-3	C-4	C-5
NR/PB-SiO <sub>2</sub> <sup>a</sup>	90/10	C-3	C-4	C-4
	80/20	C-3	C-4	C-4
	70/30	C-3	C-4	C-4
NR/HPB-SiO <sub>2</sub> <sup>b</sup>	90/10	B-2	C-3	C-3
	80/20	B-2	B-2	B-3
	70/30	nc <sup>c</sup>	A-2	A-2

\*Classification of cracking on the surface of rubber specimens. A: A small number of cracking. B: A large of number cracking. C: Numberless cracking. 1. That which cannot be seen with eyes but can be confirmed with 10 times magnifying glass. 2. That which can be confirmed with naked eyes. 3. That which the deep and comparatively long (below 1 mm). 4. That which the deep and long (above 1 mm and below 3 mm). 5. That which about to crack more than 3 mm or about to severe.

<sup>a</sup> PB-SiO<sub>2</sub> at M/H<sub>2</sub>O of 0.2, SDS of 5 wt%, KPS of 3 wt% and SiO<sub>2</sub> of 10 wt% based on BD monomer.

<sup>b</sup> HPB-SiO<sub>2</sub> at 98.6 %HD.

<sup>c</sup> The cracking was not appeared on the surface of the rubber composites.

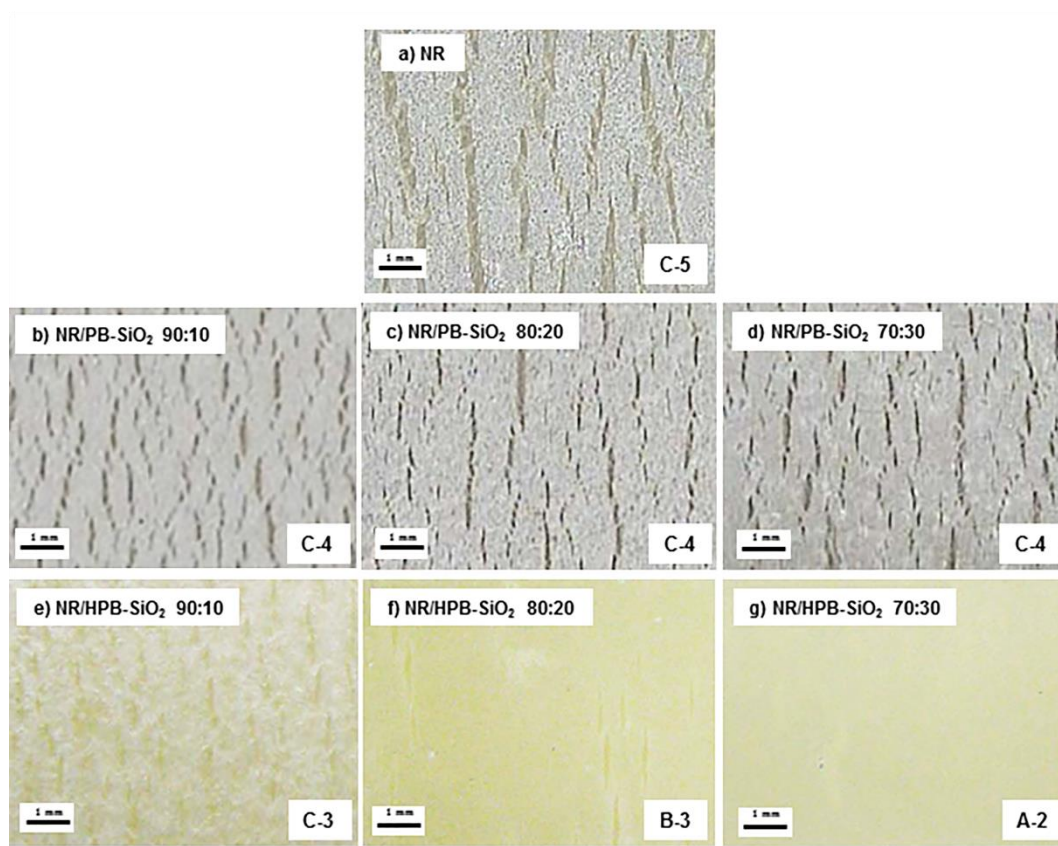


**Figure 5. 13** Surface of NR/PB-SiO<sub>2</sub> and NR/HPB-SiO<sub>2</sub> composites after ozone exposure for 72 h; (a) NR, (b) NR/PB-SiO<sub>2</sub> (90:10), (c) NR/PB-SiO<sub>2</sub> (80:20), (d) NR/PB-SiO<sub>2</sub> (70:30), (e) NR/HPB-SiO<sub>2</sub> (90:10), (f) NR/HPB-SiO<sub>2</sub> (80:20), (g) NR/HPB-SiO<sub>2</sub> (70:30).

## CHAPTER VI

### SBR/PS-SiO<sub>2</sub> NANOCOMPOSITES: PHYSICAL PROPERTIES

#### 6.1 Introduction

The addition of inorganic fillers into polymers is well known as being a beneficial way to improve the properties of the polymers. In fact, among the numerous organic/inorganic composites, polymer/silica composites are the most commonly reported in the literature. They have received much attention in recent years and have been employed in a variety of applications. Styrene butadiene rubber (SBR) films are widely used in coating and packaging due to their excellent properties such as high strength, high stiffness, good wet and dry adhesion, low gas and vapor permeability, and high transparency. Some properties could be improved by adding only a small amount of silica particles. In this study, polystyrene (PS)-SiO<sub>2</sub> were selected for blending with SBR latex to form a new SBR/PS-SiO<sub>2</sub> nanocomposites having improved mechanical, thermal and gas barrier properties while maintaining high transparency leading to a high potential for application in the coating and packaging field.

In this research work, a monodispersion of PS-SiO<sub>2</sub> nanoparticles with a uniform particle size distribution and core/shell morphology were prepared by differential microemulsion polymerization (DMP). The effect of silica loading and surfactant concentration on monomer conversion, grafting efficiency, silica encapsulation efficiency and particle size were studied. For SBR/PS-SiO<sub>2</sub> composite films, the mechanical properties, the thermal properties and oxygen and water vapor permeability were investigated.



## 6.2 Characterization of PS-SiO<sub>2</sub> Nanocomposites

Figure 6.1 shows the FTIR spectrum of SiO<sub>2</sub> modified with VTS and PS-SiO<sub>2</sub> nanoparticles to demonstrate successful functionalization and encapsulation on the silica nanoparticles. In the FTIR spectrum of modified SiO<sub>2</sub> (Figure 6.1a), the most intensive absorption band at 1097 cm<sup>-1</sup>, including the less intense bands at 800 and 473 cm<sup>-1</sup> are attributed to the vibration absorption of Si-O-Si groups. Moreover, the absorbance band at 3428 cm<sup>-1</sup> is assigned to the surface hydroxyl group (O-H) of silica. The absorption peaks at 3061 and 2957 cm<sup>-1</sup> relate to C-H and CH<sub>2</sub> stretching of the VTS groups. The bands at 1612 cm<sup>-1</sup> (C=C) and 1409 cm<sup>-1</sup> (CH out of plane bending) are attributed to the double bonds of VTS. These results indicate that VTS silane coupling agents could be bonded with silanol groups of silica to introduce a double bond on the silica surface.

For PS-SiO<sub>2</sub> nanoparticles (Figure 6.1b), the additional bands at 2919, 2846 and 1453 cm<sup>-1</sup> are related to the C-H asymmetric stretching, C-H symmetric stretching and C-H in plane bending in CH<sub>2</sub> groups, respectively. The peaks at 3102 and 1942 cm<sup>-1</sup> are assigned to the C-H symmetric stretching and overtone C-H out of plane bending in the aromatic ring, respectively. In addition, the C=C stretching skeletal in aromatic ring are apparent at 1598 and 1492 cm<sup>-1</sup>. C-H out of plane bending in the aromatic monosubstituted ring is evident at 756 and 697 cm<sup>-1</sup> [71]. These results confirm that the silica nanoparticle has been successfully encapsulated by PS via DMP.

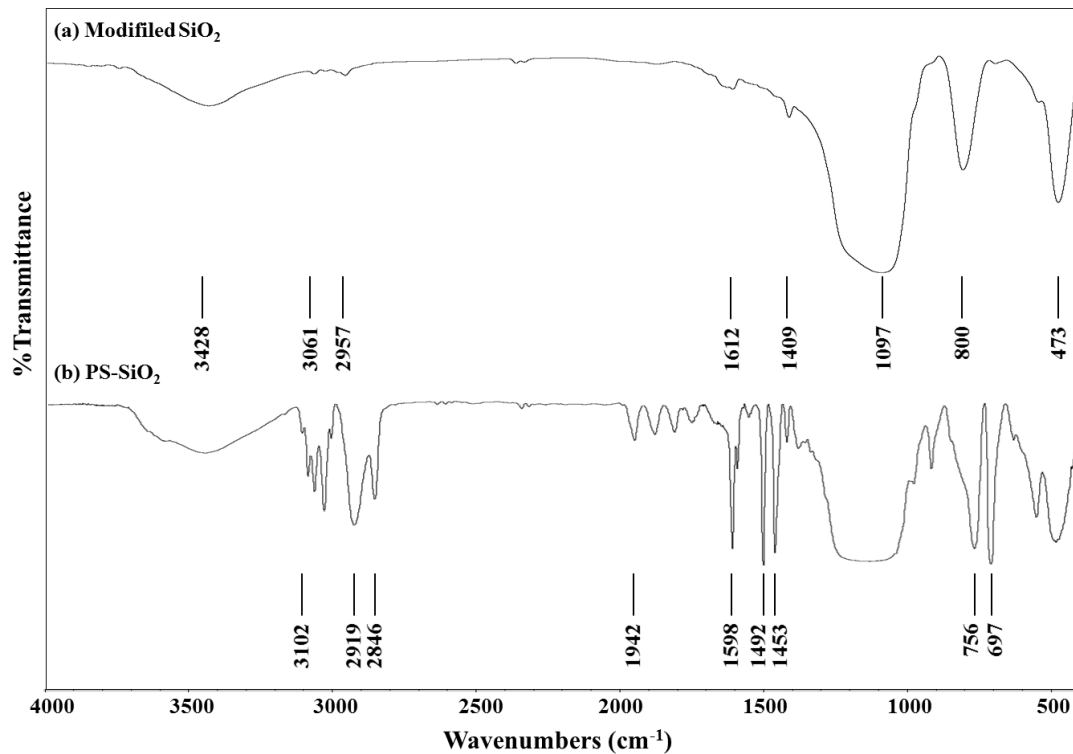


Figure 6.1 FTIR spectrum of (a) Modified SiO<sub>2</sub> and (b) PS-SiO<sub>2</sub>.

### 6.3 Effect of Process Parameters

#### 6.3.1 Effect of Silica Loading

The amount of silica loading had a significant effect on monomer conversion, silica encapsulation efficiency and particle size as shown in Figure 6.2a. The monomer conversion and silica encapsulation efficiency decreased while the particle size increased from 31.6 nm to 40.2 nm with an increase in silica loading from 5 to 20 wt%. This implies that at high silica loading, more aggregation of silica particles occurred and some SiO<sub>2</sub> particles were not encapsulated, resulting in low encapsulation efficiency and large particle size. It is probable that, the aggregation of silica particles was due to the decreased number of monomer-swollen micelles and therefore, particle stability and the final conversion decreased. For PS-SiO<sub>2</sub> synthesis, a silica loading of 5 to 10 wt% was appropriate for the SiO<sub>2</sub> encapsulation with a high monomer conversion (92-

87%), high silica encapsulation efficiency (90-82%) and small particle size (31-34 nm) via DMP. The effect of silica loading on the characteristics of PS-SiO<sub>2</sub> nanoparticles are shown in Figure 6.2b. The latex became more transparent with a decrease in silica loading. However, the DMP of ST on modified SiO<sub>2</sub> could provide PS-SiO<sub>2</sub> nanoparticles with a monodispersion of silica in the PS latex. Therefore, this novel method could enhance the compatibility and dispersion of silica in the PS matrix, reduce the silica-silica interaction resulting in a homogeneous PS-SiO<sub>2</sub> nanocomposite latex.

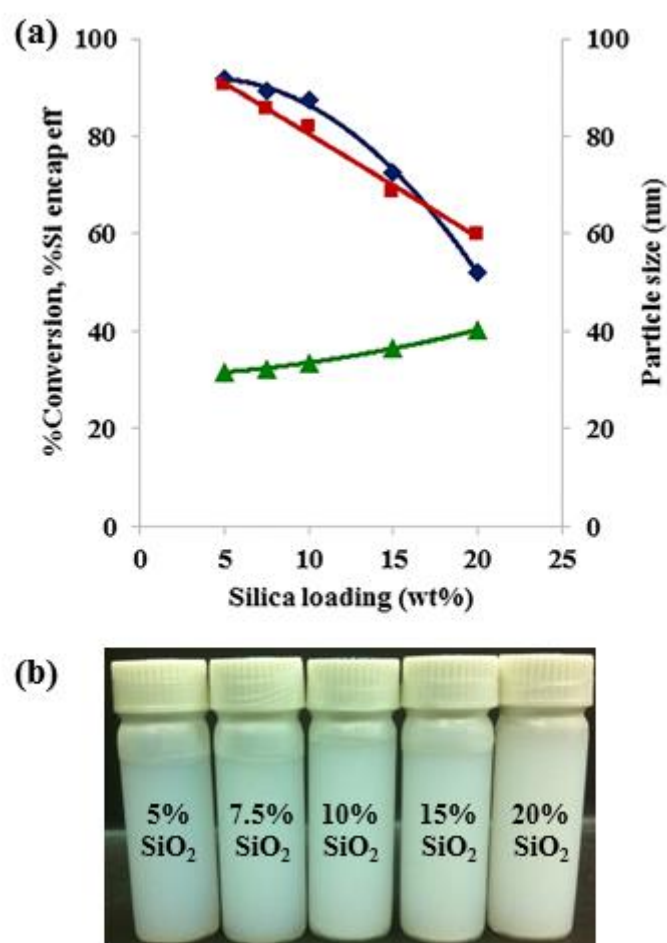


**Figure 6. 2** Effect of silica loading on; (a) (◆) %Conversion, (■) %Si encapsulation eff, (▲) Particle size and (b) characteristics of the latex. Condition:  $M/H_2O = 0.3$ , SDS = 3 wt%, KPS = 2 wt% based on monomer.

### 6.3.2 Effect of Surfactant Concentration

SDS was used as an anionic surfactant for encapsulation of nanosilica with PS at a concentration above the critical micelle concentration (CMC). The concentration of surfactant had a great influence on monomer conversion, polymer grafting efficiency and particle size as illustrated in Figure 6.3a. The monomer conversion increased from 72 to 94% with an increase in surfactant concentration from 1 to 10%. An increase in the SDS amount increased the number of monomer-swollen micelles which act as a reaction domain leading to an increase in the polymerization rate and the final conversion [106, 107]. However, the grafting efficiency decreased from 80% to 37% on increasing the surfactant concentration from 1 to 10 wt% based on monomer. This result implies that at a high surfactant concentration, the free PS (homopolymer) occurred instead of the encapsulation of SiO<sub>2</sub> within PS. When the surfactant concentration increased, the monomer was polymerized progressively faster and its chance to react with macroradicals was reduced resulting in limiting the graft polymerization and favoring the homopolymerization [113].

Moreover, the particle size decreased from 43 nm to 24 nm with an increase in the surfactant concentration from 1 to 10 wt% based on monomer. This can be explained in that at a high surfactant concentration, more micelles were generated and micellar nucleation could dominate over homogeneous nucleation while coagulative nucleation was neglected [108, 109]. Thus, more homogeneous latex particles were produced resulting in a smaller particle size. The surfactant concentration has a significant effect on the characteristics of the PS-SiO<sub>2</sub> nanoparticle latex as shown in Fig. 5.3b. This indicated that the PS-SiO<sub>2</sub> particles showed a trend of decreasing diameter and the latex became more transparent with an increase in surfactant concentration.

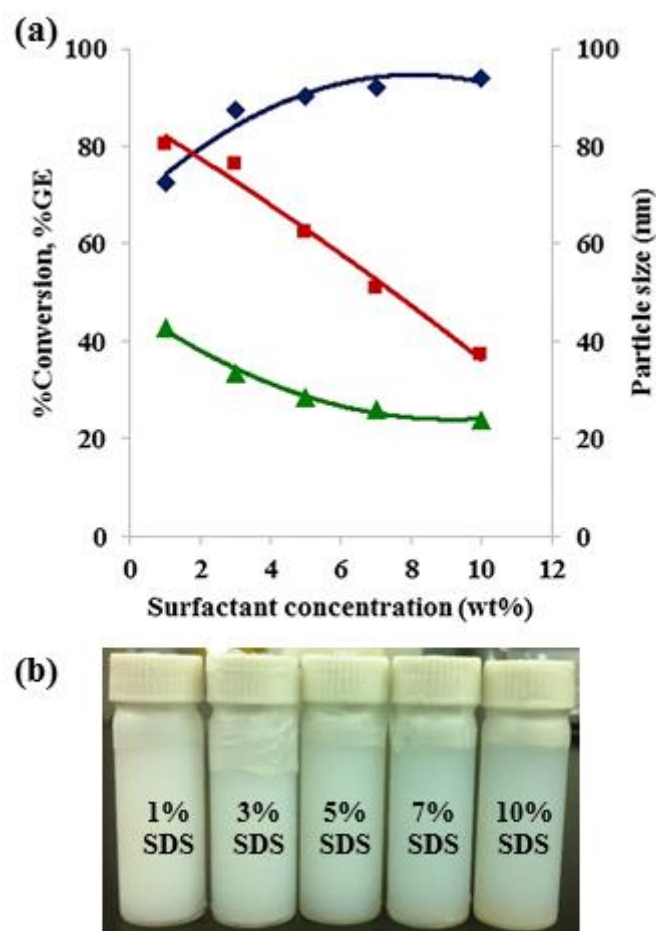


**Figure 6.3** Effect of surfactant concentration on; (a) (◆) %Conversion, (■) %GE, (▲) Particle size and (b) characteristics of the latex. Condition:  $\text{SiO}_2 = 10 \text{ wt\%}$ ,  $M/\text{H}_2\text{O} = 0.3$ ,  $\text{KPS} = 2 \text{ wt\%}$  based on monomer.

#### 6.4 Morphology of PS- $\text{SiO}_2$ Nanocomposites

Morphology of PS- $\text{SiO}_2$  nanoparticles observed by TEM is illustrated in Figure 6.4. These morphologies showed the encapsulation of darker  $\text{SiO}_2$  cores with lighter polymeric layer shells around the core. Interestingly, the  $\text{SiO}_2$  nanoparticles as regular spheres were well dispersed in the polymer latex and no agglomeration morphology of composite particles was predominantly observed. Therefore,  $\text{SiO}_2$  nanoparticles were encapsulated with a PS shell, indicating that core-shell nanoparticles were successfully produced from DMP. The particle size of the PS- $\text{SiO}_2$  nanocomposite as

seen from the TEM photograph were about 40 nm, 30 nm and 25 nm at 1 wt%, 3 wt% and 10 wt% surfactant concentration respectively in good agreement with the DLS characterization. Additionally, the thickness of PS shell decreased with increasing surfactant concentration. This implies that the grafting efficiency decreased with an increasing surfactant concentration resulting in a reduction in the PS shell thickness. However, the SiO<sub>2</sub> nanoparticles were well dispersed in the PS latex and uniform in size and a core-shell spherical morphology of the PS-SiO<sub>2</sub> nanocomposite was produced.

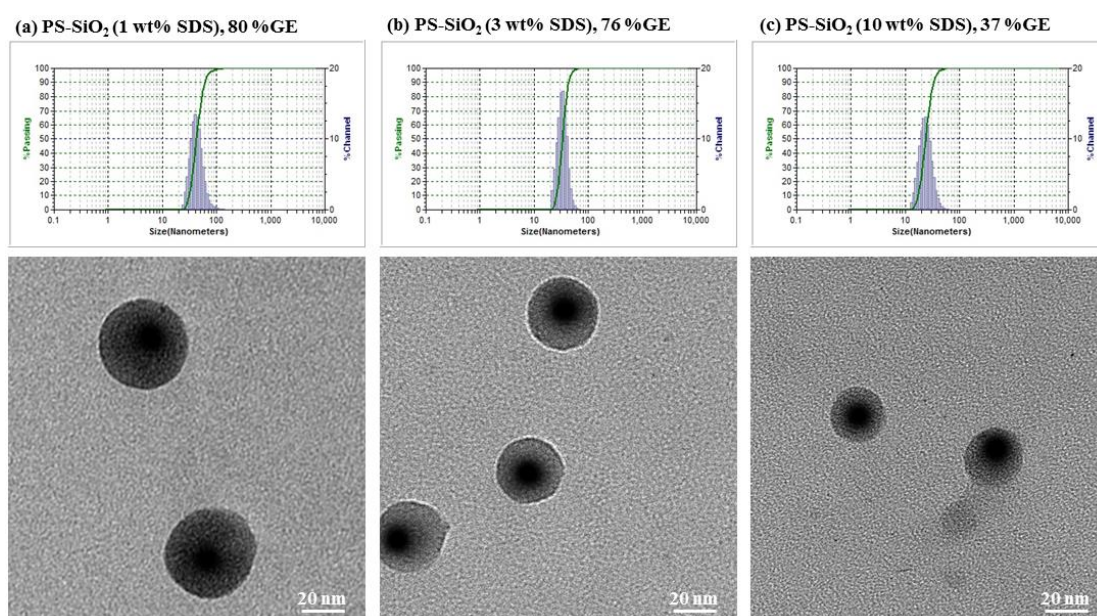


**Figure 6. 4** TEM imaging of PS-SiO<sub>2</sub> nanocomposite samples (a) 1 wt% SDS, (b) 3 wt% SDS and (c) 10 wt% SDS at 10 wt% silica loading. Condition: SiO<sub>2</sub> = 10 wt%, M/H<sub>2</sub>O = 0.3, KPS = 2 wt% based on monomer.

### 6.5 Thermal Properties of PS-SiO<sub>2</sub> Nanoparticles

The silica loading affected the decomposition temperature of PS-SiO<sub>2</sub> nanoparticles as shown in Fig. 6.5. The thermograms of PS and PS-SiO<sub>2</sub> show one-step polymer degradation and provided smooth weight loss curves, indicating the good

compatibility between PS and nano-SiO<sub>2</sub>. The decomposition of the PS and PS-SiO<sub>2</sub> was observed at temperatures over the range of 350 to 500 °C. The initial decomposition temperature ( $T_{id}$ ) and the temperature at the maximum of mass loss rate ( $T_{max}$ ) of all nanoparticle samples are presented in Table 6.1. The  $T_{id}$  and  $T_{max}$  of all PS-SiO<sub>2</sub> were higher than that of pure PS. It is obvious that the  $T_{id}$  of PS-SiO<sub>2</sub> was not significantly increased. However, the  $T_{max}$  of PS-SiO<sub>2</sub> samples increased from 408.3 °C to 420.4 °C with an increase in SiO<sub>2</sub> loading from 0 to 10 wt% based on monomer due to the high thermal resistance of the nanofiller and the hindered thermal movement of the polymer molecule chains. The inorganic phase could restrict the movement of the polymer chains with the effect of a high interaction in the organic-inorganic composite, resulting in more difficult scission of the polymer chains and an increase in the decomposition temperature [90, 130]. However,  $T_{max}$  was decreased at high silica loading (15-20 wt%) due to an agglomeration of nano-SiO<sub>2</sub> in the PS matrix resulting in a reduction of the thermal resistance. Therefore, the PS-SiO<sub>2</sub> nanoparticle at a silica loading of 10 wt% exhibited high thermal stability.

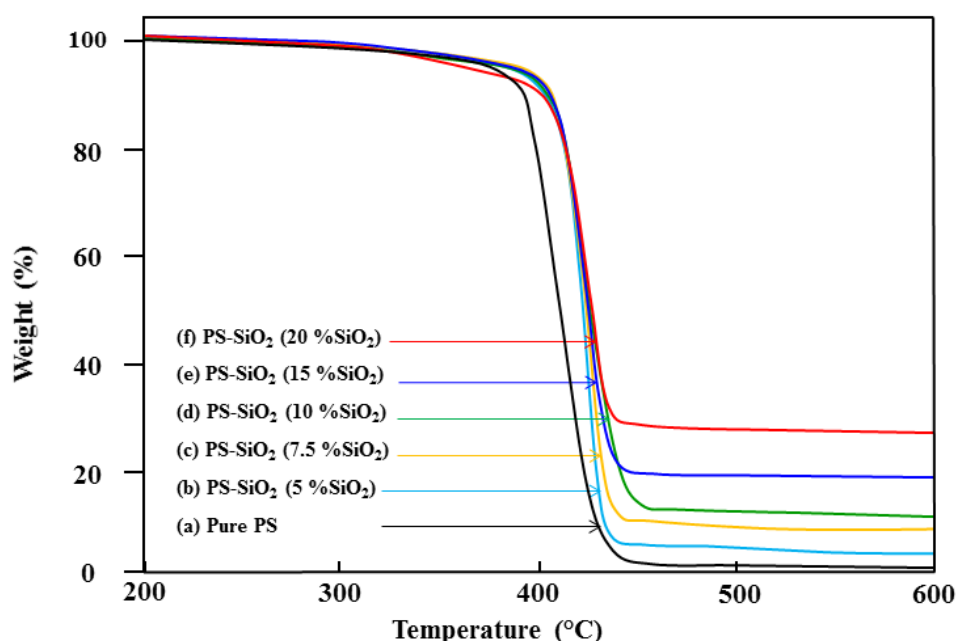


**Figure 6. 5** TGA thermograms of (a) Pure PS, (b) PS-SiO<sub>2</sub> (5 %SiO<sub>2</sub>), (c) PS-SiO<sub>2</sub> (7.5 %SiO<sub>2</sub>), (d) PS-SiO<sub>2</sub> (10 %SiO<sub>2</sub>), (e) PS-SiO<sub>2</sub> (15 %SiO<sub>2</sub>) and (f) PS-SiO<sub>2</sub> (20 %SiO<sub>2</sub>).

**Table 6. 1** Thermal properties of PS-SiO<sub>2</sub><sup>a</sup> nanocomposites.

SiO <sub>2</sub> (wt%)	%weight loss	T <sub>id</sub> (°C)	T <sub>max</sub> (°C)
0	98.4	387.5	408.3
5	93.6	396.7	413.7
7.5	89.1	395.8	415.9
10	85.8	389.9	420.4
15	80.1	392.2	418.5
20	74.0	392.1	415.5

<sup>a</sup> PS-SiO<sub>2</sub> preparation condition: M/H<sub>2</sub>O = 0.3, SDS = 3 wt%, KPS = 2 wt% based on monomer.

## 6.6 Thermal Properties of SBR/PS-SiO<sub>2</sub> Composites

The DSC thermograms of the SBR, SBR/PS-SiO<sub>2</sub> composites are shown in Figure 6.6 which indicate a one-step baseline shift around -30 to -15 °C. Therefore, all the samples have a single glass transition temperature (T<sub>g</sub>). The T<sub>g</sub> of the unfilled SBR and SBR/PS-SiO<sub>2</sub> composites at various blend ratios are presented in Table 6.2. The T<sub>g</sub> of SBR/PS-SiO<sub>2</sub> were slightly higher than that of unfilled SBR ( $\Delta T_g = 0.6-1.4$  °C). The increase in T<sub>g</sub> of SBR/PS-SiO<sub>2</sub> composites could be explained in that the T<sub>g</sub> of PS-SiO<sub>2</sub> at 10 wt% SiO<sub>2</sub> loading (104.3 °C) was much higher than that of unfilled SBR. Additionally, the T<sub>g</sub> of SBR/PS-SiO<sub>2</sub> composites slightly increased with increasing silica content. These phenomena could be explained in that the effect of a high interaction and interfacial area between SBR matrix and PS-SiO<sub>2</sub> nanoparticles caused increased restricting strength of PS-SiO<sub>2</sub> on the SBR molecules leading to an increase in T<sub>g</sub> [91].

The T<sub>id</sub> and T<sub>max</sub> of the unfilled SBR and SBR/PS-SiO<sub>2</sub> composites at various blend ratios are summarized in Table 6.2. The T<sub>id</sub> of SBR/PS-SiO<sub>2</sub> at blend ratios of 90:10 and 80:20 is 399.8 and 401.8 °C, respectively. It can be seen that T<sub>id</sub> of SBR/PS-SiO<sub>2</sub> did not significantly changed compared with unfilled SBR (400.2 °C). The T<sub>max</sub> of SBR/PS-SiO<sub>2</sub> composites slightly increased from 436.6 °C to 439.4 °C with an increase PS-SiO<sub>2</sub> loading in the composite from 0 to 20 wt% (SiO<sub>2</sub> content = 0 – 1 wt%). This



result implies that PS-SiO<sub>2</sub> could be uniformly dispersed in the SBR matrix resulting in the high thermal stability of the composites.

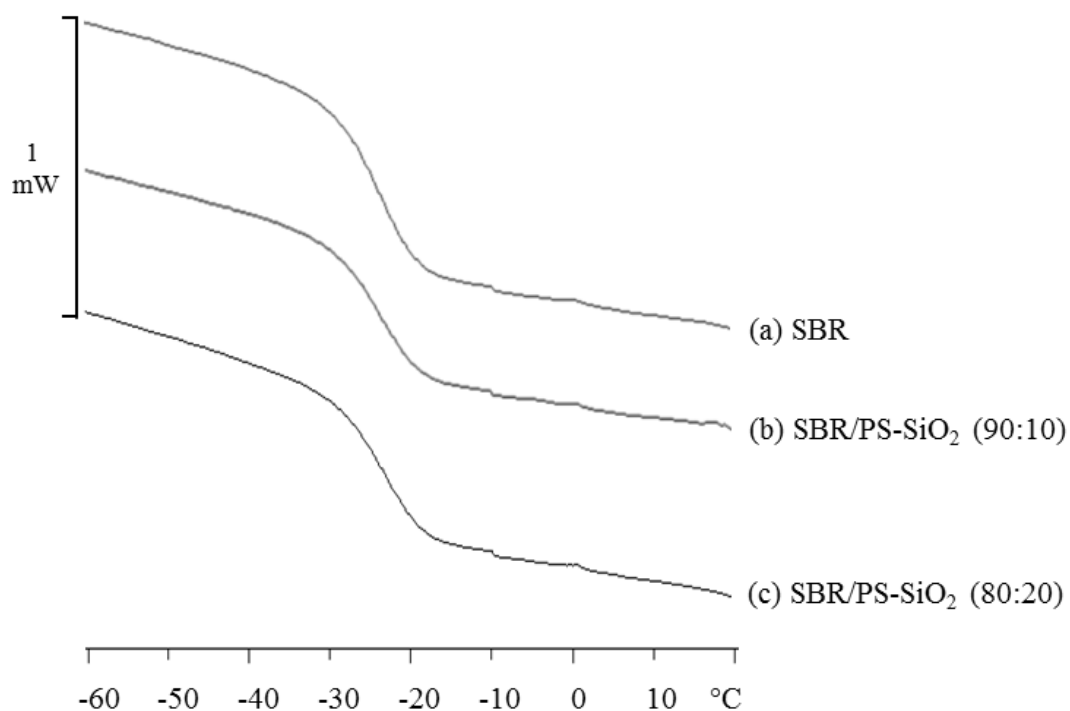


**Figure 6. 6** DSC thermograms of (a) SBR, (b) SBR/PS-SiO<sub>2</sub> (90:10) and (c) SBR/PS-SiO<sub>2</sub> (80:20).

**Table 6. 2** Thermal properties of SBR/PS-SiO<sub>2</sub> composite films.

SBR/PS-SiO <sub>2</sub> <sup>a</sup> (wt./wt.)	SiO <sub>2</sub> content <sup>b</sup> (wt.%)	T <sub>g</sub> (°C)	T <sub>id</sub> (°C)	T <sub>max</sub> (°C)
100/0	-	-24.8	400.2	436.6
90/10	1.0	-24.2	399.8	437.5
80/20	2.0	-23.4	401.8	439.4

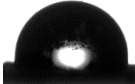
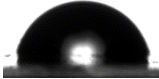

<sup>a</sup> PS-SiO<sub>2</sub> preparation condition: M/H<sub>2</sub>O = 0.3, SiO<sub>2</sub>= 10 wt%, SDS = 3 wt%, KPS = 2 wt% based on monomer.

<sup>b</sup> Silica content based on total rubber.

## 6.7 Surface Properties of SBR/PS-SiO<sub>2</sub> Composites

Table 6.3 shows the water contact angles of the PS-SiO<sub>2</sub> filled SBR composites with different PS-SiO<sub>2</sub> loading (SBR/PS-SiO<sub>2</sub> ratio of 100:0, 90:10 and 80:20). It can be seen that the water contact angles decreased with an increase of PS-SiO<sub>2</sub> loading in SBR, suggesting that more SiO<sub>2</sub> content in filled SBR composites led to the higher hydrophilicity of the SBR composite surface. When the PS-SiO<sub>2</sub> loading increased from 0 to 20 wt% (SiO<sub>2</sub> content = 0 – 2 wt%), the contact angle of the filled SBR surface increased from 98.4° to 64.7°. This result indicated that the reactive hydroxyl groups of the PS-SiO<sub>2</sub> nanoparticle exhibited an enhanced effect on the hydrophilic surface of the SBR composite films. For application in the coating and packaging field, the surface properties will influence the oxygen and water vapor permeability of SBR/PS-SiO<sub>2</sub> composites films. At high PS-SiO<sub>2</sub> loading, the transmission rate of oxygen and water vapor may increase due to an increase in the hydrophilic surface of the SBR composite films.

**Table 6.3** Contact angle of SBR/PS-SiO<sub>2</sub> composite films.

SBR/PS-SiO <sub>2</sub> <sup>a</sup> (wt/wt)	SiO <sub>2</sub> content <sup>b</sup> (wt%)	Contact angle in degree	Water droplet
100/0	-	98.4±4.8	
90/10	1.0	73.1±1.8	
80/20	2.0	64.7±1.8	

<sup>a</sup> PS-SiO<sub>2</sub> preparation condition: M/H<sub>2</sub>O = 0.3, SiO<sub>2</sub> = 10 wt%, SDS = 3 wt%, KPS = 2 wt% based on monomer.

<sup>b</sup> Silica content based on total polymer.

## 6.8 Mechanical Properties of SBR/PS-SiO<sub>2</sub> Composites

The PS-SiO<sub>2</sub> synthesized under optimal conditions (M/H<sub>2</sub>O = 0.3, SiO<sub>2</sub> = 10 wt%, SDS = 3 wt%, KPS = 2 wt% based on monomer) was selected for blending with SBR for mechanical testing. The effect of the amount of PS-SiO<sub>2</sub> (SBR/PS-SiO<sub>2</sub> ratio of 100:0, 90:10 and 80:20) on the tensile strength, 300% modulus and elongation at break of SBR/PS-SiO<sub>2</sub> composites are summarized in Table 6.4. The tensile strength of the SBR/PS-SiO<sub>2</sub> increased from 13.2 MPa to 16.8 MPa with an increase in the PS-SiO<sub>2</sub> loading from 0 to 20 wt% (SiO<sub>2</sub> content = 0 – 2 wt%). It is obvious that the PS-SiO<sub>2</sub> nanoparticles provide a reinforcing effect on the composites prepared from the SBR latex. The increase in the tensile strength may be due to the fact that the PS-SiO<sub>2</sub> nanoparticles were homogeneously distributed in the SBR matrix. The modulus at 300% strain of all SBR/PS-SiO<sub>2</sub> composites was much higher than that of unfilled SBR. It increased from 2.05 MPa to 4.47 MPa with an increase in the PS-SiO<sub>2</sub> loading from 0 to 20 wt% (SiO<sub>2</sub> content = 0 – 2 wt%). This implied that the improvement in the modulus of the SBR composites was due to the high interaction between the nanosized PS-SiO<sub>2</sub> and SBR matrix, and thus the stiffness of PS-SiO<sub>2</sub> could hinder the SBR main chain movement. For elongation at break, it can be seen that unfilled SBR exhibited the highest elongation at break at 610%. However, the elongation at break tended to decrease with an increase in the PS-SiO<sub>2</sub> nanofiller amount due to the hard and stiff nature of the PS-SiO<sub>2</sub> nanoparticles. This indicated that the addition of stiff PS-SiO<sub>2</sub> nanoparticles can reduce the elongation at break of the composites.

**Table 6. 4** Mechanical properties of SBR/PS-SiO<sub>2</sub> composites films.

SBR/PS-SiO <sub>2</sub> <sup>a</sup> (wt/wt)	SiO <sub>2</sub> content <sup>b</sup> (wt%)	Tensile strength (MPa)	300% Modulus (MPa)	Elongation at break (%)
100/0	-	13.2 ± 0.97	2.05 ± 0.59	610 ± 9
90/10	1.0	15.7 ± 0.57	3.22 ± 0.07	559 ± 13
80/20	2.0	16.8 ± 0.47	4.47 ± 0.21	520 ± 14

<sup>a</sup> PS-SiO<sub>2</sub> preparation condition: M/H<sub>2</sub>O = 0.3, SiO<sub>2</sub> = 10 wt%, SDS = 3 wt%, KPS = 2 wt% based on monomer.

<sup>b</sup> Silica content based on total polymer.

## 6.9 Morphology of SBR/PS-SiO<sub>2</sub> Composites

The surface morphology of unfilled SBR and PS-SiO<sub>2</sub> filled SBR matrix at various blend ratios (SBR/PS-SiO<sub>2</sub> ratio of 100:0, 90:10 and 80:20) was observed by SEM as shown in Figure 6.7. It can be seen that the surface of unfilled SBR was quite smooth (Figure 6.7a). For the addition of PS-SiO<sub>2</sub> into the SBR matrix, SEM micrographs showed that SBR/PS-SiO<sub>2</sub> composites exhibited rougher surfaces compared with the unfilled SBR. Moreover, the surface roughness of SBR/PS-SiO<sub>2</sub> composites tended to increase with an increase blend ratio (Figure 6.7b and 6.7c). However, the surface of SBR/PS-SiO<sub>2</sub> composites showed good compatibility between the nanofiller PS-SiO<sub>2</sub> and the SBR surface. This indicated that PS-SiO<sub>2</sub> had high interfacial adhesion and good compatibility with the SBR matrix resulting in an increase in interaction bonding and the dispersion of the SBR composite. Thus, good miscibility of the PS-SiO<sub>2</sub> (prepared by DMP) in the SBR matrix could be achieved and that mechanical properties of the SBR composites could be dramatically improved.

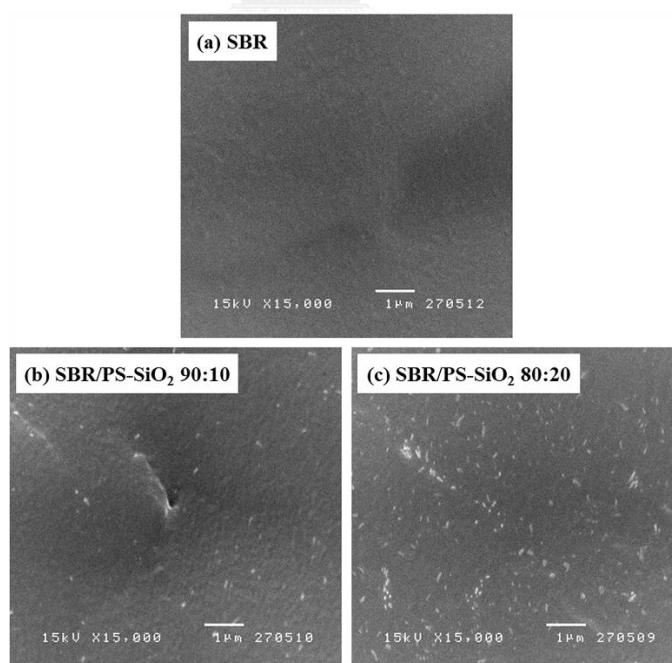


**Figure 6. 7** SEM micrographs (15000×) of (a) SBR, (b) SBR/PS-SiO<sub>2</sub> (90:10) and (c) SBR/PS-SiO<sub>2</sub> (80:20).

## CHAPTER VII

### CONCLUSIONS AND RECOMMENDATIONS

#### 7.1 Conclusions

**i) Preliminary Study on Synthesis of Styrene Butadiene Copolymer Nanoparticles via Differential Microemulsion Polymerization**

Using the technique of differential microemulsion polymerization, styrene butadiene copolymer (SBR) with at small particle size (39 nm) and narrow size distribution are prepared and stabilized at a very low SDS concentration of 3 wt% based on monomer as well as a high solid content of 14.7% was obtained. The monomer to water ratio, SDS and KPS concentration significantly affected the monomer conversion, polymer content and particle size of SBR. The SBR with a uniform size was spherical with a smooth surface as confirmed by TEM.

**ii) Preparation of Styrene Butadiene Copolymer-Silica Nanocomposites via Differential Microemulsion Polymerization and NR/SBR-SiO<sub>2</sub> Membrane for Pervaporation of Water-Ethanol Mixture**

Styrene butadiene copolymer-SiO<sub>2</sub> nanoparticles were synthesized via differential microemulsion polymerization. From a study of process parameter effects, the silica loading, monomer to water ratio, SDS and KPS concentration significantly affected the monomer conversion, grafting efficiency, silica encapsulation efficiency and particle size of SBR-SiO<sub>2</sub>. A high monomer conversion (87%), grafting efficiency (76%) and small particle size (43 nm) with narrow size distribution was obtained at optimum reaction conditions at a silica loading of 10 wt.%, monomer to water ratio of 0.2, SDS concentration of 3 wt.% and KPS concentration of 2 wt.%. From TEM photographs of the SBR-SiO<sub>2</sub>, it can be seen that the VTS-SiO<sub>2</sub> was completely encapsulated with SBR indicating a core-shell morphology with SiO<sub>2</sub> as the core and

the SBR as shell whose thickness depended on the grafting efficiency. A NR/SBR-SiO<sub>2</sub> nanocomposite as a novel membrane made from a green polymer was prepared for pervaporation of water-ethanol mixtures. The NR/SBR-SiO<sub>2</sub> membrane performance was strongly influenced by the feed mixture composition and SBR-SiO<sub>2</sub> loading in the membrane. The membranes show high water selectivity and the water partial flux increased with increasing SBR-SiO<sub>2</sub> loading and feed water concentration due to an increase of reactive hydroxyl groups. Thus, SBR-SiO<sub>2</sub> nanocomposites have good potential for future applications.

### **iii) Synthesis of Polybutadiene-Silica Nanoparticles via Differential Microemulsion Polymerization and their Hydrogenated Nanoparticles by Diimide Reduction**

PB-SiO<sub>2</sub> nanocomposites with SiO<sub>2</sub> as core and PB as shell were successfully synthesized via differential microemulsion polymerization, and then were hydrogenated via diimide reduction to produce the HPB-SiO<sub>2</sub> nanocomposite. These novel composites (PB-SiO<sub>2</sub> and HPB-SiO<sub>2</sub>) could be used as a nanofiller in natural rubber blends. From the study of process parameter effects on the synthesis of PB-SiO<sub>2</sub>, a high monomer conversion (81.5%), grafting efficiency (78.5%) and small particle size (27 nm) with narrow size distribution was obtained at optimal reaction conditions at a silica loading of 10 wt%, monomer to water ratio of 0.2, SDS concentration of 5 wt% and KPS concentration of 3 wt%. For diimide hydrogenation, an increase in the concentration of hydrazine hydrate and hydrogen peroxide had a beneficial effect on the PB-SiO<sub>2</sub> hydrogenation. The highest HD (98.6 %) of HPB-SiO<sub>2</sub> was achieved under optimal conditions and the thermal stability of HPB-SiO<sub>2</sub> was significantly improved. For thermal properties of the NR composites, NR/HPB-SiO<sub>2</sub> had two maximum decomposition temperatures attributed to NR and HPB-SiO<sub>2</sub>, while the NR/PB-SiO<sub>2</sub> had only one maximum decomposition temperature. However, the thermal properties of NR/HPB-SiO<sub>2</sub> were subsequently improved as compared to an unfilled NR and NR/PB-SiO<sub>2</sub>. For mechanical properties of NR/PB-SiO<sub>2</sub> and NR/HPB-SiO<sub>2</sub> composites, the tensile strength and modulus of the composites were higher than those of unfilled NR,

indicating that compatibility of NR, PB-SiO<sub>2</sub> and HPB-SiO<sub>2</sub> occurred resulting in an increase in the mechanical and thermal properties of NR composites. Moreover, the incorporation of HPB-SiO<sub>2</sub> as a novel nanofiller in NR could prevent ozone-induced degradation favoring an improvement in ozone resistance. Thus, HPB-SiO<sub>2</sub> can be used as a nanoreinforcing filler and thermal and ozone stabilizer for NR composites.

#### iv) SBR/PS-SiO<sub>2</sub> Nanocomposites: Physical Properties

Well-dispersed PS-SiO<sub>2</sub> with a small particle size and a narrow size distribution was successfully synthesized by differential microemulsion polymerization using SDS and KPS as the surfactant and initiator, respectively. Nanosized SiO<sub>2</sub>-PS core-shell particles were achieved whose PS shell thickness depended on the grafting efficiency as confirmed by TEM. From process parameter effects, a high monomer conversion (87.4%), grafting efficiency (76.3%), silica encapsulation efficiency (81.9%) and small particle size (33.5 nm) with narrow size distribution was obtained at optimal reaction conditions at a silica loading of 10 wt%, monomer to water ratio of 0.3, SDS concentration of 3 wt% and KPS concentration of 2 wt%. The composites of SBR/PS-SiO<sub>2</sub> were successfully prepared by latex blending. From the mechanical properties, it is seen that the incorporation of an appropriate amount of PS-SiO<sub>2</sub> apparently improved the tensile strength and modulus at 300% strain, whereas the elongation at break deteriorated with the incorporation of PS-SiO<sub>2</sub> nanoparticles. The thermal properties showed that, the glass transition temperature ( $T_g$ ) and maximum decomposition temperature ( $T_{max}$ ) increased with the addition of PS-SiO<sub>2</sub> nanoparticles in the SBR matrix. Therefore, the synthesis of PS-SiO<sub>2</sub> core-shell nanoparticles with good dispersion is of importance from both an academic and industrial point of view.

## 7.2 Recommendations

Further research on the preparation of new polymer-silica nanocomposites should be concerned with the following aspects:

1. It is desirable to achieve high thermal stability and good mechanical properties of acrylonitrile–butadiene rubber (NBR), thus, the incorporation of nanosilica via differential microemulsion polymerization could be potentially applied to synthesize NBR-SiO<sub>2</sub> nanocomposites using modified silica, acrylonitrile and butadiene as starting materials.
2. It is clear that a high hydrogenation degree and thermal stability of PB-SiO<sub>2</sub> have been achieved via diimide reduction. Therefore, diimide hydrogenation of other composite such as styrene-butadiene rubber (SBR)-SiO<sub>2</sub> in latex form should be further studied.
3. NR filled with SBR-SiO<sub>2</sub>, PB-SiO<sub>2</sub> and HPB-SiO<sub>2</sub> nanocomposites, as well as SBR filled with PS-SiO<sub>2</sub> clearly exhibited a dramatic improvement in mechanical properties, thermal stability and ozone resistance. Hence, this suggested that the use of SBR-SiO<sub>2</sub>, PB-SiO<sub>2</sub>, HPB-SiO<sub>2</sub> and PS-SiO<sub>2</sub> filled in PB and NBR should be further studied to increase their performance under aggressive environments.



## REFERENCES

- [1] Atik SS, Thomas JK. Polymerized microemulsions. *Journal of the American Chemical Society*. 1981;103:4279-80.
- [2] Desai SD, Gordon RD, Gronda AM, Cussler EL. Polymerized microemulsions. *Current Opinion in Colloid & Interface Science*. 1996;1:519-22.
- [3] Eastoe J, Warne B. Nanoparticle and polymer synthesis in microemulsions. *Current Opinion in Colloid & Interface Science*. 1996;1:800-5.
- [4] Stoffer JO, Bone T. Polymerization in water-in-oil microemulsion systems. I. *Journal of Polymer Science: Polymer Chemistry Edition*. 1980;18:2641-8.
- [5] Larpent C. *Microemulsion Polymerization. Colloidal Polymers: Synthesis and Characterization*. New York: CRC Press; 2003.
- [6] Fendler JH, Fendler EJ. *Catalysis in micellar and macromoleular systems*. New York: Academic Press; 2012.
- [7] Candau F. *Polymerization in Microemulsions*. New York: Gordon and Breach; 1992.
- [8] Candau F. *Polymerization in Microemulsions*. New York: Marcel Dekker; 1999.
- [9] Gan LM, Chew CH, Lye I, Imae T. Microemulsion polymerization of styrene. *Polymer Bulletin*. 1991;25:193-8.
- [10] Roy S, Devi S. Mechanism of microemulsion polymerization of methyl methacrylate: Experimental evidence. *Journal of Applied Polymer Science*. 1996;62:1509-16.
- [11] Larpent C, Bernard E, Richard J, Vaslin S. Polymerization in microemulsions with polymerizable cosurfactants: A route to highly functionalized nanoparticles. *Macromolecules*. 1997;30:354-62.
- [12] He GW, Pan QM, Rempel GL. Synthesis of poly(methyl methacrylate) nanosize particles by differential microemulsion polymerization. *Macromolecular Rapid Communications*. 2003;24:585-8.
- [13] He GW, Pan QM, Rempel GL. Modeling of differential microemulsion polymerization for synthesizing nanosized poly(methyl methacrylate) particles. *Industrial & Engineering Chemistry Research*. 2007;46:1682-9.

- [14] Yuan L, Wang Y, Pan MZ, Rempel GL, Pan QM. Synthesis of poly(methyl methacrylate) nanoparticles via differential microemulsion polymerization. *European Polymer Journal*. 2013;49:41-8.
- [15] Sun Y, Zhang Z, Wong CP. Study on mono-dispersed nano-size silica by surface modification for underfill applications. *Journal of Colloid and Interface Science*. 2005;292:436-44.
- [16] Morris JE. *Nanopackaging: Nanotechnologies and Electronics Packaging*. New York: Springer; 2008.
- [17] Conradi M. Nanosilica-Reinforced Polymer Composites. *Material and Thechnology*. 2013;47:285-93.
- [18] Bagwe RP, Hilliard LR, Tan W. Surface modification of silica nanoparticles to reduce aggregation and nonspecific binding. *Langmuir*. 2006;22:4357-62.
- [19] Ma XK, Lee NH, Oh HJ, Kim JW, Rhee CK, Park KS, et al. Surface modification and characterization of highly dispersed silica nanoparticles by a cationic surfactant. *Colloids and Surfaces A: Physicochemical and Engineering Aspects*. 2010;358:172-6.
- [20] Ahn SH, Kim SH, Lee SG. Surface-modified silica nanoparticle-reinforced poly(ethylene 2,6-naphthalate). *Journal of Applied Polymer Science*. 2004;94:812-8.
- [21] Ramier J, Chazeau L, Gauthier C, Guy L, Bouchereau MN. Grafting of silica during the processing of silica-filled SBR: Comparison between length and content of the silane. *Journal of Polymer Science Part B: Polymer Physics*. 2006;44:143-52.
- [22] Zou H, Wu S, Shen J. Polymer/silica nanocomposites: preparation, characterization, properties, and applications. *Chemical Reviews*. 2008;108:3893-957.
- [23] Jesionowski T, Krysztafkiewicz A. Influence of silane coupling agents on surface properties of precipitated silicas. *Applied Surface Science*. 2001;172:18-32.
- [24] Liu Q, Ding J, Chambers DE, Debnath S, Wunder SL, Baran GR. Filler-coupling agent-matrix interactions in silica/polymethylmethacrylate composites. *Journal of Biomedical Materials Research*. 2001;57:384-93.
- [25] Haldorai Y, Lyoo WS, Noh SK, Shim J-J. Ionic liquid mediated synthesis of silica/polystyrene core-shell composite nanospheres by radical dispersion polymerization. *Reactive and Functional Polymers*. 2010;70:393-9.

- [26] Lin J, Siddiqui JA, Ottenbrite RM. Surface modification of inorganic oxide particles with silane coupling agent and organic dyes. *Polymers for Advanced Technologies*. 2001;12:285-92.
- [27] Sun SS, Li CZ, Zhang L, Du HL, Burnell-Gray JS. Effects of surface modification of fumed silica on interfacial structures and mechanical properties of poly(vinyl chloride) composites. *European Polymer Journal*. 2006;42:1643-52.
- [28] Schaefer DW, Justice RS. How Nano Are Nanocomposites? *Macromolecules*. 2007;40:8501-17.
- [29] Krishnamoorti R, Vaia RA. Polymer nanocomposites. *Journal of Polymer Science Part B: Polymer Physics*. 2007;45:3252-6.
- [30] Balazs AC, Emrick T, Russell TP. Nanoparticle polymer composites: where two small worlds meet. *Science*. 2006;314:1107-10.
- [31] Rong MZ, Zhang MQ, Zheng YX, Zeng HM, Walter R, Friedrich K. Structure–property relationships of irradiation grafted nano-inorganic particle filled polypropylene composites. *Polymer*. 2001;42:167-83.
- [32] Pérez LD, Giraldo LF, López BL, Hess M. Reinforcing of Elastomers with Mesoporous Silica. *Macromolecular Symposia*. 2006;245-246:628-40.
- [33] Wu CL, Zhang MQ, Rong MZ, Friedrich K. Silica nanoparticles filled polypropylene: effects of particle surface treatment, matrix ductility and particle species on mechanical performance of the composites. *Composites Science and Technology*. 2005;65:635-45.
- [34] Huang L, Zhan RB, Lu YF. Mechanical properties and crystallization behavior of polypropylene/nano-SiO<sub>2</sub> composites. *Journal of reinforced plastics and composites*. 2006;25:1001-12.
- [35] Kontou E, Niaounakis M. Thermo-mechanical properties of LLDPE/SiO<sub>2</sub> nanocomposites. *Polymer*. 2006;47:1267-80.
- [36] Reddy CS, Das CK. HLDPE/organic functionalized SiO<sub>2</sub> nanocomposites with improved thermal stability and mechanical properties. *Composite Interfaces*. 2005;11:687-99.
- [37] Kontou E, Anthoulis G. The effect of silica nanoparticles on the thermomechanical properties of polystyrene. *Journal of Applied Polymer Science*. 2007;105:1723-31.

- [38] Yang F, Nelson GL. PMMA/silica nanocomposite studies: Synthesis and properties. *Journal of Applied Polymer Science*. 2004;91:3844-50.
- [39] Ou CF, Hsu MC. Preparation and characterization of cyclo olefin copolymer (COC)/silica nanoparticle composites by solution blending. *Journal of Polymer Research*. 2007;14:373-8.
- [40] Rong MZ, Zhang MQ, Zheng YX, Zeng HM, Walter R, Friedrich K. Irradiation graft polymerization on nano-inorganic particles: An effective means to design polymer-based nanocomposites. *Journal of Materials Science Letters*. 2000;19:1159-61.
- [41] Zhang MQ, Rong MZ, Zeng HM, Schmitt S, Wetzel B, Friedrich K. Atomic force microscopy study on structure and properties of irradiation grafted silica particles in polypropylene-based nanocomposites. *Journal of Applied Polymer Science*. 2001;80:2218-27.
- [42] Lee J, Hong CK, Choe S, Shim SE. Synthesis of polystyrene/silica composite particles by soap-free emulsion polymerization using positively charged colloidal silica. *Journal of Colloid and Interface Science*. 2007;310:112-20.
- [43] Schmid A, Fujii S, Armes SP. Synthesis of micrometer-sized silica-stabilized polystyrene latex particles. *Langmuir*. 2005;21:8103-5.
- [44] Schmid A, Fujii S, Armes SP, Leite CAP, Galembeck F, Minami H, et al. Polystyrene–Silica Colloidal Nanocomposite Particles Prepared by Alcoholic Dispersion Polymerization. *Chemistry of Materials*. 2007;19:2435-45.
- [45] Stejskal J, Kratochvil P, Armes SP, Lascelles SF, Riede A, Helmstedt M, et al. Polyaniline dispersions .6. Stabilization by colloidal silica particles. *Macromolecules*. 1996;29:6814-9.
- [46] Schmid A, Fujii S, Armes SP. Polystyrene-silica nanocomposite particles via alcoholic dispersion polymerization using a cationic azo initiator. *Langmuir*. 2006;22:4923-7.
- [47] Percy MJ, Michailidou V, Armes SP, Perruchot C, Watts JF, Greaves SJ. Synthesis of Vinyl Polymer–Silica Colloidal Nanocomposites via Aqueous Dispersion Polymerization. *Langmuir*. 2003;19:2072-9.
- [48] Zhu A, Shi Z, Cai A, Zhao F, Liao T. Synthesis of core–shell PMMA–SiO<sub>2</sub> nanoparticles with suspension–dispersion–polymerization in an aqueous system and

its effect on mechanical properties of PVC composites. *Polymer Testing*. 2008;27:540-7.

[49] Duan L, Chen M, Zhou S, Wu L. Synthesis and characterization of poly(N-isopropylacrylamide)/silica composite microspheres via inverse pickering suspension polymerization. *Langmuir*. 2009;25:3467-72.

[50] Mayes AG, Mosbach K. Molecularly imprinted polymer beads: suspension polymerization using a liquid perfluorocarbon as the dispersing phase. *Analytical Chemistry*. 1996;68:3769-74.

[51] Li H, You B, Gu GX, Wu LM, Chen GD. Particle size and morphology of poly[styrene-co-(butyl acrylate)]/nano-silica composite latex. *Polymer International*. 2005;54:191-7.

[52] Zeng Z, Yu J, Guo Z-X. Preparation of epoxy-functionalized polystyrene/silica core-shell composite nanoparticles. *Journal of Polymer Science Part A: Polymer Chemistry*. 2004;42:2253-62.

[53] Zhang K, Zheng LL, Zhang XH, Chen X, Yang B. Silica-PMMA core-shell and hollow nanospheres. *Colloids and Surfaces A: Physicochemical and Engineering Aspects*. 2006;277:145-50.

[54] Zhang K, Chen HT, Chen X, Chen ZM, Cui ZC, Yang B. Monodisperse silica-polymer core-shell microspheres via surface grafting and emulsion polymerization. *Macromolecular Materials and Engineering*. 2003;288:380-5.

[55] Reculosa S, Mingotaud C, Bourgeat-Lami E, Duguet E, Ravaine S. Synthesis of daisy-shaped and multipod-like silica/polystyrene nanocomposites. *Nano Letters*. 2004;4:1677-82.

[56] Bourgeat-Lami E, Espiard P, Guyot A. Poly(Ethyl Acrylate) Latexes Encapsulating Nanoparticles of Silica .1. Functionalization and Dispersion of Silica. *Polymer*. 1995;36:4385-9.

[57] Espiard P, Guyot A. Poly(Ethyl Acrylate) Latexes Encapsulating Nanoparticles of Silica .2. Grafting Process onto Silica. *Polymer*. 1995;36:4391-5.

[58] Espiard P, Guyot A, Perez J, Vigier G, David L. Poly(Ethyl Acrylate) Latexes Encapsulating Nanoparticles of Silica .3. Morphology and Mechanical-Properties of Reinforced Films. *Polymer*. 1995;36:4397-403.

- [59] Ding XF, Zhao JZ, Liu YH, Zhang HB, Wang ZC. Silica nanoparticles encapsulated by polystyrene via surface grafting and in situ emulsion polymerization. *Materials Letters*. 2004;58:3126-30.
- [60] Mahdavian AR, Ashjari M, Makoo AB. Preparation of poly (styrene–methyl methacrylate)/SiO<sub>2</sub> composite nanoparticles via emulsion polymerization. An investigation into the compatibilization. *European Polymer Journal*. 2007;43:336-44.
- [61] Qiang W, Wang Y, He P, Xu H, Gu H, Shi D. Synthesis of asymmetric inorganic/polymer nanocomposite particles via localized substrate surface modification and miniemulsion polymerization. *Langmuir*. 2008;24:606-8.
- [62] Boutti S, Bourgeat-Lami E, Zydowicz N. Silica/polyamide nanocomposite synthesis via an original double emulsification process in miniemulsion. *Macromolecular Rapid Communications*. 2005;26:1860-5.
- [63] Qiao XG, Chen M, Zhou J, Wu LM. Synthesis of raspberry-like silica/polystyrene/silica multilayer hybrid particles via miniemulsion polymerization. *Journal of Polymer Science Part A: Polymer Chemistry*. 2007;45:1028-37.
- [64] Zhou J, Zhang SW, Qiao XG, Li XQ, Wu LM. Synthesis of SiO<sub>2</sub>/poly(styrene-co-butyl acrylate) nanocomposite microspheres via miniemulsion polymerization. *Journal of Polymer Science Part A: Polymer Chemistry*. 2006;44:3202-9.
- [65] Zhang SW, Zhou SX, Weng YM, Wu LM. Synthesis of SiO<sub>2</sub>/polystyrene nanocomposite particles via miniemulsion polymerization. *Langmuir*. 2005;21:2124-8.
- [66] Chow PY, Gan LM. Microemulsion processing of silica-polymer nanocomposites. *Journal of nanoscience and nanotechnology*. 2004;4:197-202.
- [67] Xu P, Wang HT, Tong R, Du QG, Zhong W. Preparation and morphology of SiO<sub>2</sub>/PMMA nanohybrids by microemulsion polymerization. *Colloid and Polymer Science*. 2006;284:755-62.
- [68] Tiarks F, Landfester K, Antonietti M. Silica nanoparticles as surfactants and fillers for latexes made by miniemulsion polymerization. *Langmuir*. 2001;17:5775-80.
- [69] Qi DM, Bao YZ, Weng ZX, Huang ZM. Preparation of acrylate polymer/silica nanocomposite particles with high silica encapsulation efficiency via miniemulsion polymerization. *Polymer*. 2006;47:4622-9.

- [70] Kickelbick G. Concepts for the incorporation of inorganic building blocks into organic polymers on a nanoscale. *Progress in Polymer Science*. 2003;28:83-114.
- [71] Chuayjuljit S, Boonmahitthisud A. Natural rubber nanocomposites using polystyrene-encapsulated nanosilica prepared by differential microemulsion polymerization. *Applied Surface Science*. 2010;256:7211-6.
- [72] Kongsinlark A, Rempel GL, Prasassarakich P. Synthesis of monodispersed polyisoprene–silica nanoparticles via differential microemulsion polymerization and mechanical properties of polyisoprene nanocomposite. *Chemical Engineering Journal*. 2012;193-194:215-26.
- [73] Singha NK, Bhattacharjee S, Sivaram S. Hydrogenation of diene elastomers, their properties and applications: A critical review. *Rubber Chemistry and Technology*. 1997;70:309-67.
- [74] Pasto DJ. A theoretical study of the disproportionation reactions of diimide ( $N_2H_2$ ) species. *Journal of the American Chemical Society*. 1979;101:6852-7.
- [75] Parker DK, Roberts RF, Schiessl HW. A New Process for the Preparation of Highly Saturated Nitrile Rubber in Latex Form. *Rubber Chemistry and Technology*. 1992;65:245-58.
- [76] He Y, Daniels ES, Klein A, ElAasser MS. Hydrogenation of styrene-butadiene rubber (SBR) latexes. *Journal of Applied Polymer Science*. 1997;64:2047-56.
- [77] De Sarkar M, De PP, Bhowmick AK. Diimide reduction of carboxylated styrene–butadiene rubber in latex stage. *Polymer*. 2000;41:907-15.
- [78] Xie H-Q, Li X-D, Liu X-Y, Guo J-S. Hydrogenation and neutralization of carboxylic styrene-butadiene latex to form thermoplastic elastomer with excellent thermooxidation resistance. *Journal of Applied Polymer Science*. 2002;83:1375-84.
- [79] Xie H-Q, Li X-D, Guo J-S. Hydrogenation of nitrile-butadiene rubber latex to form thermoplastic elastomer with excellent thermooxidation resistance. *Journal of Applied Polymer Science*. 2003;90:1026-31.
- [80] Lin XW, Pan QM, Rempel GL. Gel formation in diimide-hydrogenated polymers. *Journal of Applied Polymer Science*. 2005;96:1122-5.
- [81] Mahittikul A, Prasassarakich P, Rempel GL. Diimide hydrogenation of natural rubber latex. *Journal of Applied Polymer Science*. 2007;105:1188-99.

- [82] Simma K, Rempel GL, Prasassarakich P. Improving thermal and ozone stability of skim natural rubber by diimide reduction. *Polymer Degradation and Stability*. 2009;94:1914-23.
- [83] Kongsinlark A, Rempel GL, Prasassarakich P. Hydrogenated polyisoprene-silica nanoparticles and their applications for nanocomposites with enhanced mechanical properties and thermal stability. *Journal of Nanoparticle Research*. 2013;15:1-16.
- [84] Crosby AJ, Lee JY. Polymer nanocomposites: the “nano” effect on mechanical properties. *Polymer reviews*. 2007;47:217-29.
- [85] Rong MZ, Zhang MQ, Zheng YX, Zeng HM, Friedrich K. Improvement of tensile properties of nano-SiO<sub>2</sub>/PP composites in relation to percolation mechanism. *Polymer*. 2001;42:3301-4.
- [86] Bikiaris DN, Papageorgiou GZ, Pavlidou E, Vouroutzis N, Palatzoglou P, Karayannidis GP. Preparation by melt mixing and characterization of isotactic polypropylene/SiO<sub>2</sub> nanocomposites containing untreated and surface-treated nanoparticles. *Journal of Applied Polymer Science*. 2006;100:2684-96.
- [87] Suzuki N, Ito M, Yatsuyanagi F. Effects of rubber/filler interactions on deformation behavior of silica filled SBR systems. *Polymer*. 2005;46:193-201.
- [88] Peng Z, Kong LX, Li SD, Chen Y, Huang MF. Self-assembled natural rubber/silica nanocomposites: Its preparation and characterization. *Composites Science and Technology*. 2007;67:3130-9.
- [89] Liu X, Zhao SH. Measurement of the condensation temperature of nanosilica powder organically modified by a silane coupling agent and its effect evaluation. *Journal of Applied Polymer Science*. 2008;108:3038-45.
- [90] Ray SS, Okamoto M. Polymer/layered silicate nanocomposites: a review from preparation to processing. *Progress in Polymer Science*. 2003;28:1539-641.
- [91] Shang XY, Zhu ZK, Yin J, Ma XD. Compatibility of soluble polyimide/silica hybrids induced by a coupling agent. *Chemistry of Materials*. 2002;14:71-7.
- [92] Li SD, Peng Z, Kong LX, Zhong JP. Thermal degradation kinetics and morphology of natural rubber/silica nanocomposites. *Journal of nanoscience and nanotechnology*. 2006;6:541-6.



- [93] Feng XS, Huang RYM. Liquid separation by membrane pervaporation: A review. *Industrial & Engineering Chemistry Research*. 1997;36:1048-66.
- [94] Wijmans JG, Baker RW. The Solution-Diffusion Model - a Review. *Journal of Membrane Science*. 1995;107:1-21.
- [95] Kataoka T, Tsuru T, Nakao S-i, Kimura S. Permeation equations developed for prediction of membrane performance in pervaporation, vapor permeation and reverse osmosis based on the solution-diffusion model. *JOURNAL OF CHEMICAL ENGINEERING OF JAPAN*. 1991;24:326-33.
- [96] Okada T, Yoshikawa M, Matsuura T. A study on the pervaporation of ethanol/water mixtures on the basis of pore flow model. *Journal of Membrane Science*. 1991;59:151-68.
- [97] Okada T, Matsuura T. Predictability of transport equations for pervaporation on the basis of pore-flow mechanism. *Journal of Membrane Science*. 1992;70:163-75.
- [98] Okada T, Matsuura T. A new transport model for pervaporation. *Journal of Membrane Science*. 1991;59:133-49.
- [99] Liu YL, Hsu CY, Su YH, Lai JY. Chitosan-silica complex membranes from sulfonic acid functionalized silica nanoparticles for pervaporation dehydration of ethanol-water solutions. *Biomacromolecules*. 2005;6:368-73.
- [100] Khayet M, Villaluenga JPG, Valentin JL, Lopez-Manchado MA, Mengual JI, Seoane B. Filled poly(2,6-dimethyl-1,4-phenylene oxide) dense membranes by silica and silane modified silica nanoparticles: characterization and application in pervaporation. *Polymer*. 2005;46:9881-91.
- [101] Guo R, Ma X, Hu C, Jiang Z. Novel PVA-silica nanocomposite membrane for pervaporative dehydration of ethylene glycol aqueous solution. *Polymer*. 2007;48:2939-45.
- [102] Zhao Q, Qian JW, Zhu CX, An QF, Xu TQ, Zheng Q, et al. A novel method for fabricating polyelectrolyte complex/inorganic nanohybrid membranes with high isopropanol dehydration performance. *Journal of Membrane Science*. 2009;345:233-41.
- [103] Sun D, Li BB, Xu ZL. Pervaporation of ethanol/water mixture by organophilic nano-silica filled PDMS composite membranes. *Desalination*. 2013;322:159-66.

- [104] Orlov AS, Kiselev SA, Kiseleva EA, Budeeva AV, Mashukov VI. Determination of styrene-butadiene rubber composition by attenuated total internal reflection infrared spectroscopy. *Journal of applied spectroscopy*. 2013;80:47-53.
- [105] Wei RZ, Luo YW, Li ZS. Synthesis of structured nanoparticles of styrene/butadiene block copolymers via RAFT seeded emulsion polymerization. *Polymer*. 2010;51:3879-86.
- [106] Wang H, Pan QM, Rempel GL. Diene-Based Polymer Nanoparticles: Preparation and Direct Catalytic Latex Hydrogenation. *Journal of Polymer Science Part A: Polymer Chemistry*. 2012;50:2098-110.
- [107] Wang H, Pan QM, Rempel GL. Organic solvent-free catalytic hydrogenation of diene-based polymer nanoparticles in latex form: Part I. Preparation of nano-substrate. *Journal of Polymer Science Part A: Polymer Chemistry*. 2012;50:4656-65.
- [108] Liu JM, Pan QM. Synthesis of nanosized poly(ethyl acrylate) particles via differential emulsion polymerization. *Journal of Applied Polymer Science*. 2006;102:1609-14.
- [109] Ouzineb K, Heredia MF, Graillat C, McKenna TF. Stabilization and kinetics in the emulsion copolymerization of butyl acrylate and methyl methacrylate. *Journal of Polymer Science Part A: Polymer Chemistry*. 2001;39:2832-46.
- [110] Wang H, Pan QM, Rempel GL. Micellar nucleation differential microemulsion polymerization. *European Polymer Journal*. 2011;47:973-80.
- [111] Kiatkamjornwong S, Apiwattanon S, Rikukawa M, Ogata N. Super-fine particles of poly(styrene-co-methyl methacrylate) by dispersion copolymerization. *Colloids and Surfaces A: Physicochemical and Engineering Aspects*. 1999;153:229-40.
- [112] Norakankorn C, Pan Q, Rempel GL, Kiatkamjornwong S. Synthesis of core/shell structure of glycidyl-functionalized poly(methyl methacrylate) latex nanoparticles via differential microemulsion polymerization. *European Polymer Journal*. 2009;45:2977-86.
- [113] Romanaguirre M. Elucidating the graft copolymerization of methyl methacrylate onto wood-fiber. *Carbohydrate Polymers*. 2004;55:201-10.
- [114] Norakankorn C, Pan QM, Rempel GL, Kiatkamjornwong S. Synthesis of Poly(methyl methacrylate) Nanoparticles Initiated by Azobisisobutyronitrile Using a Differential

Microemulsion Polymerization Technique. *Journal of Applied Polymer Science*. 2009;113:375-82.

[115] Ismail H, Freakley PK, Sutherland I, Sheng E. Effects of Multifunctional Additive on Mechanical-Properties of Silica Filled Natural-Rubber Compound. *European Polymer Journal*. 1995;31:1109-17.

[116] Liu XH, Sun YA, Deng XH. Studies on the pervaporation membrane of permeation water from methanol/water mixture. *Journal of Membrane Science*. 2008;325:192-8.

[117] Amnuaypanich S, Patthana J, Phinyocheep P. Mixed matrix membranes prepared from natural rubber/poly(vinyl alcohol) semi-interpenetrating polymer network (NR/PVA semi-IPN) incorporating with zeolite 4A for the pervaporation dehydration of water-ethanol mixtures. *Chemical Engineering Science*. 2009;64:4908-18.

[118] Tanchareernrat T, Rempel GL, Prasassarakich P. Preparation of styrene butadiene copolymer-silica nanocomposites via differential microemulsion polymerization and NR/SBR-SiO<sub>2</sub> membranes for pervaporation of water-ethanol mixtures. *Chemical Engineering Journal*. 2014;258:290-300.

[119] Nallasamy P, Anbarasan PM, Mohan S. Vibrational spectra and assignments of cis- and trans-1,4-polybutadiene. *Turkish Journal of Chemistry*. 2002;26:105-11.

[120] Piya-areetham P, Prasassarakich P, Rempel GL. Aqueous-phase hydrogenation of nanosized polyisoprene emulsion using rhodium catalysts. *European Polymer Journal*. 2013;49:2584-95.

[121] Xia HS, Zhang CH, Wang Q. Study on ultrasonic induced encapsulating emulsion polymerization in the presence of nanoparticles. *Journal of Applied Polymer Science*. 2001;80:1130-9.

[122] Suppaibulsuk B, Rempel GL, Prasassarakich P. Synthesis of styrene-g-polyisoprene nanoparticles by emulsion polymerization and its effect on properties of polyisoprene composites. *Polymers for Advanced Technologies*. 2012;23:1473-83.

[123] Santee ER, Chang R, Morton M. 300 MHz proton NMR of polybutadiene: Measurement of cis-trans isomeric content. *Journal of Polymer Science: Polymer Letters Edition*. 1973;11:449-52.

[124] Zhou S, Bai H, Wang J. Hydrogenation of acrylonitrile-butadiene rubber latexes. *Journal of Applied Polymer Science*. 2004;91:2072-8.

- [125] Hinchiranan N, Lertweerasirikun W, Poonsawad W, Rempel GL, Prasassarakich P. Hydrogenated Natural Rubber Blends: Aspect on Thermal Stability and Oxidative Behavior. *Journal of Applied Polymer Science*. 2009;113:1566-75.
- [126] Piya-areetham P, Prasassarakich P, Rempel GL. Organic solvent-free hydrogenation of natural rubber latex and synthetic polyisoprene emulsion catalyzed by water-soluble rhodium complexes. *Journal of Molecular Catalysis A: Chemical*. 2013;372:151-9.
- [127] Piya-areetham P, Rempel GL, Prasassarakich P. Hydrogenated nanosized polyisoprene as a thermal and ozone stabilizer for natural rubber blends. *Polymer Degradation and Stability*. 2014;102:112-21.
- [128] Razumovsky SD, Podmasteriyev VV, Zaikov G. Kinetics of the growth of cracks on polyisoprene vulcanizates in ozone. *Polymer Degradation and Stability*. 1986;16:317-24.
- [129] Sahakaro K, Datta RN, Baaij J, Noordermeer JWM. Blending of NR/BR/EPDM by reactive processing for tire sidewall applications. III. Assessment of the blend ozone- and fatigue-resistance in comparison with a conventional NR/BR compound. *Journal of Applied Polymer Science*. 2007;103:2555-63.
- [130] Esthappan SK, Kuttappan SK, Joseph R. Effect of titanium dioxide on the thermal ageing of polypropylene. *Polymer Degradation and Stability*. 2012;97:615-20.



## APPENDIX A

Data of Mechanical Properties of NR/SBR-SiO<sub>2</sub>**Table A- 1** Tensile strength, 300% modulus and elongation at break of NR/SBR-SiO<sub>2</sub> composites membranes.

Samples	NR	NR/SBR-SiO <sub>2</sub> <sup>c</sup>			
Ratio <sup>a</sup> (wt/wt)	100/0	90/10	80/20	70/30	60/40
SiO <sub>2</sub> cont. <sup>b</sup> (wt%)	-	1.0	2.0	3.0	4.0
Tensile strength (MPa)	18.9	21.1	23.0	26.4	27.7
	17.4	19.0	23.1	24.2	26.7
	16.5	19.4	20.3	24.1	22.5
Mean	17.6	19.8	22.1	24.9	25.6
SD	1.2	1.1	1.6	1.3	2.8
300% Modulus (MPa)	1.45	1.52	1.49	1.52	1.64
	1.26	1.37	1.55	1.50	1.56
	1.33	1.37	1.42	1.63	1.55
Mean	1.35	1.42	1.49	1.55	1.58
SD	0.1	0.09	0.07	0.07	0.05
Elongation at break (%)	830	816	796	792	777
	846	826	827	822	833
	851	845	838	823	784
Mean	842	829	820	812	798
SD	11	15	22	18	31

<sup>a</sup> Ratio of NR to SBR-SiO<sub>2</sub>.<sup>b</sup> Silica content based on total rubber.<sup>c</sup> SBR-SiO<sub>2</sub> condition: M/H<sub>2</sub>O = 0.2, SiO<sub>2</sub>= 10 wt%, SDS = 5 wt%, KPS = 2 wt% based on monomer.

## APPENDIX B

Data of Mechanical Properties of NR/PB-SiO<sub>2</sub> and NR/HPB-SiO<sub>2</sub>**Table B- 1** Mechanical properties of NR/PB-SiO<sub>2</sub> and NR/HPB-SiO<sub>2</sub> composites before and after ageing.

samples	Ratio <sup>c</sup> (wt/wt)	SiO <sub>2</sub> content <sup>d</sup> (wt%)	Tensile strength (MPa)			300% Modulus (MPa)			Elongation at break (%)		
			Be <sup>e</sup>	Af <sup>f</sup>	%Re <sup>g</sup>	Be <sup>e</sup>	Af <sup>f</sup>	%Re <sup>g</sup>	Be <sup>e</sup>	Af <sup>f</sup>	%Re <sup>g</sup>
			age	age		age	age		age	age	
NR	-	-	20	12.6	63.0	1.87	1.13	60.4	662	579	87.5
NR/PB-	90/10	1.0	22.6	16.9	74.8	1.95	1.37	70.3	698	640	91.7
SiO <sub>2</sub> <sup>a</sup>	80/20	2.0	23.1	18.0	77.9	2.15	1.66	77.2	711	672	94.5
	70/30	3.0	25.3	19.5	77.1	2.29	1.85	80.8	721	654	90.7
NR/HPB-	90/10	1.0	23.7	21.6	91.1	2.08	1.96	94.2	658	645	98.0
SiO <sub>2</sub> <sup>b</sup>	80/20	2.0	25.2	23.4	92.9	2.27	2.15	94.7	642	628	97.8
	70/30	3.0	28.3	26.9	95.1	2.49	2.43	97.6	627	592	94.4

<sup>a</sup> PB-SiO<sub>2</sub> condition: M/H<sub>2</sub>O = 0.2, SiO<sub>2</sub>= 10 wt%, SDS = 5 wt%, KPS = 3 wt% based on monomer

<sup>b</sup> HPB-SiO<sub>2</sub> at 98.6 %HD

<sup>c</sup> Ratio of NR to PB-SiO<sub>2</sub> or NR to HPB-SiO<sub>2</sub>

<sup>d</sup> Silica content based on total rubber

<sup>e</sup> Properties before thermal ageing

<sup>f</sup> Properties after thermal ageing

<sup>g</sup> %Retention= (Properties after ageing/Properties before ageing) x 100

**Table B-2** Tensile strength, 300% modulus and elongation at break of NR/PB-SiO<sub>2</sub> and NR/HPB-SiO<sub>2</sub> composites before and after ageing.

Samples	NR			NR/PB-SiO <sub>2</sub>						NR/HPB-SiO <sub>2</sub>					
	100/0	90/10	70/30	80/20	90/10	70/30	80/20	90/10	80/20	70/30	90/10	80/20	70/30		
SiO <sub>2</sub> cont.	0	1.0	3.0	2.0	1.0	3.0	2.0	1.0	2.0	3.0	1.0	2.0	3.0		
	Be age	Af age	Be age	Af age	Be age	Af age	Be age	Af age	Be age	Af age	Be age	Af age	Be age	Af age	
Tensile strength (MPa)	20.0	12.3	22.2	16.8	24.5	17.7	26.4	20.4	23.5	21.1	24.2	23.4	28.2	27.8	
	20.5	13.1	23.5	17.5	20.7	18.9	25.0	19.6	23.2	22.5	25.9	24.3	28.8	26.1	
	19.5	12.5	22.0	16.3	24.2	17.4	24.5	18.5	24.4	21.2	25.5	22.5	27.8	26.7	
Mean	20.0	12.6	22.6	16.9	23.1	18.0	25.3	19.5	23.7	21.6	25.2	23.4	28.3	26.9	
SD	0.5	0.4	0.8	0.6	2.1	0.8	1.0	1.0	0.6	0.8	0.9	0.9	0.5	0.9	
300%	1.78	1.05	2.01	1.40	2.20	1.65	2.33	1.90	2.01	1.94	2.37	2.08	2.47	2.39	
Modulus (MPa)	1.86	1.15	1.92	1.45	2.07	1.73	2.27	1.91	2.15	1.92	2.20	2.23	2.54	2.45	
	1.96	1.20	1.93	1.26	2.18	1.60	2.26	1.75	2.07	2.03	2.23	2.13	2.45	2.46	
Mean	1.87	1.13	1.95	1.37	2.15	1.66	2.29	1.85	2.08	1.96	2.27	2.15	2.49	2.43	
SD	0.09	0.08	0.05	0.10	0.07	0.07	0.04	0.09	0.07	0.06	0.09	0.08	0.05	0.04	
Elongation at break (%)	639	568	711	630	712	672	712	643	649	653	643	613	634	584	
	682	577	702	656	715	664	727	658	657	638	629	639	629	602	
	665	591	681	635	707	681	725	662	667	645	653	633	619	590	
Mean	662	579	698	640	711	672	721	654	658	645	642	628	627	592	
SD	22	12	15	14	4	9	8	10	9	8	12	14	8	9	



## APPENDIX C

Data of Mechanical Properties of SBR/PS-SiO<sub>2</sub>**Table C- 1** Tensile strength, 300% modulus and elongation at break of SBR/PS-SiO<sub>2</sub> composites membranes.

Samples	SBR	SBR/PS-SiO <sub>2</sub> <sup>c</sup>	
Ratio <sup>a</sup> (wt/wt)	100/0	90/10	80/20
SiO <sub>2</sub> cont. <sup>b</sup> (wt%)	-	1.0	2.0
Tensile strength (MPa)	14.3	15.2	16.4
	13.0	15.5	17.3
	12.4	16.3	16.6
Mean	13.2	15.7	16.8
SD	0.97	0.57	0.47
300% Modulus (MPa)	1.49	3.20	4.25
	2.67	3.17	4.67
	2.00	3.30	4.48
Mean	2.05	3.22	4.47
SD	0.59	0.07	0.21
Elongation at break (%)	602	574	534
	619	549	519
	610	555	507
Mean	610	559	520
SD	9	13	14

<sup>a</sup> Ratio of SBR to PS-SiO<sub>2</sub>.<sup>b</sup> Silica content based on total rubber.<sup>c</sup> PS-SiO<sub>2</sub> condition: M/H<sub>2</sub>O = 0.3, SiO<sub>2</sub>= 10 wt%, SDS = 3 wt%, KPS = 2 wt% based on monomer.

## APPENDIX D

Data of SBR-SiO<sub>2</sub> Synthesis**Table D- 1** Data of effect of silica loading on SBR-SiO<sub>2</sub>.

%SiO <sub>2</sub>	Exp. Run	Particle size (nm)	Average particle size (nm)	Conversion (%)	Average conversion (%)	%Si encap. eff.	Average %Si encap. eff.
5	1	30.8	30.6	93.2	91.9	89.7	91.8
	2	30.4		90.6		93.9	
7.5	1	31.7	31.4	89.1	88.7	87.2	88.0
	2	31.1		88.3		88.8	
10	1	33.2	33.7	86.3	87.5	82.6	83.5
	2	34.2		88.7		84.4	
15	1	35.0	35.9	65.6	64.2	67.3	68.9
	2	36.8		62.8		70.5	
20	1	42.6	43.2	51.8	52.6	55.9	57.8
	2	43.8		53.4		59.3	

Condition: M/H<sub>2</sub>O = 0.2, KPS = 2 wt%, SDS = 5 wt% based on monomer.

**Table D- 2** Data of effect of surfactant concentration on SBR-SiO<sub>2</sub>.

%SDS	Exp. Run	Particle size (nm)	Average particle size (nm)	Conversion (%)	Average conversion (%)	%GE	Average %GE
1	1	52.6	54.0	76.4	77.1	82.4	83.0
	2	55.3		77.8		83.6	
3	1	36.8	37.5	88.5	86.6	75.9	75.5
	2	38.2		84.7		75.1	
5	1	33.2	33.7	86.3	87.5	56.4	57.6
	2	34.2		88.7		58.8	
7	1	27.5	26.0	88.7	89.2	50.2	48.7
	2	24.4		89.7		47.2	
10	1	21.8	22.5	94.6	93.3	32.5	33.8
	2	23.2		92.0		35.1	

Condition: M/H<sub>2</sub>O = 0.2, KPS = 2 wt%, SiO<sub>2</sub> = 10 wt% based on monomer

**Table D- 3** Data of effect of monomer to water ratio on SBR-SiO<sub>2</sub>.

M/H <sub>2</sub> O	Exp. Run	Particle size (nm)	Average particle size (nm)	Conversion (%)	Average conversion (%)	%GE	Average %GE
0.1	1	25.9	26.6	19.4	20.1	36.8	37.9
	2	27.2		20.8		39.0	
0.15	1	32.6	32.6	41.7	41.7	41.9	41.9
0.2	1	33.2	33.7	86.3	87.5	56.4	57.6
	2	34.2		88.7		58.8	
0.25	1	35	35	88.6	88.6	71.1	71.1
0.3	1	38.9	39.6	97.9	98.6	76.9	78.3
	2	40.3		99.3		79.7	
0.4	1	42.2	42.9	95.0	95.3	73.1	72.8
	2	43.5		95.6		72.5	
0.5	1	44.8	44.7	90.7	91.2	70.2	68.1
	2	44.6		91.7		66	

Condition: SDS = 5 wt%, KPS = 2 wt%, SiO<sub>2</sub> = 10 wt% based on monomer

**Table D- 4** Data of effect of initiator concentration on SBR-SiO<sub>2</sub>.

%KPS	Exp. Run	Particle size (nm)	Average particle size (nm)	Conversion (%)	Average conversion (%)	%GE	Average %GE
0.5	1	28.0	28.9	3.6	3.3	82.1	82.2
	2	29.8		3.0		82.3	
1	1	33.7	34.0	82.7	84.2	77.4	78.1
	2	34.3		85.7		78.8	
2	1	36.8	37.5	88.5	86.6	75.9	75.5
	2	38.2		84.7		75.1	
3	1	45.1	45.6	90.5	91.9	73.8	74.0
	2	46.0		93.3		74.2	
4	1	39.5	40.7	90.7	89.0	71.5	70.1
	2	41.8		87.3		68.7	

Condition: M/H<sub>2</sub>O = 0.2, SDS = 3 wt%, SiO<sub>2</sub> = 10 wt% based on monomer

## APPENDIX E

Data of PB-SiO<sub>2</sub> Synthesis**Table E- 1** Data of effect of silica loading on PB-SiO<sub>2</sub>.

%SiO <sub>2</sub>	Exp. Run	Particle size (nm)	Average particle size (nm)	Conversion (%)	Average conversion (%)	%Si encap. eff.	Average %Si encap. eff.
5	1	23.4	23.6	94.3	95.9	93.7	92.4
	2	23.8		97.5		91.1	
7.5	1	26.4	25.6	88.0	88.3	86.4	85.7
	2	24.8		88.6		85.0	
10	1	27.1	27.3	82.7	81.5	83.1	83.5
	2	27.5		80.3		83.9	
15	1	31.6	30.8	75.8	76.2	72.7	73.7
	2	30.0		76.6		74.7	
20	1	32.5	32.2	72.3	71.3	65.6	66.4
	2	31.9		70.3		67.2	

Condition: M/H<sub>2</sub>O = 0.2, KPS = 3 wt%, SDS = 5 wt% based on monomer

**Table E- 2** Data of effect of surfactant concentration on PB-SiO<sub>2</sub>.

%SDS	Exp. Run	Particle size (nm)	Average particle size (nm)	Conversion (%)	Average conversion (%)	%GE	Average %GE
1	1	27.9	28.2	24.3	23.6	31.4	30.2
	2	28.5		22.9		29.0	
3	1	25.4	24.8	55.9	55.6	67.3	66.0
	2	24.2		55.3		64.7	
5	1	26.0	25.3	74.8	75.2	81.5	82.7
	2	24.6		75.6		83.9	
7	1	22.3	21.6	82.7	83.3	82.3	83.3
	2	20.9		83.9		84.3	
10	1	18.6	18.9	91.5	90.2	72.1	70.3
	2	19.2		88.9		68.5	

Condition: M/H<sub>2</sub>O = 0.2, KPS = 2 wt%, SiO<sub>2</sub> = 10 wt% based on monomer

**Table E- 3** Data of effect of monomer to water ratio on PB-SiO<sub>2</sub>.

M/H <sub>2</sub> O	Exp. Run	Particle size (nm)	Average particle size (nm)	Conversion (%)	Average conversion (%)	%GE	Average %GE
0.1	1	18.7	19.2	57.8	59.3	76.2	76.7
	2	19.7		60.8		77.2	
0.2	1	22.3	21.6	82.7	83.3	82.3	83.3
	2	20.9		83.9		84.3	
0.3	1	22.5	22.0	76.4	75.5	83.9	83.5
	2	21.5		74.6		83.1	
0.4	1	22.7	22.8	64.2	63.4	71.7	71.4
	2	22.9		62.6		71.1	
0.5	1	22.9	23.2	60.8	61.7	68.5	68.1
	2	23.5		62.6		67.7	

Condition: SDS = 7 wt%, KPS = 2 wt%, SiO<sub>2</sub> = 10 wt% based on monomer

**Table E- 4** Data of effect of initiator concentration on PB-SiO<sub>2</sub>.

%KPS	Exp. Run	Particle size (nm)	Average particle size (nm)	Conversion (%)	Average conversion (%)	%GE	Average %GE
1	1	24.1	24.3	73.8	74.7	88.2	87.4
	2	24.5		75.6		86.6	
2	1	26.0	25.3	74.8	75.2	81.5	82.7
	2	24.6		75.6		83.9	
3	1	28.2	27.3	82.7	81.5	77.7	78.5
	2	26.4		80.3		79.3	
4	1	29.3	28.4	83.2	83.7	65.1	63.3
	2	27.5		84.2		61.5	
5	1	29.8	30.1	98.0	97.7	50.5	51.1
	2	30.4		97.4		51.7	

Condition: M/H<sub>2</sub>O = 0.2, SDS = 5 wt%, SiO<sub>2</sub> = 10 wt% based on monomer

## APPENDIX F

Data of PS-SiO<sub>2</sub> Synthesis**Table F- 1** Data of effect of silica loading on PS-SiO<sub>2</sub>.

%SiO <sub>2</sub>	Exp. Run	Particle size (nm)	Average particle size (nm)	Conversion (%)	Average conversion (%)	%Si encap. eff.	Average %Si encap. eff.
5	1	31.4	31.6	91.7	91.8	89.9	90.4
	2	31.8		91.9		90.9	
7.5	1	32.2	32.3	89.0	89.2	86.5	85.7
	2	32.4		89.4		84.9	
10	1	33.7	33.5	87.2	87.4	81.2	81.9
	2	33.3		87.6		82.6	
15	1	36.6	36.5	71.9	72.6	67.2	68.4
	2	36.4		73.3		69.6	
20	1	40.0	40.2	51.5	52.1	59.2	59.7
	2	40.4		52.7		60.2	

Condition: M/H<sub>2</sub>O = 0.2, KPS = 3 wt%, SDS = 5 wt% based on monomer

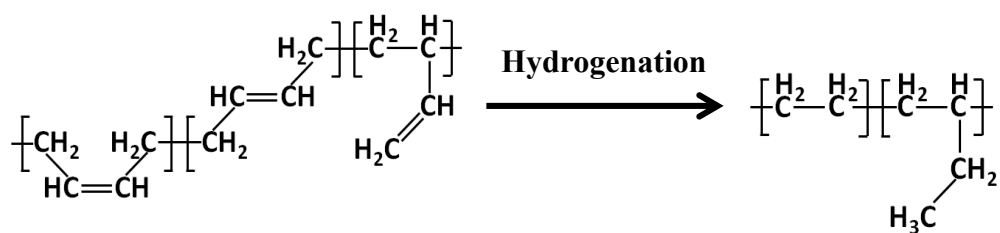
**Table F- 2** Data of effect of surfactant concentration on PS-SiO<sub>2</sub>.

%SDS	Exp. Run	Particle size (nm)	Average particle size (nm)	Conversion (%)	Average conversion (%)	%GE	Average %GE
1	1	42.3	42.7	70.7	72.7	78.5	80.4
	2	43.1		74.7		82.3	
3	1	32.5	33.5	85.5	87.4	77.4	76.3
	2	34.5		89.3		75.2	
5	1	28.3	28.6	88.7	90.3	61.5	62.1
	2	28.9		91.9		62.7	
7	1	25.2	26.0	92.0	92.2	51.5	50.8
	2	26.8		92.4		50.1	
10	1	23.3	23.8	93.1	93.9	35.8	37.0
	2	24.3		94.7		38.2	

Condition: M/H<sub>2</sub>O = 0.2, KPS = 2 wt%, SiO<sub>2</sub> = 10 wt% based on monomer

## APPENDIX G

## Calculation of %Hydrogenation

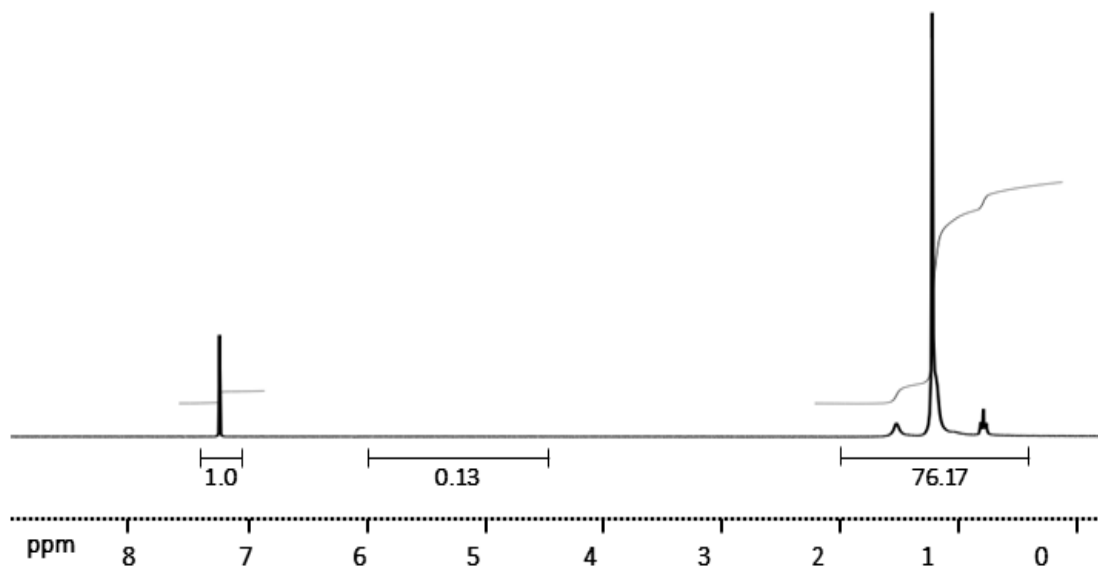


Polybutadiene

Hydrogenated polybutadiene

Proton of repeating unit except =CH in polybutadiene = 4 protons

Proton of repeating unit in hydrogenated polybutadiene = 8 protons

Figure G- 1  $^1\text{H}$ -NMR spectra of HPB-SiO<sub>2</sub> at 98.6 %HD.

where A = Peak area except double bond peak at 5.2 ppm

B = Peak area of double bond at 5.2 ppm

C = Peak area of saturated  $-\text{CH}_2-$  and  $-\text{CH}_3$

$$A = 8C + 4B$$

$$\therefore C = \frac{A - 4B}{8}$$

Total peak area = Peak area of saturated  $-\text{CH}_2-$  and  $-\text{CH}_3$  + Peak area of double bond at 5.2 ppm

$$= \left[ \frac{A - 4B}{8} \right] + B$$

$$= \frac{A + 4B}{8}$$

%Hydrogenation = [(Peak area of saturated  $-\text{CH}_2-$  and  $-\text{CH}_3$ )/(Total peak area)] $\times$  100

$$= \left[ \frac{(A - 4B)/8}{(A + 4B)/8} \right] \times 100$$

$$= \frac{A - 4B}{A + 4B} \times 100$$

For Example: A = 76.17 and B = 0.13

$$\% \text{Hydrogenation} = \frac{76.17 - 4(0.13)}{76.17 + 4(0.13)} \times 100$$

$$= 98.64\%$$



## APPENDIX H

Data of Diimide Hydrogenation of Nanosized PB-SiO<sub>2</sub>**Table H- 1** Data of effect of N<sub>2</sub>H<sub>4</sub> concentration on HPB-SiO<sub>2</sub>.

N <sub>2</sub> H <sub>4</sub> /C=C	Exp. Run	Particle size (nm)	Average particle size (nm)	%HD	Average %HD
1	1	28.0	28.2	74.6	74.8
	2	28.4		75.0	
2	1	28.1	28.2	90.9	90.7
	2	28.3		90.5	
3	1	28.4	28.6	98.6	98.6
	2	28.8		98.6	
4	1	29.5	29.7	98.0	98.2
	2	29.9		98.4	
5	1	29.8	29.9	97.7	97.9
	2	30.0		98.1	

Condition: [H<sub>2</sub>O<sub>2</sub>] = 4 mol/L, [H<sub>3</sub>BO<sub>3</sub>] = 0.15 mol/L, [C=C] = 1 mol/L, T = 70 °C, time = 5 h

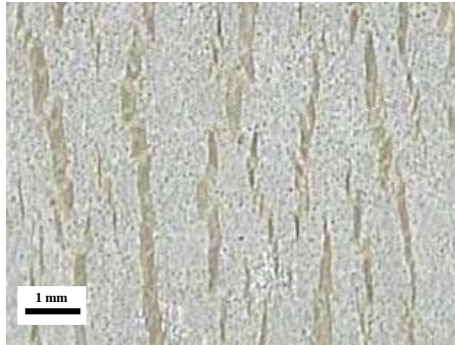
**Table H- 2** Data of effect of H<sub>2</sub>O<sub>2</sub> concentration on HPB-SiO<sub>2</sub>.

H <sub>2</sub> O <sub>2</sub> /C=C	Exp. Run	Particle size (nm)	Average particle size (nm)	%HD	Average %HD
1	1	28.1	28.2	73.5	73.7
	2	28.3		73.9	
2	1	30.2	30.2	84.2	84.0
	2	30.2		83.8	
3	1	32.0	32.4	96.7	96.4
	2	32.8		96.1	
4	1	28.4	28.6	98.6	98.6
	2	28.8		98.6	
5	1	29.5	29.6	96.8	97.0
	2	29.7		97.2	

Condition: [N<sub>2</sub>H<sub>4</sub>] = 3 mol/L, [H<sub>3</sub>BO<sub>3</sub>] = 0.15 mol/L, [C=C] = 1 mol/L, T = 70 °C, time = 5 h

## APPENDIX I

**Classification of Cracking on the Surface of NR Composites  
for Ozone Resistance Testing**



Type of cracking

= Appearance of cracking-Number of cracking

= C-5

Number of Cracking

- A: A small number of cracking.
- B: A large of number cracking.
- C: Numerous cracking.

Appearance of Cracking จุฬาลงกรณ์มหาวิทยาลัย

- 1: That which cannot be seen with eyes but can be confirmed with 10 times magnifying glass.
- 2: That which can be confirmed with naked eyes.
- 3: That which the deep and comparatively long (below 1 mm).
- 4: That which the deep and long (above 1 mm and below 3 mm).
- 5: That which about to crack more than 3 mm or about to severe.

## VITA

Miss Thanyaporn Tancharernrat was born on October 24, 1988 in Ratchaburi, Thailand. She received her B.Sc. (Second class honors) degree from the Department of Chemical Technology, Chulalongkorn University in 2011. She continued studying for a Doctoral Degree in Chemical Technology, Chulalongkorn University. She has received the Royal Golden Jubilee Scholarship from Thailand Research Fund for her Ph.D. study. Thanyaporn also served as a teaching assistant for undergraduate courses “Chemical Engineering Thermodynamic”, “Applied Mathematics in Chemical Engineering” and “Fuels Testing Laboratory”. She carried out her Ph.D. research for one year (2013-2014) at “Advanced Rubber Technology and Applied Catalysis Laboratory” in Department of Chemical Engineering, University of Waterloo, ON, Canada.

### Journal Publication:

1. Tancharernrat, T., Rempel, G.L., and Prasassarakich, P. Preparation of Styrene Butadiene Copolymer-Silica Nanocomposites via Differential Microemulsion Polymerization and NR/SBR-SiO<sub>2</sub> Membranes for Pervaporation of Water-Ethanol Mixtures. *Chemical Engineering Journal* 258 (2014) 290-300.
2. Tancharernrat, T., Rempel, G.L., and Prasassarakich, P. Synthesis of Polybutadiene-Silica Nanoparticles via Differential Microemulsion Polymerization and their Hydrogenated Nanoparticles by Diimide Reduction. *Polymer Degradation and Stability* 118 (2015) 69-81.
3. Tancharernrat, T., Rempel, G.L., and Prasassarakich, P. SBR/PS-SiO<sub>2</sub> Nanocomposites: Physical Properties and Gas Permeability. To be submitted to *Express Polymer Letters* (2015).

### Conference Presentation:

1. Tancharernrat, T., Rempel, G.L., and Prasassarakich, P. (2014) “Synthesis of Styrene Butadiene Copolymer-Silica Nanoparticles via Differential Microemulsion Polymerization”. The 9th Mathematics and Physical Sciences Graduate Congress (9thMPSGC), January 8 – 10, 2014 at University of Malaya, Malaysia. (Oral presentation)
2. Tancharernrat, T., Rempel, G.L., and Prasassarakich, P. (2014) “Preparation of Polybutadiene-Silica Nanoparticles via Differential Microemulsion Polymerization and their Hydrogenated Nanoparticles by Diimide Reduction”. The 4th Polymer Conference of Thailand (4thPCT), March 20 – 21, 2014 at Pathumwan Princess Hotel, Bangkok, Thailand. (Oral presentation).
3. Tancharernrat, T., Rempel, G.L., and Prasassarakich, P. (2014) “Synthesis of Styrene Butadiene Copolymer-Silica Nanoparticles via Differential Microemulsion Polymerization”. The Royal Golden Jubilee Ph.D. Congress XV (RGJ-Ph.D. Congress XV), May 28 – 30, 2014 at Jomtien Palm Beach Hotel, Chonburi, Thailand. (Oral presentation)
4. Tancharernrat, T., Rempel, G.L., and Prasassarakich, P. (2014) “Preparation of Polybutadiene-Silica Nanoparticles via Differential Microemulsion Polymerization and their Hydrogenated Nanoparticles by Diimide Reduction”. The 2014 IUPAC World Polymer Congress, July 6 – 11, 2014 at Chiangmai International Convention and Exhibition Centre, Chiangmai, Thailand. (Poster presentation).
5. Tancharernrat, T., Rempel, G.L., and Prasassarakich, P. (2015) “Preparation of Polybutadiene-Silica Nanoparticles via Differential Microemulsion Polymerization and their Hydrogenated Nanoparticles by Diimide Reduction”. Nanotech France 2015 International Conference & Exhibition, June 15 – 17, 2015 at Pôle Universitaire Léonard de Vinci, Paris, France. (Poster presentation).